Guidance Algorithm for an Air-to-Air Boost Phase Interceptor

Master Thesis Report

J.L. Broekhuizen

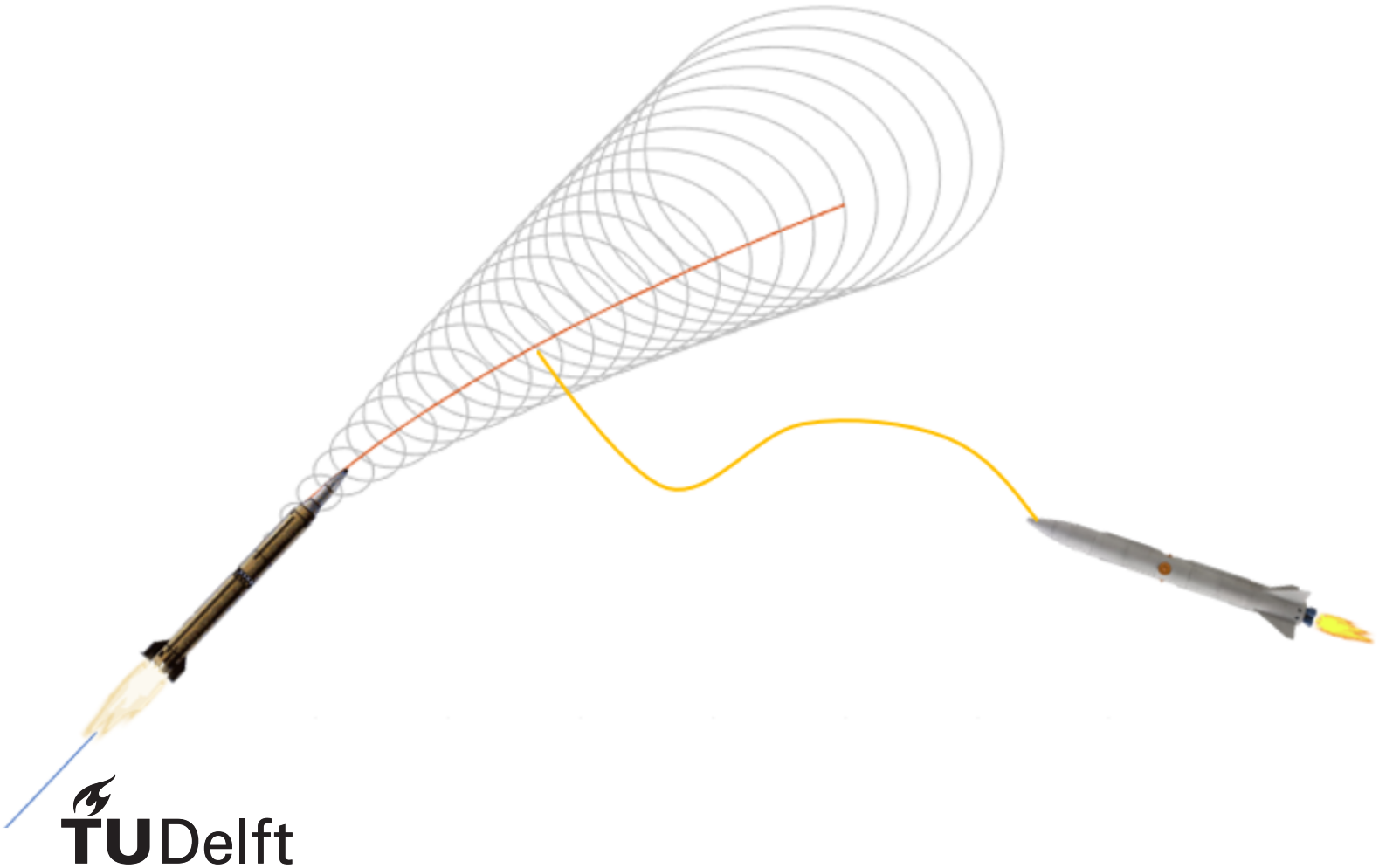

TU Delft

Guidance Algorithm for an Air-to-Air Boost Phase Interceptor

Master Thesis Report

by

J.L. Broekhuizen

Student number: 4292499
Project duration: 1 June, 2017 – 16 November, 2018
Thesis supervisors: Ir. W. Halswijk, TNO
Dr. Ir. M. Voskuijl, TU Delft

An electronic version of this thesis is available at `http://repository.tudelft.nl/`.

TU Delft

Abstract

Current Ballistic Missile (BM) defence systems intercept an incoming threat in its terminal phase, and to some extend during its coast phase. During the boost phase of a BM, the initial velocity of the BM is low and the hot exhaust plume is easy to spot for infrared sensors, which provides a good opportunity for interception. To do so, the Network Centric Airborne Defense Element (NCADE) is a missile in development, which is to be launched from a 5^{th} generation fighter aircraft. A tracking algorithm model has already been developed at TNO, which performs the tracking and trajectory prediction of the BM, based on the location measurements performed by the IR sensors of both the aircraft and the missile. Tracking a BM and predicting its trajectory poses a challenge, as the mass, thrust and acceleration cannot be measured directly, resulting in an uncertainty in the trajectory prediction. The NCADE therefore must be able to intercept the BM in its boost phase, considering the uncertainties in the trajectory prediction. The main research goal of this thesis is to develop a guidance algorithm for the NCADE, which plans a trajectory of an air launched missile, intercepting a BM in its boost phase. To do so, the NCADE has been modelled, and the tracking algorithm has been implemented. The actual guidance is performed using trajectory optimisation.

The NCADE is designed to disable its target by means of kinetic penetration, meaning that there is no explosive warhead present. The missile is derived from the AIM120D AMRAAM, with a similar outer shape and suspension points. The NCADE consists of two stages, where the first stage is equipped with a solid booster for a fast acceleration. Control deflections are provided with aerodynamic surfaces. The second stage, also called Kill Vehicle (KV), is equipped with an IR sensor to determine the location of the target. Some sensor inaccuracy is present due to the amount of pixels used in the sensor. Control inputs on the second stage are performed using monopropellant pulses. Both control inputs and thrust of the KV use monopropellant from the same source, meaning that when the monopropellant tank is depleted, both control deflections and thrust cannot be delivered. To calculate different trajectories of the NCADE, the equations of motion are set up, where the NCADE is modelled as a 3 degrees of freedom point mass. Aerodynamic coefficients are obtained using software applying empirical methods, for which an extended database of projectiles is available. Verification of the equations is performed using a validated generic missile model, made by TNO using Simulink.

The calculation of the guidance relies on a location of the target in the future. Therefore, a trajectory prediction must be performed, for which the states of the BM must be determined. There are however only position measurements of the BM available, from which a more extended set of states of the BM must be derived. This is performed using an Extended Kalman Filter (EKF), which was developed during an earlier study. The filter initiates with a guess of the states of the BM, and continuously updates those as new readings of the BM become available. Using the Kalman states, a trajectory prediction is performed. The Kalman states require a certain tracking period to converge to the correct values, to be able to calculate usable trajectory predictions. The quality of the tracking prediction is quantified by a score, which is forwarded to the guidance algorithm to be able to take the significant uncertainties in the trajectory prediction into account. The certainty score improves when the tracking duration increases and when the trajectory prediction is nearby in the future. The certainty results are forwarded to the guidance algorithm by means of coefficients of a polynomial.

Due to the complexity of the control system of the NCADE and the uncertain target trajectory, trajectory optimisation is applied in the guidance algorithm. Trajectory optimisation aims to decrease the defined performance index, which is in this case the divert cone minus the uncertainty ellipse of the trajectory prediction, to maximise the probability for interception. The divert cone of the NCADE is a volume which the missile is able to reach on a certain time, given its states and reserve fuel. The divert cone is calculated using a separate shooting optimisation algorithm, which maximises the distance in three ENU frame directions. To maximise the probability of interception, a shooting method is applied, which uses candidate solutions in the form of functions describing the control input, to calculate the performance index. Using constraints, the missile is directed towards an interception point. Constraints are also applied to bound the magnitude of the controls, and at the trajectory itself to remain physical feasible.

To investigate the behaviour of the guidance algorithm, simulations of interceptions of the NCADE have been performed on a modelled Scud BM, using a range of launch locations and tracking settings. The opti-

mum results are presented in control deflection functions of the NCADE, which achieve the flight with the minimised performance index. When only the tracking uncertainty is minimised, flight time t_f is minimised, as the prediction becomes less reliable when a longer trajectory prediction is performed. When only the size of the divert cone is to be maximised, the propellant of the sustainer, used for control and propulsion, is saved to increase the divert cone. Because of this, the altitude of the flight is increased, and t_f must become larger, because less monopropellant is applied to increase the velocity at the beginning of the sustain phase. The optimum solution is a compromise between the divert cone size and t_f. As the duration of the tracking time increases, the target trajectory prediction becomes more reliable, so the maximisation of the divert cone becomes more prominent. However, this results in the maximum range to decrease, since there is less time for interception, and the altitude of the target has increased. When the launch location is positioned further from the target, the reduction of t_f becomes more prominent and the divert cone decreases. In conclusion, the optimisation routine performs the compromise between the amount of reserve propellant available, and the uncertainty of the trajectory prediction.

Preface

I would like to thank my friends, of who I asked tons of patience, and my family for their never ending support. My girlfriend does not know me differently than being a stressed thesis student, which I hope could be different from now on. I am grateful for all support of my supervisor at TNO, Wouter Halswijk. His enthusiasm for the subject made me persistent in finishing my work. Besides his apparent infinite knowledge of all aspects of missiles, I would like to thank all TNO colleagues for their support and knowledge. There was always time for help with my troubles. This thesis could not have been completed without Mark Voskuijl, my supervisor at the TU Delft. The military subject has an ethical edge on it, nevertheless, Mark supervised my work and he did so with great devotion. He can be either assisting with hard to understand subjects, or improving the structure with obvious yet overseen remarks.
Thank you all!

J.L. Broekhuizen

Rijswijk, November 2018

Contents

List of Figures

List of Tables

Nomenclature

Table 1: Latin Variables

Sign	Variable	Unit
A	Axial force	(N)
a	Basis function coefficient	$(-)$
B	Side force	(N)
C_A	Axial Coefficient	$(-)$
C_N	Normal Coefficient	$(-)$
C_S	Prediction certainty score	$(-)$
C_X	Axial Coefficient output term	$(-)$
c	Constraint	$(-)$
D_B	Sideways DACS deflection	(N)
D_N	Upwards DACS deflection	(N)
E	Pitching control force	(N)
E	Divert Cone Size	(m)
$\dot{E}$	Change in position, east	$(^m/_s)$
F	Force	(N)
$\mathbf{F}^a$	Force in the aerodynamic frame	(N)
$\mathbf{F}^b$	Force in the body frame	(N)
g	gravitational acceleration	$(^m/_{s^2})$
H	Hamiltonian	$(-)$
H_C	Jacobian	$(-)$
I_{sp}	Specific Impulse	(s)
J	Performance index	$(-)$
L	Lagrangian	$(-)$
M	Mach number	$(-)$
m	Mass	(kg)
N	Normal force	(N)
N'	PN coefficient	$(-)$
$\dot{N}$	Change in position, north	$(^m/_s)$
n_c	Sideways acceleration command	$(-)$
P_E	Uncertainty Ellipse	(m)
R	Yawing control force	(N)
R_C	Covariance Matrix	$(-)$
Rd	Random value	$(-)$
S	Reference surface	(m^2)
S_0	Start location	(m)
T	Thrust	(N)

t_f	time to flight	(s)
t_s	simulation time	(s)
t	time	(s)
$\dot{U}$	Change in position, up	$(^{m}/_{s})$
$\mathbf{u}$	Control function/vector	$(-)$
V	Velocity	$(^{m}/_{s})$
V_T	Target Velocity	$(^{m}/_{s})$
W	Weight	(N)
X_M	Interceptor ECEF Coordinates	(m)
X_T	BM ECEF Coordinates	(m)
$\mathbf{x}$	State function/vector	$(-)$

Table 2: Greek Variables

Sign	Variable	Unit
α	Angle of attack	(rad)
β	Sideslip angle	(rad)
γ	Path angle	(rad)
θ	Pitch angle	(rad)
λ	Adjoint	$(-)$
$\dot{\lambda}$	Observation angle rate	$^{rad}/_{s})$
ξ	Angle between acceleration and velocity vector	(rad)
ρ	Density	$(^{kg}/_{m^3})$
σ	Standard Deviation	$(-)$
Ψ	Heading	(rad)
χ	Azimuth	(Rad)

Abbreviations

AMRAAM	Advanced Medium Range Air to Air Missile
AoA	Angle of Attack
BM	Ballistic Missile
BPI	Boost Phase Interception
CG	Centre of Gravity
CP	Centre of Pressure
DACS	Divert and Attitude Control System
DAS	Distributed Aperture System
DOF	Degrees Of Freedom
ECEF	Earth Centred Earth Fixed
ECI	Earth Centred Inertial
EKF	Extended Kalman Filter
ENU	East-North-Up
EOM	Equations Of Motion
FBD	Free Body Diagram
FOV	Field Of View
FPA	Focal Plane Array
GMM	Generic Missile Model
HAN	HydroxylAmmonium Nitrate
IFOV	Instantaneous Field Of View
IR	InfraRed
IRST	Infrared Search and Track
IVOF	Instantaneous Field Of View
JSF	Joint Strike Fighter
KF	Kalman Filter
KV	Kill Vehicle
NCADE	Network Centric Airborne Defense Element
NED	North East Down
NLP	NonLinear Programming
PIP	Predicted Intercept Point
PN	Proportional Navigation
PRODAS	Projectile Rocket Ordinance Design & Analysis System
SQP	Sequential Quadratic Programming
TFOV	Total Field Of View
TNO	Nederlandse Organisatie voor toegepast-natuurwetenschappelijk onderzoek
TU	Technische Universiteit
WEZ	Weapon Engagement Zone

1 Introduction

1.1. Research Work Motivation

In the cold war, a large amount of firepower for a counter attack was used to keep the enemy from striking first (Neufeld, 1995 [26]). Nowadays, focus has shifted to repelling possible threats. Incoming Ballistic Missiles (BM) can be shot down on arrival, by surface-launched missiles. These have as downside that intercepted threats can still cause damage to the homeland. Advances in Infrared Search and Track (IRST) instruments on 5^{th} generation fighter aircraft have stimulated the development of a dedicated airborne BM interceptor, called the Network Centric Airborne Defense Element (NCADE) (Tackett, 2006 [36]). The NCADE is an air-to-air missile which fits inside current weapon bays of fighter aircraft, since its outer shape is similar to the AIM-120D Advanced Medium-Range Air-to-Air Missile (AMRAAM). It features two stages equipped with a passive infrared seeker. The second stage is a Kill Vehicle (KV), making the weapon a hit-to-kill type, meaning that an explosive charge is absent. Advantages of using an air-launched anti-BM boost phase interceptor system are the added line of defence and the easy lock on the hot exhaust plume. Another advantage is that the debris of the BM is not able to achieve its target, decreasing damage to friendly territory (Bardanis, 2004 [3]).

1.2. Research Aims and Objectives

For common air-to-air interception missiles, proportional navigation guidance algorithms are commonly applied, which rely on predictable accelerations of the target and the missile itself (Nesline and Zarchan, 1981 [25]). The challenge for BM interception is the large acceleration and the changing mass, making proportional navigation unusable for hit-to-kill missiles. The developer of the NCADE system, Raytheon, is unlikely to share specific technical details on how guidance laws are implemented. This poses a challenge to completely determine the performance and operational capability of the weapon system. TNO aims to develop a fly-out simulation model of a dedicated BM boost phase interceptor. As a start, a tracking algorithm is already established, which tracks an accelerating target, considering its decrease in mass. Due to the large varying acceleration of the target, the track prediction is not accurate enough for straightforward guidance algorithms. Other studies have proven that trajectory optimisation is theoretically possible for guidance of a fast accelerating missile as the NCADE, but do not consider the uncertain nature of the trajectory of the target. The main research goal is to develop a guidance algorithm which calculates the trajectory of an air launched missile, which intercepts a BM in its boost phase, considering the uncertainties of the trajectory prediction. The main research question is therefore formulated as:
How can the guidance of an air launched missile with the purpose of intercepting a ballistic missile in its boost phase be developed, by applying a flight trajectory optimisation algorithm to cope with the uncertainties of the prediction of the ballistic missile's trajectory?

1.3. Methodology

The thesis work starts with the literature study, which provides the required state-of-the-art knowledge of the aspects of BM interception. The thesis work then continues by modelling an air-to-air missile, for which the NCADE is chosen. The tracking procedure is analysed, and a guidance algorithm is set up and tested.

1.3.1. Literature Study
The thesis work start with a literature research (Chapter 2). Defence against BMs is already operational using surface based interception missiles, from which valuable lessons can be learned. The theory about the tracking of BMs is studied as well. The literature study provides the theoretic base for air launched missiles and the general strategies for the optimisation of flight.

1.3.2. Modelling the Air-to-air Ballistic Missile Boost Phase Interceptor
A dedicated air-to-air BM boost phase interceptor is to be modelled. The model will be based upon the NCADE, since it is the only known missile under development for this purpose, to the best of the author's knowledge. Its development is a reason for this thesis work. A certain amount of analysis already has been performed, which is extended to be able to calculate flight trajectories (Halswijk and Benoist, 2014 [10]). The Equations Of Motion (EOM) are derived. Verification of those EOM is performed by running a set of cases, and compare it with a validated Simulink model, in which a model of the NCADE is simulated (TNO, 2012 [39]).

1.3.3. Tracking
The tracking algorithm is assessed. This assessment can be used as an input for the trajectory optimisation process, which should adjust the trajectory accordingly. Besides the estimation of the BM's states, the IR sensors produce sensor noise, for which assumptions must be made. The actual uncertainty is identified and its behaviour is investigated.

1.3.4. Trajectory Optimisation
A guidance algorithm is developed, using a flight optimisation strategy which is determined. The control problem is defined and the NCADE with its target are implemented. The optimiser is completed by implementing constraints, and a NonLinear Programming (NLP) algorithm to solve the optimisation problem.

1.3.5. Simulations
The results will provide insight in what kind of flight strategies are most optimal for intercepting hard-to-track targets, with for example control functions of the propellant consumption and the chosen flight altitude. A set of test cases is defined and run to investigate the behaviour of the interceptor. Variations will be applied to the launch conditions, the tracking procedure and the defined performance index which is to be minimised.

2

Ballistic Missile Defence Background

The thesis work is supported by a literature study, to investigate the current knowledge about the interception of BMs. The first practical Ballistic Missiles (BM) originated from World War Two, which could at that time engage without any defence means by the enemy (Neufeld, 1995 [26]). As BMs started became more technical advanced and posed an increasingly larger threat, counter measurements were being developed. Operational counter measurements exist of a system to track the target, whereafter a missile is fired to intercept the threat, either equipped or not equipped with an explosive charge (Mantle, 2004 [21]). This report focuses on a missile which is launched from an aircraft, instead of a ground based system, being the NCADE. A Kalman Filter (KF) is developed in an earlier study to track the BM. Guidance algorithms already exist for air-launched weapons, which apply trajectory optimisation to calculate the optimal path towards interception. They do not however include the difficulties of the prediction of the BM's trajectory.

2.1. Ballistic Missile Defence

BMs are designed to carry an explosive, nuclear or biochemical load from a launch position towards enemy territory. To defend against incoming BMs, missile systems where developed, were high accuracy became an increasingly important design aspect.

2.1.1. Ballistic Missiles

BMs can be distinguished from other types of missiles for their ballistic portion of the flight (Figure 2.1, #1). They have typical ranges from 150 km of the smaller tactical missiles to 10.000 km for the largest intercontinental BMs (Neufeld, 1995 [26]). The larger types commonly consist of multiple stages. During the initial boost phase, the BM burns all of its fuel to increase its velocity, and guides its flight towards its target by attaining an azimuth angle, set by its guidance algorithm. The boost phase is characterised by initially a large mass of the missile due to the fuel load, and an exhaust plume which can be easily detected using infrared (IR) sensors (Postol, 2001 [30]). The boost phase can take up to three minutes where maximum accelerations up to 10 $^{m}/_{s^2}$ can be achieved, depending on the type. Note that the acceleration increases significantly during the boost phase, since the mass of the BM decreases. After burnout, the BM enters its midcourse, taking the longest duration of the trajectory (John C. Lonnquest, 1996 [16]) (Figure 2.1, #5-#6). The terminal phase is the last portion of the flight, where most current defensive measurements are deployed (#7-#8).

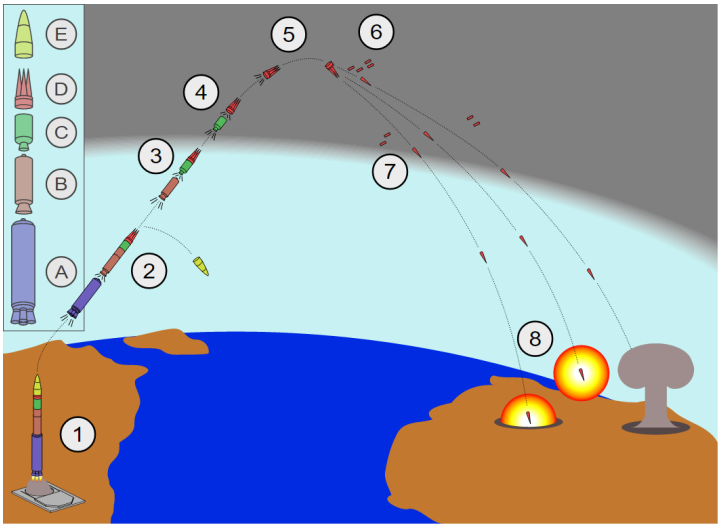

Source: https://nationalinterest.org/
Figure 2.1: Ballistic Missile Flight Phases

2.1.2. Current Ballistic Missile Defence

BM defence became operational during the late 1950's, when the Nike-Zeus system was developed (Parsch, 2001 [28]). It was a ground based missile, which accelerated towards the incoming target, using an initial thrust generated by a fast-burning booster. It was equipped with a nuclear warhead, which exploded in proximity of the threat, since guidance was not sufficiently accurate to aim for penetration of the target. Tracking, as well as guidance, where provided by ground based computers. As guidance algorithms evolved, warheads of BM defence systems could decrease in size and weight due to a decreasing miss distance, which resulted in an increased amount of available fuel in the missile. This continued until the warhead was completely omitted, resulting in hit-to-kill missiles such as the Terminal High Altitude Area Defense (THAAD), which maximises its range for interception of BMs in their coast phase (Yingbo and Yong, 2010 [44]). Control is commonly performed using commanded guidance, where a ground station tracks its shot missile and the target, and transmits new control commands to the missile.

2.1.3. Boost Phase Interception

The boost phase of the BM promises a potential opportunity for interception, due to its initially low velocity, its relatively large mass and the exhaust plume, which could be detected from 100's of kilometres away, depending on the circumstances (Halswijk and Benoist, 2014 [10]). The disadvantages of Boost Phase Interception (BPI) is that the launch platform must be close to the actual BM launch site, contrary to the defence systems based at the homeland for the terminal phase. Therefore, launch possibilities are limited to sea-based or air-based. A theoretical study has been performed, where a BM is intercepted using the ship-launched, multi-stage, warhead equipped SM-6 missile (Lukacs, 2006 [20]). Theoretically, this proved to be a success, but the difficulty of predicting the trajectory of the target was not included. Also, since the missile is launched from a ship, the target is to be intercepted in vicinity of the sea, which would not always be possible. Another study of the same work group was conducted, to adjust the direct flight optimisation routine to be applied for the NCADE (Lu, 2011 [19]). This was possible to do so, but again only theoretically, with all the future states of the BM known to the guidance algorithm. The launch platform was chosen to be an Unmanned Aerial Vehicle (UAV), which could be deployed above enemy territory.

2.2. Kalman Filter Tracking

At TNO, a study has been conducted to find a BM boost phase tracking algorithm (Riegman, 2016 [31]). For this, a Kalman Filter (KF) is applied, which is able to filter disturbances in the measurements. A KF predicts the future state of the object to be tracked, using a linear relation between the states. It then proceeds to perform the measurement and compares the two states together, of which the error can be determined. This is then used to set the Kalman gain, which is used to weigh the combined results of the measurement and the prediction. This way, if the measurement turns out to be noisy, the values for the prediction are weighted

more. If the sensor data is accurate, the filter will rely increasingly on the measurement. This filter is therefore continuously improving itself, making it light in calculations and versatile. States which are not directly measured can be derived. The KF made at TNO, used for the tracking of BMs in their boost phase, is extended to handle non-linear state relations (Riegman, 2016 [31]). It is known as an Extended Kalman Filter (EKF), which operates by continuously updating the Jacobian of the states. The filter is further discussed in Chapter 4.

2.3. Trajectory Optimisation

A common guidance algorithm for air-to-air missiles is proportional navigation (Nesline and Zarchan, 1981 [25]). However, due to the uncertain target trajectory prediction and the propellant system of the NCADE, a trajectory optimisation algorithm is required for interception. Previous studies performed to investigate the feasibility of BPI employed trajectory optimisation algorithms for the guidance ((Lukacs, 2006 [20]) and (Lu, 2011 [19])). When the optimisation problem has been defined, the problem is solved by either indirect or direct methods (Hargraves and Paris, 1987 [11]).

2.3.1. Proportional Navigation

Proportional Navigation (PN) has become widely implemented in missiles which intercept moving targets (Janus, 1964 [15]). The advantages are the simplicity of operation, and the ease of making specified adjustments, without large hardware changes (Nesline and Zarchan, 1981 [25]). PN operates by keeping the observation angle between the missile and the target constant (Figure 2.2). The control commands required to attain this angle are proportional to the change of the view angle $\dot{\lambda}$, reducing the algorithm to one equation (Equation 2.1). This algorithm considers the velocity of both the missile and the target.

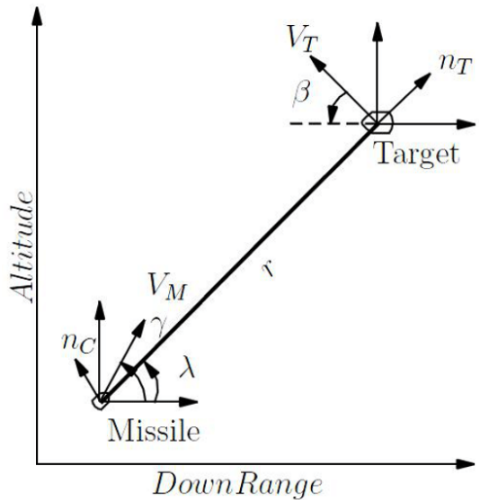

Source: Dipankar Deb, 2012
Figure 2.2: Proportional Navigation (2D)

$$n_c = N' V_c \dot{\lambda} \tag{2.1}$$

2.3.2. Trajectory Optimisation Application

Flight trajectory optimisation is aimed to find a control vector $\mathbf{u}(t)$, which minimises a certain performance index (J) (Equation 2.2). In this equation, the states are noted by $\mathbf{x}(t)$. A performance index could for example be time or fuel consumption. The solution to the problem shows the control inputs which must be applied to perform the optimum flight. Constraints are applied to bound the control deflections which are possible by the device which performs the flight, and physical limitations of the flight itself. The boundary conditions describe the states of the device at the start and end of the flight.

$$J = \Phi(\mathbf{x}_f, t_f) + \int_{t_0}^{t_f} L(\mathbf{x}(t), \mathbf{u}(t), t)\, dt \tag{2.2}$$

subject to the governing physical properties of the problem:

$$\dot{\mathbf{x}} = \mathbf{f}(\mathbf{x}(t), \mathbf{u}(t), t)\ ; t_0 \leq t \leq t_f$$

2.3.3. Indirect Trajectory Optimisation Methods

Indirect methods for flight optimisation use calculus of variations to solve the control problem. Indirect methods are different from direct methods, since the Hamiltonian is derived from the original problem (David A. Benson and Rao, 2006 [7]). Instead of finding the optimum control vector $\mathbf{u}(t)$ directly, the states and adjoint (λ) are being solved. First, the objective function is rewritten as (Equation 2.3)

$$J = \Phi[\mathbf{x}(t_f), t_f] + \int_{t_0}^{t_f} L(\mathbf{x}(t), \mathbf{u}(t), t) + \lambda^T(t)(f(\mathbf{x}(t), \mathbf{u}(t), t)\,dt \tag{2.3}$$

The Hamiltonian is defined as (Equation 2.4):

$$H(\mathbf{x}, \mathbf{u}, \lambda, t) = \lambda^{\mathbf{T}}(t) f(\mathbf{x}(t), \mathbf{u}(t), t) + L(\mathbf{x}(t), \mathbf{u}(t), t) \tag{2.4}$$

In this equation, λ is the adjoint equation. The Hamiltonian is to be minimised for the solution of the problem, which occurs if the necessary condition is met (Equation 2.5).

$$\frac{\partial H}{\partial \mathbf{u}} = 0, \;\; t_0 \leq t \leq t_f \tag{2.5}$$

The found solution is an actual minimum and not for example a saddle point, if the Legendre-Clebsch condition is met (Equation 2.6) (Visser, 2014 [40]):

$$\frac{\partial^2 H}{\partial \mathbf{u}^2} \geq 0 \tag{2.6}$$

With the found Hamiltonian being a minimum, the related states and control functions are determined (Equation 2.7).

$$\begin{aligned} \dot{\mathbf{x}}(t) &= \partial_\lambda^T H(\mathbf{x}(t), \mathbf{u}(t), \lambda, t) \\ \dot{\lambda}(t) &= -\partial_x^T H(\mathbf{x}(t), \mathbf{u}(t), \lambda, t) \end{aligned} \tag{2.7}$$

Indirect methods demand a considerable mathematical derivation of the problem, where non-linear phenomena worsen the calculations. If an initial condition changes, the complete derivation is to be redone. Also, increasing the constraints results in increasing the complexity of the problem, especially when non-linearities are introduced (David A. Benson and Rao, 2006 [7]). The advantage however is the insight the derivation provides, compared to the direct methods where a NLP solver is applied.

Indirect methods are theoretically successfully used for the interception of BM's in their boost phase (Guelman and Golan, 1995 [9]) and (Huang and Zhu, 2001 [12]). The performance index in both papers is the minimisation of the energy, with the interception location enforced as a boundary condition. Minimising the energy usage ultimately increases the energy which can be delivered to the BM, increasing the chances for a kill when hit. Unfortunately, in both applications of indirect methods, the location of the BM is known to the interceptor beforehand, so the mathematical derivation is not updated when the Predicted Interception Point (PIP) updates.

2.3.4. Direct Trajectory Optimisation Methods

Direct methods are called as such, since the performance index of the problem is directly calculated using candidate solutions of the actual problem, instead of using the Bolza form (Hargraves and Paris, 1987 [11]). Using NonLinear Programming (NLP), the performance index is to be minimised. The candidate solution is expressed with basis functions, resulting in a vector of coefficients. The gradient of the performance index is found using this vector, meaning that the impact of the change on both the performance index and the constraints is evaluated. After each iteration, a new candidate solution is attempted, until J is minimised and the constraints are met. A candidate solution can consist of a vector describing the control functions, which defines a shooting method. Inverse kinematics applies a vector of states. The third method is collocation, where both controls and states are included in the candidate solution.

Shooting Methods

A shooting method applies control functions through the problem, describing the control settings of the missile at all time nodes. The resulting trajectory is calculated using numerical integration. This results in the calculation of performance index J, which is to be minimised using a NLP algorithm. Shooting methods are relatively easy to implement and it is convenient to generalise problems (Hargraves and Paris, 1987 [11]). The shooting method is relatively slow compared to other direct methods, since integration is performed at one time step at a time. Also, since the states are dependent on the controls, the constraints are evaluated after the integration, further increasing computation time.

Inverse Kinematics
The inverse Kinematics method applies candidate solutions in form of set of states, and then proceeds to find the controls required to achieve those states (Nicolas Petit and Murray, 2001 [27]). Similar to the shooting method, a NLP algorithm minimises J. The constraints of the maximum controls are evaluated after the control functions are found, and path constraints are imposed directly to the candidate solution. Inverse kinematics become complex to implement, if non-linear effects of controls become part of the optimisation problem, which is for example the case with the 2-stage NCADE.

Collocation
Instead of applying parametrisation on either the controls or the states, collocation uses candidate solutions of both. Using equality constraints, the defect between the controls with the resulting acceleration and the candidate state is forced to zero. The optimum solution must therefore comply with both collocation constraints and physical constraints. Using this method, a larger portion of the solution space can be explored, evaluating non-feasible solutions. Integration can be performed over the whole time domain simultaneously, in contrast to the shooting method, where integration starts at the start conditions of the flight. Therefore, with collocation, the optimum solution is found sooner, but it takes a more complex implementation.

2.4. Air-to-Air Boost Phase Interception Developments

In theory, boost phase interception has been proven to be possible, given a certain target in the near future. The result is a guidance algorithm for either surface or air launched missiles. However, the main problem putting BPI into practice is the tracking procedure. The uncertainty of the target trajectory prediction, as a result of the complex trackable states of the threat, has not been implemented in a guidance algorithm to the best knowledge of the author. Fly-out models, simulations of real-time flights of missiles, or even actual implementation can therefore not be made.

3

Air-to-Air Boost Phase Interceptor Model

A weapon system for the purpose of air-to-air Boost Phase Interception (BPI) is not yet operational. One weapon system in development is the Network Centric Airborne Defense Element (NCADE), which will be modelled in this thesis as an example. The NCADE resembles the AIM-120D AMRAAM, which has the same outer shape and attachment points for suspension to the aircraft. The most notable difference is the two stage layout, which will be elaborated and analysed in this Chapter. To be able to calculate the optimum trajectory, the Equations Of Motion (EOM) of the missile are required. Since a prototype has not emerged yet, assumptions are made concerning aerodynamics, engine performance and control systems. Where possible, images of the NCADE are used, and the remainder of the required assumptions is made by examining other missile systems with comparable layouts. This Chapter provides the reasoning behind the assumptions. All results are summarised in Appendix A and B.

3.1. Equations of Motion

The EOM are required to calculate the flight path of the NCADE. First, a set of assumptions is made to reduce calculation and modelling load, without compromising the final result. Next, the reference frames are elaborated, which relate the location of the BM to the control inputs which must be applied for the NCADE to intercept. Using the Free Body Diagrams (FBD), the governing forces can be expressed.

3.1.1. Model Assumptions

The following assumptions have been made:

- Rigid Body
- Zero control lag
- Absent atmospheric disturbances
- Perfectly round earth
- ISA atmospheric conditions (1976)
- Zero roll angle

The first assumption is the infinite structural stiffness of the missile system, meaning that no aeroelastic effects occur. If any, these are assumed to be accounted for automatically. The control lag is assumed to be zero. The NCADE would most likely have a second order control system, featuring rise time and overshoot. These two effects are assumed to compensate each other, so the net control output equals the control input. Also, if this is not the case, the rate of a control deflection is assumed small compared to the total flight time. The disturbances in the atmosphere, such as wind, are discarded in this research. The roll angle is assumed to remain zero, with the missile flying with control surfaces pointed horizontally and vertically, so the y-axis of the body frame is always oriented horizontally. If the missile, experiences a roll angle disturbance, the guidance computer of the missile is assumed to accommodate the resulting error automatically. Since the moment of inertia in roll direction is small due to the missile's shape, the control deflection magnitudes are assumed negligible, and are therefore not modelled. This is a valid assumption for missiles with two

symmetry axes in the cross section, which is the case for the NCADE. The advantage is the reduced calculation effort.

3.1.2. Reference Frames

There are four reference frames used in the model, being the Earth Centred, Earth Fixed (ECEF) frame to relate the BM to the NCADE and the launch platform, the body frame of the missile, and the aerodynamic frame of the missile. The tracking procedure requires an adapted North East Down (NED) frame, explained below.

Earth Centred, Earth Fixed Frame

The locations between the target, the launch vehicle and the missile are connected using the ECEF frame. The positive Z-axis is located through the North Pole, with the X-axis through the Greenwich meridian (Figure 3.1). This frame is convenient for use in combination with a round (spherical or ellipsoid) earth model, a minimum requirement for the navigation of BMs.

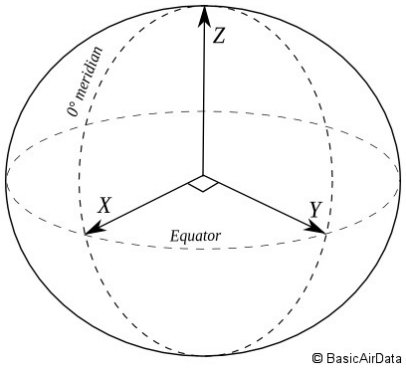

Source: https://www.basicairdata.eu/
Figure 3.1: Earth Centred, Earth Fixed Frame

Body Fixed Reference Frame

The normal force, the axial force and the control forces of the missile itself are at first expressed in the body fixed reference frame. The applied software, 'PRODAS,' used to define aerodynamic coefficients, provides normal force coefficients for this reference frame. Also, the control system of the sustainer exerts control forces perpendicular to the body. The X-axis points through the nose, and the Z-axis points downwards. The Y-axis is perpendicular to the vertical symmetry axis. To rotate from the body frame to the aerodynamic frame, α and β are required. Note that the roll angle is omitted, since it is assumed to be always zero.

Aerodynamic Reference Frame

Integration of the forces on the missile body have influence on the magnitude and direction of the velocity vector. This requires a velocity frame, which is also applied to define the angle of attack (AoA) α and sideslip angle β (Figure 3.2). The X-axis is oriented positively along the missile's velocity vector, with the Z-axis situated in the vertical symmetry axis, perpendicular to the velocity vector. The Y-axis points right.

Ballistic Missile Tracking Frame

The BM is to be tracked and its trajectory is defined in the ECEF frame. For the filtering process to work best, a rotated North East Down (NED) frame is defined, which rotates about the z-axis, using the azimuth χ as rotation angle (Figure 3.3) (Riegman, 2016 [31]). The launch location of the BM is estimated in the ECEF frame. The azimuth is assumed to be constant for the boost phase, since a BM commonly rotates in the first seconds of its launch, and retains its azimuth to reach its destination. The x axis of the NED frame is aligned with the velocity vector. This decreases the amount of states to be filtered, increasing the performance of the filter. The location of the target is transformed towards the ECEF frame, for which it requires the BMs origin, which is the first measurement in the ECEF frame. Using the filtered states of the target, the trajectory prediction is performed, again in the ECEF frame.

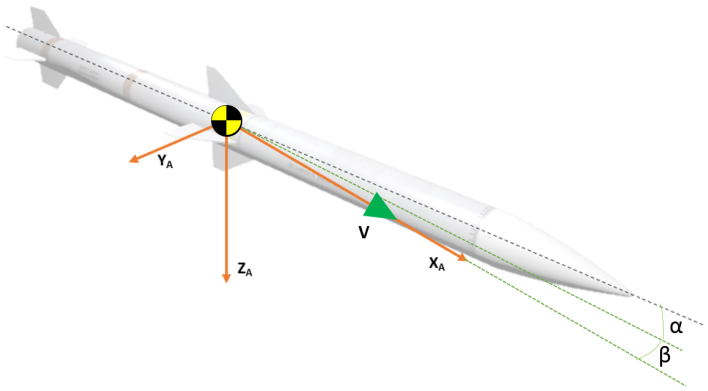

Figure 3.2: Aerodynamic Reference Frame

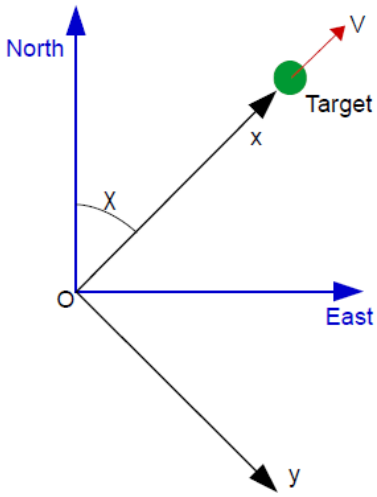

Source: Riegman, 2016
Figure 3.3: North East Down Reference Frame

3.1.3. Free Body Diagrams

The EOM are derived using free body diagrams, where acting forces are represented. In Figure 3.4, the pitching motion is described for the first stack from a side view and Figure 3.5 shows the turn from a top view. The first stack consists of the two stages, being the 1st boost stage and the 2nd sustain stage. In these Figures, V is the velocity, N is the normal force perpendicular to the body, T is the thrust, A is the axial force and W is the weight. E and R are the aerodynamic forces generated by the fins, directed in negative z direction and y direction respectively. The Centre of Gravity (CG) is shown in yellow, the Centre of Pressure (CP) where the normal force of the wings and the body combined is originated is shown in blue. The path angle with the horizon is shown as γ, and the angle between the body axis and the velocity vector is the AoA α. The second stage is not shown, as the final FBD used are 3DOF instead of 6DOF.

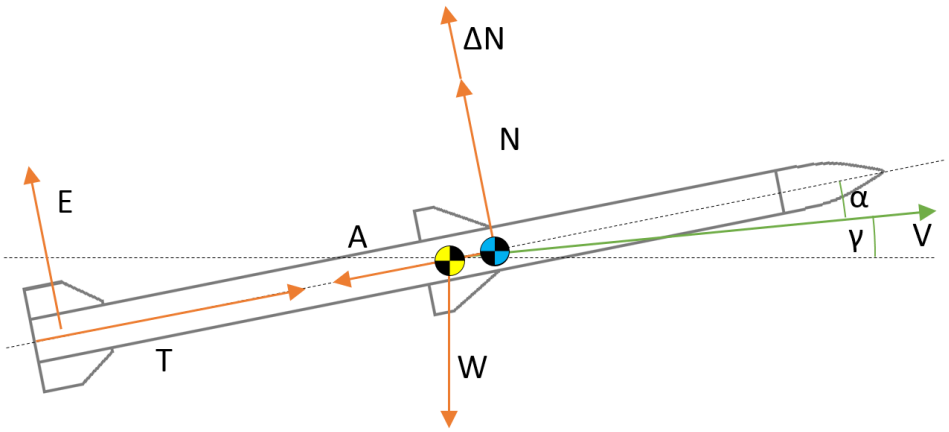

Figure 3.4: Free Body Diagram of the 1^{st} and 2^{nd} stage, side view, 6DOF

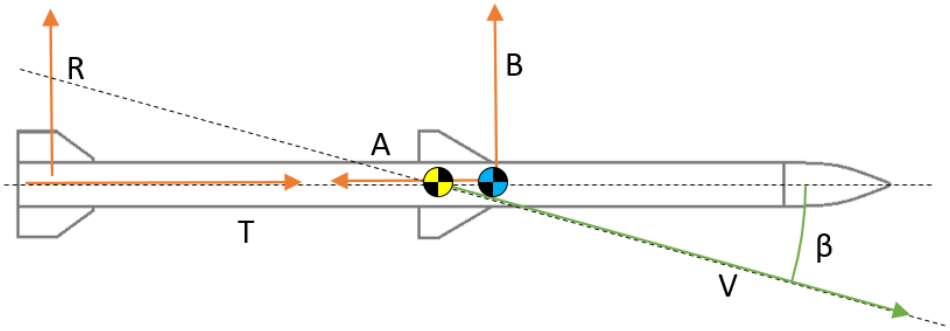

Figure 3.5: Free Body Diagram of the 1^{st} and 2^{nd} stage, top view, 6DOF

To reduce complexity of the model, the EOM are expressed in the 3DOF point mass model, which will also be used for the trajectory calculations. The CP is merging with the CG, which requires assumptions about automatic control forces in the model, further elaborated in Section 3.4. This causes the moments to become zero, so E and R are discarded, for which is assumed that the fin is designed and automatically controlled such that the CP remains at the CG (Figure 3.6). This hold also for the second stage, where the non-controllable wings and the thrust vectoring generate correcting moments (Figure 3.8). During the flight of the first stack, an AoA is attained to provide lift, and a control input can be set to either increase or decrease the AoA. This results in an increased normal force, shown as ΔN in Figure 3.6. The sustainer operates differently, by directly generating a control force D_N using its DACS, explained in Subsection 3.1.4.

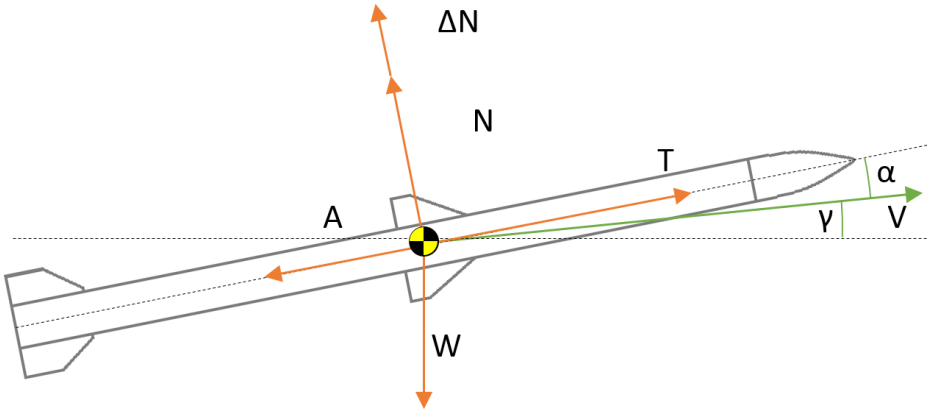

Figure 3.6: Free Body Diagram of the 1^{st} and 2^{nd} stage, side view, 3DOF

The first stack turns by generating a side slip by controlling the fins (Figure 3.7). This generates a sideways directed force B. When the turn has been conducted, the control fins automatically decrease β to continue flight in the intended heading.

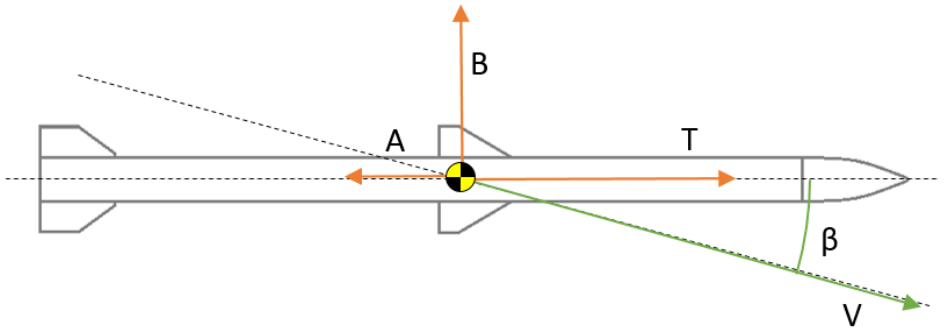

Figure 3.7: Free Body Diagram of the 1^{st} and 2^{nd} stage stage, top view, 3DOF

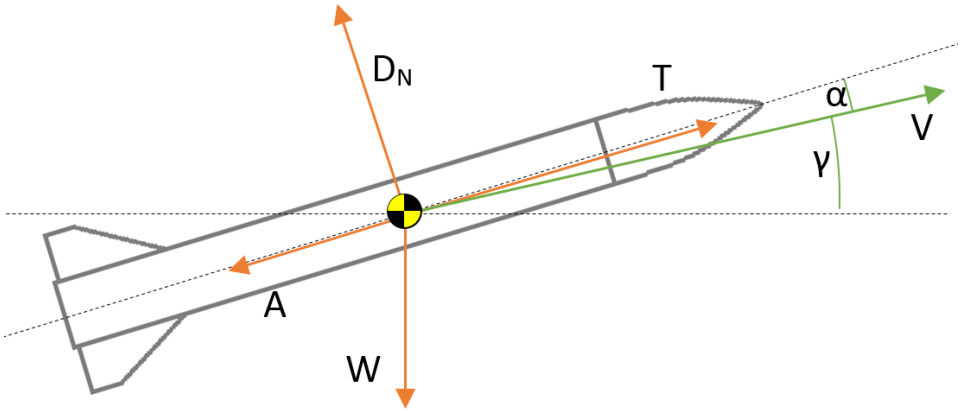

Figure 3.8: Free Body Diagram of the 2^{nd} stage, side view, 3DOF

The second stage differs from the first stage as it is able to generate a side ways directed force directly at the centre of gravity using the DACS (Figure 3.9). The wings or the thrust vectoring decrease the resulting β, so only the DACS deflection is modelled. Note that like the normal force, D_B is directed perpendicular to the missile's body.

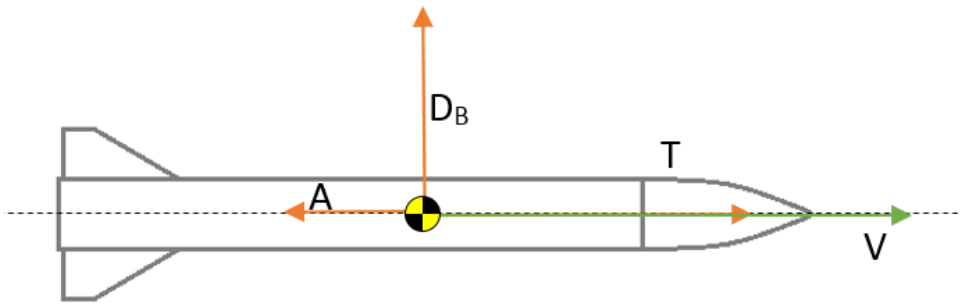

Figure 3.9: Free Body Diagram of the 2^{nd} stage, top view, 3DOF

3.1.4. Governing Forces

The missile is subject to aerodynamic and gravitational forces, and it is able to generate control forces. The sum of those forces are used to calculate the resulting accelerations. The accelerations are integrated to calculate the velocity, after which the position is calculated to describe the motion of the missile.

Normal Force

The normal force is generated by the body, the wings and the control fins. The airfoils are assumed to be symmetrical. Because the roll angle retains zero, the normal vector is opposed to the gravity, bearing the path angle γ and AoA α in mind. Due to the nature of the used empirical software, the normal force is chosen over lift (Equation 3.1). In this equation, ρ is the density, C_N the normal coefficient, which is dependent on both α and Mach number M. Note that for missiles, the reference surface S is defined as the frontal area.

$$N = \frac{1}{2}\rho V^2 C_N(\alpha, M)S \tag{3.1}$$

Linearising the normal coefficient is not practical, due to its dependency on Mach number which differs greatly. The Mach number ranges from subsonic levels to about Mach 4 in short periods of time.

Axial Force

The axial force A is also determined by a coefficient (Equation 3.2). It is directed perpendicular to the normal force, opposite of the velocity vector.

$$A = \frac{1}{2}\rho V^2 C_A(\beta, M)S \tag{3.2}$$

Thrust

Thrust is generated by the booster and the thruster of the second stage. The thrust profile of the booster depends on the burn grain and is therefore not part of the controls (Equation 3.3). The sustain phase is however able to modulate the amount of propellant going into the thruster, which makes the thrust variable during flight.

$$T = (I_{sp} g \dot{m}) dt YOLO \tag{3.3}$$

Turning

As described, an angle of attack or sideslip angle is applied in the boost phase to control the path angle or heading respectively. The difference in angle of attack is therefore added to the existing angle of attack, expressed with the normal force (Equation 3.1). The side force B is defined separately (Equation 3.4). Note that the normal coefficient is used, due to the symmetrical shape of the missile and its steady roll angle. The value of the coefficient depends on β and M.

$$B = \frac{1}{2}\rho V^2 C_N(\beta, M)S \tag{3.4}$$

During the sustain phase, turning forces are applied by the DACS system, which exhausts are located around the centre of gravity. These exert forces which can be added to the EOM, being D_N in the aerodynamic reference frame Z direction for a pitching motion, and D_B in the y direction for yawing. This is equal to the magnitude in the body frame, as the sideslip angle and the angle of attack are zero. Correcting moments are generated, by either the thrust vectoring which provides a sideways force, or by the aft wings which will encounter the sideslip angle, and this results in a moment and thus a decrease of the sideslip. The two systems are present, for when altitudes are reached in which the density is too low for the wings to be effective.

Weight

The weight is always directed from the point mass towards the centre of the earth, or in positive z direction in the velocity frame. When a non-zero path angle γ is encountered, this gravity is split into an X and a Z component.

$$W = m \cdot g \tag{3.5}$$

With g being assumed constant at $9.80665\,{}^{m}/_{s^2}$. One could argue correctly that the gravitational pull decreases with altitude, but the change of 1% per 32 km altitude is deemed insignificant. The mass of the NCADE is not fixed, but propellant is consumed in rates which cannot be neglected. First, during the boost phase, the mass flow is integrated and the result is subtracted from the initial launch mass m_0 (Equation 3.6). Note that the mass flow of solid propellant is assumed constant.

$$m = m_0 - \int_0^{t_{boost}} \dot{m}\,dt = m_0 - \dot{m}\int_0^{t_{boost}} dt \tag{3.6}$$

During staging, the empty boost stack is subtracted in an infinite small amount of time. Next, the monopropellant consumption is subtracted from the sustainer mass m_1 (Equation 3.7). The monopropellant is used by the thruster and the DACS system in two directions. Since both the DACS and thruster are all controllable, the control input u is included in the calculation, where subscript s defines the sustainer's thrust, and D the DACS system.

$$m(t) = m_1 - \int_{t_{boost}}^{t_f} |\left(u_s + u_{D_N} + u_{D_B}|\right) dt \tag{3.7}$$

Summation of all Forces in the EOM
The purpose of the EOM is to determine at each time-node the governing forces and the resulting accelerations (Equation 3.8).

$$F = \frac{d}{dt}(mV) \tag{3.8}$$

As stated before, the summation of forces is performed in the velocity frame. This means that rotations about α and β are included. The rotation matrix from the body frame towards the velocity frame about the **z** axis, when only considering sideslip angle β, is defined as (Equation 3.9):

$$\mathbb{T}_\beta = \begin{bmatrix} \cos(\beta) & \sin(\beta) & 0 \\ -\sin(\beta) & \cos(\beta) & 0 \\ 0 & 0 & 1 \end{bmatrix} \tag{3.9}$$

The transformation matrix about the **y**-axis, when only considering the AoA, is defined as (Equation 3.10):

$$\mathbb{T}_\alpha = \begin{bmatrix} \cos(\alpha) & 0 & \sin(\alpha) \\ 0 & 1 & 0 \\ -\sin(\alpha) & 0 & \cos(\alpha) \end{bmatrix} \tag{3.10}$$

When first rotating for α, and then for β gives the final transformation matrix $\mathbb{T}_{BA}$ (Equation 3.11). The roll angle is assumed to be zero at all cases, so no transformation matrix for that angle is required.

$$\mathbb{T}_{BA} = \begin{bmatrix} \cos(\beta)\cos(\alpha) & \sin(\beta) & \cos(\beta)\sin(\alpha) \\ -\sin(\beta)\cos(\alpha) & \cos(\beta) & -\sin(\beta)\sin(\alpha) \\ -\sin(\alpha) & 0 & \cos(\alpha) \end{bmatrix} \tag{3.11}$$

The weight is rotated using the path angle, as gravity always points towards the centre of the earth. Parallel to the velocity, the acceleration is determined, based on four governing forces. The axial force is a result of both C_{A0}, the α component and the β component. The positive direction is along the velocity vector, as shown in the aerodynamic reference frame (Figure 3.2). The side force only consists of the result of control inputs, either β in the boost phase or the direct control force D_B generated by the DACS during the sustain phase. Note that the sideslip angle is zero in the sustain phase, either due to the aerodynamic wings or the thrust vectoring. The summation of forces in the **z**-direction is perpendicular to the velocity vector. It consists of the normal force and the opposing gravity. The pitch angle is controlled by a force in the **z**-direction, resulting from the α control in the boost phase, or a deflection of the DACS, noted as D_N. The deflection of α leads to either an increase or decrease of the normal force. D_N could either be positive or negative, and is positive when directed towards the earth. All body forces combined ($\mathbf{F}^B$) are summarised below (Equation 3.12):

$$\begin{bmatrix} \mathbf{F}_X^b \\ \mathbf{F}_Y^b \\ \mathbf{F}_Z^b \end{bmatrix} = \begin{bmatrix} T - A - W\sin(\theta) \\ D_B + B \\ (-N + D_N) + W\cos(\theta) \end{bmatrix} \tag{3.12}$$

The forces are expressed in the aerodynamic frame, so that the resulting velocity can be determined. Performing the transformation results in:

$$\begin{bmatrix} \mathbf{F}_X^a \\ \mathbf{F}_Y^a \\ \mathbf{F}_Z^a \end{bmatrix} = \mathbb{T}_{BA} \begin{bmatrix} \mathbf{F}_X^b \\ \mathbf{F}_Y^b \\ \mathbf{F}_Z^b \end{bmatrix} = \begin{bmatrix} \cos(\beta)\cos(\alpha)\mathbf{F}_X^b - \sin(\beta)\cos(\alpha)\mathbf{F}_Y^b - \sin(\alpha)\mathbf{F}_Z^a \\ \sin(\beta)\mathbf{F}_X^b + \cos(\beta)\mathbf{F}_Y^b \\ \cos(\beta)\sin(\alpha)\mathbf{F}_X^b - \sin(\beta)\sin(\alpha)\mathbf{F}_Y^b + \cos(\alpha)\mathbf{F}_Z^b \end{bmatrix} \tag{3.13}$$

Note that the thrust misalignment due to α cannot be neglected, since missiles are generally capable of relatively high angles of attack. Also, the thrust to weight ratio is relatively high, so the magnitudes of the components would not be negligible.

The velocity vector is defined by its magnitude V, the path angle γ and the heading Ψ. The magnitude V changes due to the forces in the **x** direction of the aerodynamic frame (Equation 3.14). The mass changes through time cannot be neglected, so they are noted as a function of time (Equations 3.6 and 3.7)

$$\dot{V} = \frac{F_X^a}{m(t)} = \frac{g}{W(t)}\mathbf{F}_X^a \tag{3.14}$$

The force changing the path angle direction is generated by either a change in the normal force in the first stack, or a force of the DACS in the second stage, generating forces in the **z** direction (Equation 3.15).

$$\dot{\gamma} = \frac{1}{V}\cdot\frac{F_Z^a}{m(t)} = \frac{g}{W(t)V}\mathbf{F}_Z^a \tag{3.15}$$

To change the heading, the same method as changing the path angle is required, by now exerting a force in **y** direction of the aerodynamic frame (Equation 3.16).

$$\dot{\Psi} = \frac{1}{V}\cdot\frac{F_y}{m(t)} = \frac{g}{W(t)V}\mathbf{F}_Y^a \tag{3.16}$$

Integration is performed using an explicit Euler integration method, giving the following set of equations for the changes in the velocity vector (Equations 3.17 -3.19). In these equations, the time step is not fixed, as different discretisation methods are possible for the different stages.

$$V_{i+1} = V_i + \dot{V}_i \cdot dt_i \tag{3.17}$$

$$\gamma_{i+1} = \gamma_i + \dot{\gamma}_i \cdot dt_i \tag{3.18}$$

$$\Psi_{i+1} = \Psi_i + \dot{\Psi}_i \cdot dt_i \tag{3.19}$$

Since body frame accelerations are used, it is logical to express the position change in the local ENU frame (Equations 3.20-3.22), whereafter the position in ECEF is calculated. For this action, a validated off-the-shelf converter is used. Since both the velocities V_i and V_{i+1} are known, the trapezoidal rule is applied for integration.

$$\dot{E} = \frac{V_{i+1}+V_i}{2}\cdot\sin\left(\frac{\gamma_{i+1}+\gamma_i}{2}\right) \tag{3.20}$$

$$\dot{N} = \frac{V_{i+1}+V_i}{2}\cdot\cos\left(\frac{\Psi_{i+1}+\Psi_i}{2}\right) \tag{3.21}$$

$$\dot{U} = \frac{V_{i+1}+V_i}{2}\cdot\sin\left(\frac{\Psi_{i+1}+\Psi_i}{2}\right) \tag{3.22}$$

Forward Euler integration is then applied, to add the position changes to the current location. Off-the-shelf validated axis rotation scripts are applied to convert the position changes from the ENU reference frame to ECEF coordinates (TNO, **(year?)** [38]).

3.2. Aerodynamics

As discussed, the required coefficients resulting from the EOM are the normal coefficient and the axial force coefficient. These coefficients depend on both the experienced angle of attack or sideslip angle, and the Mach number. To obtain all required coefficients, the software tool PRODAS is used. PRODAS requires the aerodynamic shape of the missile, for which an estimation has been performed, since not all data is available.

3.2.1. Aerodynamic Coefficient Analysis Software

The applied software package is Projectile Rocket Ordinance Design & Analysis System, Version 3 (PRODAS V3). The software is commonly applied for any projectile design, and handles aerodynamic analysis up to Mach 8 (Arrow-Tech, 2013 [2]). The manufacturer of the software: Arrow Tech, apply the Missile DATCOM datasheet, which means that empirical methods are applied to achieve an aerodynamic prediction of a preliminary missile design (Daniel J. Lesieutre, 2002 [6]). Extensive fin-on-body data of the so-called 'Triservice

systematic fin-on-body force and moment database' is therefore used, from which data is obtained and interpolated for the applied design. Missile DATCOM also includes extensive vortex modelling. A comparison study showed that normal coefficients can be predicted fairly consistent to an angle of attack of 25^o, after which the software starts to deviate from the used experimental data (Lesieutre, 2017 [18]). PRODAS itself provides the coefficients as function of the angle of attack, where the normal coefficient is calculated using Equation 3.23, and the The axial force coefficient is determined using Equation 3.24. C_{Na}, C_{X0} and C_{X2} are outputs of the software.

$$C_N = C_{Na} \sin \alpha \tag{3.23}$$

$$C_A = C_{X0} + C_{X2} \sin(\alpha^2) \tag{3.24}$$

3.2.2. Aerodynamic Shape

PRODAS requires an aerodynamic outer shape of the missile system, to apply the empirical methods resulting in aerodynamic coefficients. The complete set of dimensions of neither the NCADE nor the AMRAAM is published, so assumptions are made on the dimensions of the AMRAAM, and applied for the NCADE. This ultimately comes down to performing measurements and estimations of ratios found on pictures (Figures 3.10 and 3.11). The design of the NCADE has not been finalised, so any deviations are unavoidable. Known values for the length and width of the AMRAAM are respectively $3.66m$ and $0.1778m$. The wingspan of the AMRAAM AIM-120D version, with clipped wings, measures $482mm$. Unknowns are the length of the second stage and the remaining dimensions of the fins, for which assumptions have been made. These assumptions are based on published images as shown in Figures 3.10 and 3.11, where ratios have been determined and scaled to dimensions. The results of the dimension analysis are shown in Figures 3.12 and 3.13. Measurement specifics are included in Appendix A.

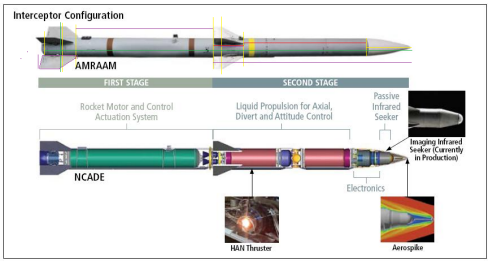

Source: http://missiledefenseadvocacy.org
Figure 3.10: NCADE and AMRAAM Comparison

Source: http://tr.eyeni.info/
Figure 3.11: AMRAAM Fin Close-up

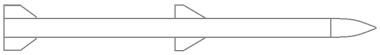

Figure 3.12: Resulting Outer Shape of the First Stack

Figure 3.13: Resulting Outer Shape of the Second Stage

3.2.3. Aerodynamic Coefficients

The aerodynamic coefficients of interest are the normal coefficient C_N and axial coefficient C_A. Note that the sideslip coefficient values of C_B are equal to the normal coefficient due to the symmetry of the missile. In Figure 3.14, the normal coefficient and the axial coefficient of the first stack are plotted, the remainder of the coefficients are included in Appendix B.

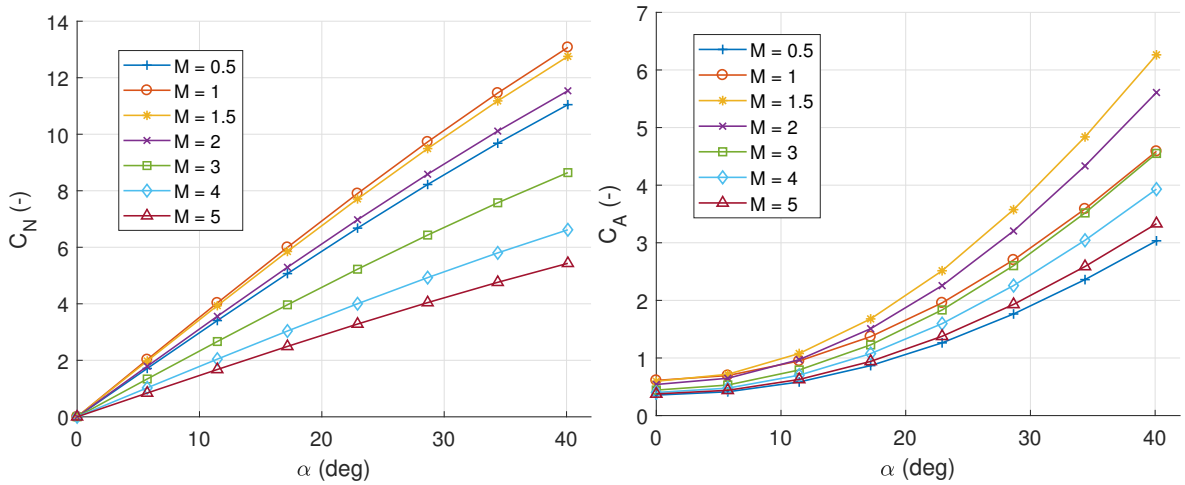

(a) Normal Force Polars, at Various Mach Numbers

(b) Axial Force Polars, at Various Mach Numbers

Figure 3.14: Aerodynamic Coefficient Plots, 1st stack

For the lift polars, it can be observed that with increasing Mach number, the normal coefficient decreases. A stall does not seem to be included in the methods used by PRODAS, as the coefficient increases at the highest angles of attack. The values are relatively high in magnitude, for example compared to commercial aviation, since PRODAS makes use of the frontal surface area of the projectile. Comparing the coefficients before and after separation of the first stage, the second stage has lower values for its aerodynamic coefficients, since the frontal surface area does not change during staging, but the lifting surface decreases. The polars cross the origin of the graph, since symmetrical lifting surfaces are assumed. The axial coefficient polars show a quadratic shape, with a decrease when the Mach number increases. Notable is the coefficients at Mach 1 which have the highest values. This is explained by the transonic regime, where wave drag is highest. Figure 3.15 shows the C_N/C_A plot.

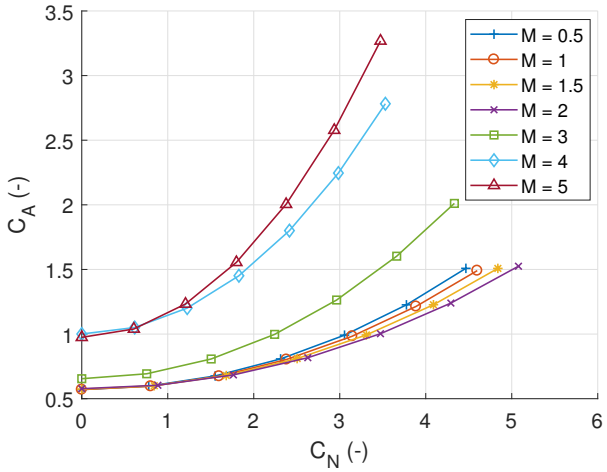

Figure 3.15: Normal Force / Axial Coefficient Plot, at Various Mach Numbers

3.3. Propulsion

The NCADE is a two-stage missile, with a solid booster as first stage for the initial acceleration, and a second stage which proceeds to penetrate the BM, for which it is called 'Kill Vehicle' (KV). The KV has a Divert and Attitude Control System (DACS), which is employed for control deflections, and four engines directed aft for propulsion. Both the DACS and the thrust generating thrusters make use of the same monopropellant tanks.

3.3.1. Propulsion of the Boost Stage

The AMRAAM is a single stage missile, with a solid booster to generate thrust. The grain of the booster exists of one fast-burning grain for the initial acceleration, and three slower burning grains. This way, a boost phase and sustain phase are distinguished. Together, the boost of the missile lasts about five seconds (Moore, 2011 [24]). Comparing the AMRAAM and the NCADE, one can observe that the booster of the NCADE is slightly shorter, since the missile consists of two stages (Figure 3.16b). The AMRAAM's electrical equipment takes a significant volume, which is assumed to be smaller in the NCADE, due to the difference in sensor equipment. Only one type of solid propellant burn grain is assumed to be present in the NCADE. The mass flow is estimated as 11.25 $^{kg}/_{s}$ (Halswijk and Benoist, 2014 [10]), and the I_{sp} is set as 250s, a high value for a solid booster, which is realistic for modern propellants. The thrust force is concluded as $2.76 \cdot 10^4 N$ (Equation 3.25). The thrust profile is assumed to be constant throughout the burn, which is a common assumption (Siouris, 2004 [35]). To put the thrust into perspective, the average acceleration in vacuum would be 22.4g. Note that the design condition is chosen at a certain altitude, which is assumed to be a convenient fighter aircraft cruising altitude for the purpose of patrol missions. For different altitudes, the I_{sp} will change, due to over/under expansion. The time window of the flight of the NCADE is small enough to discard the altitude for the performance of the booster.

$$F_T = I_{SP} \cdot \dot{m} \cdot g \tag{3.25}$$

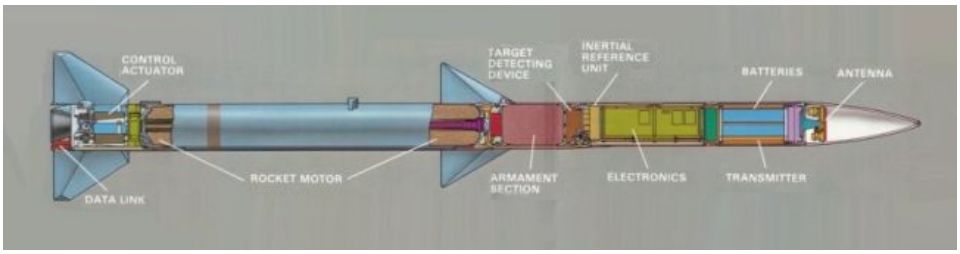

Source: Designation-Systems.Net
(a) AIM-120A AMRAAM

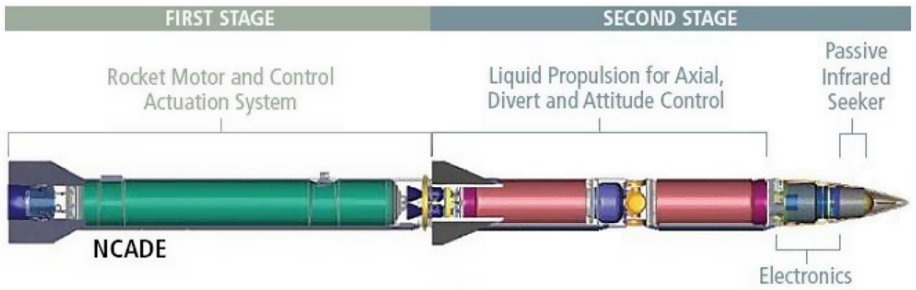

Source: GlobalSecurity.org
(b) NCADE

Figure 3.16: Comparison Between the AIM-120A AMRAAM and the NCADE's Propulsion System Systems

On the booster stage, the NCADE features control fins, and therefore thrust vectoring on the solid booster is assumed absent. The thrust vector is assumed to be perfectly parallel to the body.

3.3.2. Propulsion of the Sustain Phase

The sustainer operates using a HydroxylAmmonium Nitrate (HAN) based monopropellant (Tackett, 2006 [36]). HAN exists of an oxidiser, a fuel and an amount of water. Water is added for the purpose of being a solvent and controlling viscosity and combustion conditions, but worsens the performance of the propellant (Fukuchi B. Apollo, 2010 [8]). With a water weight component of 20%, the I_{sp} is estimated between 215s and 230s (Jankovsky, 1996 [14]) Because the NCADE is a new system in development, the I_{sp} is taken at the highest of this estimation range. For the tests in both [8] and [14], Laval nozzles have been used. The four thrusters of the sustainer of the NCADE are also modelled as Laval nozzles. With an estimated mass flow of 2.4 kg/s through all four thrusters, the total force maximises at $5.41 \cdot 10^3 N$ (Equation 3.25). The thrusters are throttable, so a lower thrust can be demanded from the engines.

3.4. Control Systems

This Section will complete the assumptions of the control system, in order to apply the EOM. The control system of the NCADE is divided into two stages. When the first stage is active, only the control fins at the rear are used. When separation occurs and the fins are discarded and control inputs are provided by the DACS on the second stage.

3.4.1. Control Surfaces on the Boost Stage

The control fin layout is assumed to be similar to the AMRAAM AIM 120D variant, featuring four non-moving wings located near the centre of gravity of the first stack providing lift, and four fins aft providing moment control and stability. The control fins of the NCADE are assumed to be all-movable, featured likewise on the AMRAAM. When the first stage drops, the fixed wings remain aft on the second stage, providing aerodynamic stability.

Control System Layout

For the first stack, the control fins of the booster are used to perform a so-called skid-to-turn movement of the NCADE. They provide a force perpendicular on the velocity vector, with a distance from the centre of gravity, resulting in a moment. This changes the sideslip angle β. As a result, a sidewise force is generated, which accelerates the missile into a turn. When the correct heading is achieved, the fins deflection is decreased and the sideslip angle is reduced. Pitching occurs in an equal manner, where α is either increased or decreased, which changes the magnitude of the normal force. This way, control inputs for the first stack are modelled by α and β.

Control System Performance

Investigation of the pictures of the design of the NCADE shows the same clipped wings as in the AIM-120D missile, designed to fit in small weapon bays of stealth fighters, limiting the spans of both the wings and the control surfaces to 0.45 m. The missile is assumed to be symmetrical. Airfoils of both wings and fins are assumed to be symmetrical. The limit of the control system depends on the stall angle, after which the control force worsens. After 30^o of angle of attack, flow separation starts at the aerodynamic surfaces of the AIM-120D (Thomas Tyrell and Marton, 2014 [37]), so this is chosen to represent the maximum stall angle for both the angle of attack and the sideslip of the NCADE. This is not an irregular value for missiles (Maynes and Gebert, 1999 [23]).

3.4.2. Divert Attitude Control System on the Sustain Stage

For the control of the second stage, the missile relies on the DACS system, since the high altitudes achieved decreases the effect of control surfaces. It consists of four aerospike engines (Figure 3.17), which are generally less efficient than Laval nozzles, especially in the Mach 1-Mach 3 range (J. W. Cornelisse and Wakker, 1979 [13]). An advantage is that in off-design conditions in terms of atmospheric pressure, the performance fluctuates less. Additionally, the aerospike's compacter layout makes it favourable for installation. The DACS is located near the centre of gravity of the missile, so a sideways directed force is generated. This inevitably will result in a sideslip angle, which is to be corrected. Because the second stage is assumed to have four non-moving wings at the tail, the missile is aerodynamically stable and would correct the sideslip by a rotation. Another possibility is that the DACS is not at the centre of gravity, but slightly in front, resulting in a moment, which turns the nose into the incoming flow. This cannot be confirmed, since not enough data is available, and therefore the CG offset idea is disregarded. If the air density becomes too low for the wings to correct for the

sideslip, the KV could make use of its thrust vectoring, which directs the thrust force aft of the body sideways, creating a correcting moment.

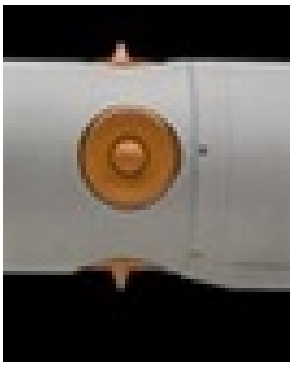

Source: GlobalSecurity.org
Figure 3.17: NCADE Aerospike Detail

Control System Layout
The DACS could be operational during the boost phase, or exclusively when separation occurs. The first option could be beneficial, since all control deflection during the first portion of the flight has an effect on the remainder of the flight. However, deflections of the DACS will require precious propellant, also usable to increase the NCADE's kinetic energy. Therefore, during the first stage boost of the NCADE, only deflections of the control surfaces are demanded. The same I_{sp} value is used for the aerospike thrusters,as the performance of the aerospike engine is hard to determine (J. W. Cornelisse and Wakker, 1979 [13]).

Control System Performance
To be able to model the DACS, a performance estimation is performed. Investigation has shown that kill vehicles are commonly designed with manoeuvring acceleration capabilities between 19.6 $^{m}/_{s^2}$ and 39.2 $^{m}/_{s^2}$ (Yingbo and Yong, 2010 [44]). Note that these values are for kill vehicles with propellant exclusively used for manoeuvring in the endgame, using a small amount of propellant. The NCADE is therefore assumed to have an acceleration capability at $20^{m}/_{s^2}$, since the kinetic kill vehicles are commonly not equipped with the relatively larger tank and amount of thrusters as installed on the NCADE. With the uncertainty of the target, higher divert accelerations would be favourable to the designers of the missile. The design point is taken at roughly half of the amount of monopropellant, which is $15kg$. In combination with the empty weight of the KV, the average weight equals $59Kg$, which results in a maximum divert thrust of $1.2 \cdot 10^3 N$. Using Equation 3.25, the mass flow results in $0.53^{Kg}/_{s}$, with an I_{sp} of 230, equal to the ΔV thruster.

3.5. Verification

The verification of the calculations is performed using the Generic Missile Model (GMM), developed at TNO Weapon Systems using Simulink. The GMM, also referred to as 'Validated Model,' calculates trajectories from generic missile data (TNO, 2012 [39]), by implementing a guidance algorithm, calculate the accelerations due to exerting forces. The accelerations are integrated resulting in the velocity and finally the position of the missile. The model has been applied to perform simulations of various missiles, for which actual data is used to validate the calculations. The outputs of this model are compared to the output given by the developed 3DOF model for the guidance algorithm, referred to as '3DOF model.' During the verification process, the integration of the velocity is verified by comparing the resulting position. Next, the EOM are verified, and finally, the impact of time step sizes is investigated.

3.5.1. Verification Test Cases

The NCADE exists of a complex layout, being a two stage missile system with various control layouts. The GMM is therefore only running the boost phase of the NCADE, after which a ballistic trajectory is flown, with the mass of the second stage still on the missile's body. This prevents the Simulink model from requiring different aerodynamic coefficients and a drop in mass. However, the effects of forces both in x and z direction are verified in this process. The investigated case is launched at $10km$ altitude with a 0^{o} heading, and an

initial pitch of 45° is given. The applied inputs are shown in Table 3.1. The C_{A0} lookup table is provided, so the aerodynamic forces can be calculated for all conditions (Figure B.1b).

Table 3.1: Generic Missile Model Verification Input

Input	Value
Empty Mass	103 kg
Propellant mass	45 kg
I_{sp}	250 s
S	0.0249 m^2
Booster $\dot{m}$	12.5 $^{kg}/_{s}$

First, the velocity output of the Simulink model is integrated and transformed to the ECEF frame using the 3DOF model. This will verify the applied forward Euler integration method and the implemented frame transformations. The second verification step is the comparison of velocity vectors which both programs calculated. Both the velocity magnitude and the path angle are compared. Last, the effect of the time step size is investigated.

3.5.2. Verification Process Outcomes

The boost phase of the Scud BM takes 62 seconds to complete, and the tracking threshold was set to 15s. In theory, the longest flight of the simulation takes 47s to complete. Therefore, the verification procedure is performed for $t_s = 45s$ and $t_s = 60s$.

Velocity Integration

For the verification of both the integration of the velocity and the reference frame transformations, the GMM velocity results are inserted in the forward Euler integration segment of the 3DOF model. The difference in location between the GMM and the 3DOF model is not visible in plots, which indicates a sufficient accurate integration method. The defect expressed in percentage is $0.7240 \cdot 10^{-3}$% for the $t_s = 45s$ case and $0.7240 \cdot 10^{-3}$% for $t_s = 60s$. The percentage is calculated using Equation 3.26. The calculated percentage provides the relative error in relation to the average values of the states. The errors are small enough to be negligible.

Overall Verification

The results of the overall verification process are shown in Figures 3.18 and 3.19. For these calculations, similar time steps are applied for both simulations, with $dt = 0.37s$ on average, since Simulink is optimising its own time discretisation. The states, altitude h, longitude, V and γ show a convincing similarity for the taken period. The differences expressed in percentage are shown in Table 3.2, which are presumed sufficiently low.

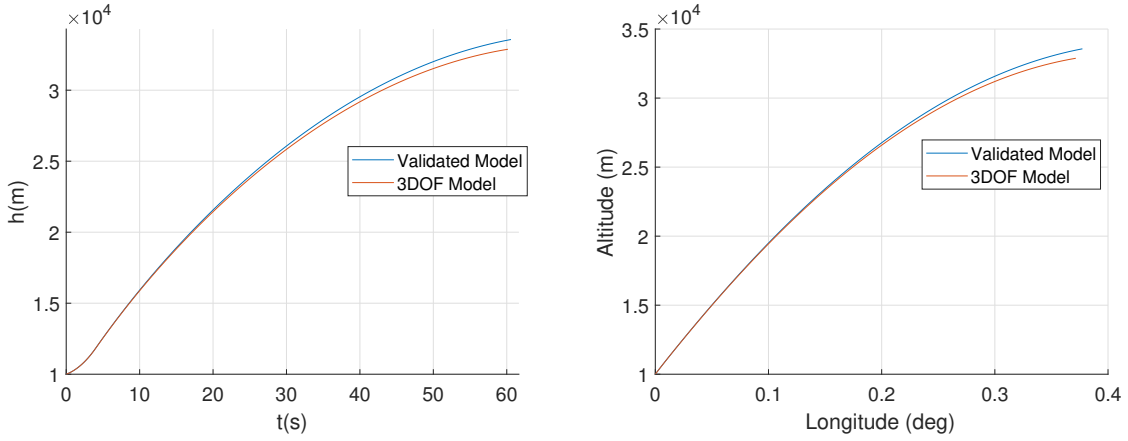

(a) Altitude Comparison

(b) Longitude Comparison

Figure 3.18: Differences between the GMM and the 3DOF model (1)

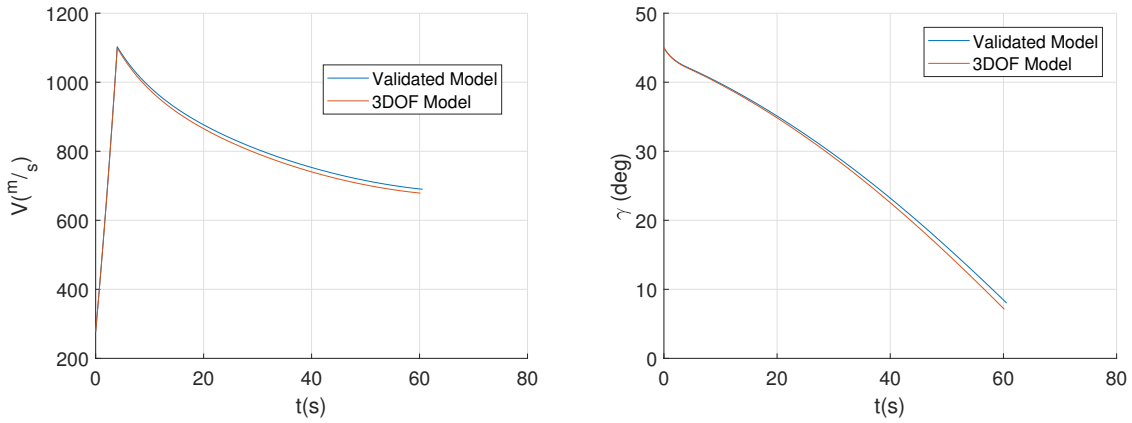

(a) Velocity Magnitude Comparison

(b) Path Angle Comparison

Figure 3.19: Comparison between the GMM and the 3DOF model

$$\left|X_{GMM}(t) - X_{3dof}(t)\right| / \frac{(X_{GMM}(1) + X_{GMM}(N))}{2} * 100\% \tag{3.26}$$

Table 3.2: Comparison between the GMM and 3DOF model (2)

State	Difference at $t_s = 45s$ (%)	Difference at $t_s = 60s$ (%)
h	0.513	0.737
V	0.631	0.613
γ	0.609	1.142
Longitude	0.387	0.442

Time Discretisation

Different time discretisations have been tested, to test their effect on the accuracy. The altitude is investigated, as it represents X,Y and Z of the ECEF frame combined, after integrating the accelerations twice. The result is plotted in Figure 3.20, where the accuracy calculated with Equation 3.26. The time discretisation consists of two parts, one for the boost phase and one for the sustain phase. The boost period takes 4 seconds and the end of the simulation is taken at both $45s$ and $60s$ after launch. As threshold, a 0.5% accuracy is desired, as a comprimise between calculation time, and accuracy of the results. Therefore, the time discretisation setting $n = 163$ is the chosen, which means that the boost phase contains 37 nodes and the sustain phase 126.

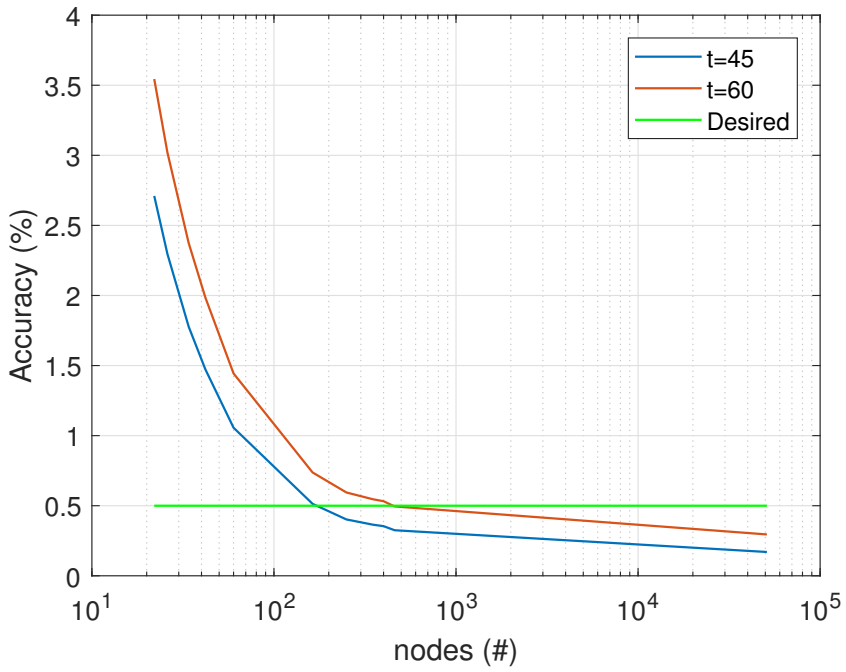

Figure 3.20: Effect of the Discretisation Settings on the Accuracy

4

Tracking

This chapter concerns the model of the process which leads to the prediction of the trajectory of a BM threat model. For this to be accomplished, an accurate BM model is required. A model for the observation is provided, including a model for the disturbance resulting from inaccuracies in the used sensors. These inaccuracies are mainly caused by the Infrared (IR) sensors, for which assumptions are to be made. An Extended Kalman Filter (EKF) filters the noise and estimates a set of states of the BM, which provides the input to perform a trajectory prediction. The BM model, the EKF and the trajectory prediction were already established at TNO (Riegman, 2016 [31]). The updates include an updated sensor noise model, the trajectory prediction assessment, and certain settings of the EKF have been investigated and tweaked for an improved performance. The result of the tracking process is a trajectory prediction with an estimated quality score, which is directly applied by the guidance algorithm of the interceptor.

4.1. Ballistic Missile Measurements

This section describes the Simulink model used to obtain a target of a BM which is to be tracked. With this target, a tracking procedure can be initiated. The model is usable for multiple inputs of targets. For this thesis, a Scud missile is chosen and described.

4.1.1. Ballistic Missile Simulation

A model of a BM is required for the interception algorithm, which is already established at TNO. The NCADE is most likely applied for tactical BMs, which poses a shorter range than Intercontinental Ballistic Missiles. Long range BMs are launched from silos, commonly located far in enemy territory. As inputs, the model requires masses of the BM, including empty mass, payload mass and propellant mass, using the corresponding centre of gravity. Multi-stage inputs are also possible, where the second stage, including propellant, is the payload of the previous stage. As aerodynamic input, coefficients for lift and drag are used, which could be obtained using PRODAS. The burn out time is to be specified, from which the mass flow is concluded. Together with a given thrust, the I_{sp} is determined. The model applies six degrees of freedom (6DOF), so the mass moments of inertia are also an input.
Next, the trajectory modelling is performed, using a Simulink program. Guidance is performed by controlling the attitude, where the current attitude is compared to the attitude required to achieve a target. At each time discretisation step of $dt = 0.2s$, all acting forces are considered in the Earth Centred Inertial (ECI) frame and converted to the ECEF frame. Outputs include, besides accelerations, velocities and positions, also the Euler angles and AoA.

4.1.2. Ballistic Missile Data

As input, the Scud missile is chosen, of which four versions are operated by various armed forces around the globe. This has also been chosen, since data on the Scud is already available at TNO. In short, the Scud is a liquid fuel propelled tactical BM, guided using inertial guidance. The maximum operating range lies between 190km and 550km, due to the various versions and payloads (CSIS, 2016 [5]). A typical achieved altitude is around 80km, with a total time of flight in the range of 5-6 minutes (Wade, 2016 [42]). Running the model, similar values are obtained, for a maximum altitude of 76km (Figure 4.1a), with a Mach number reaching

almost 5 at the end of the boost phase (Figure 4.1b). Note that the coast phase of the BM is not considered for interception in this thesis.

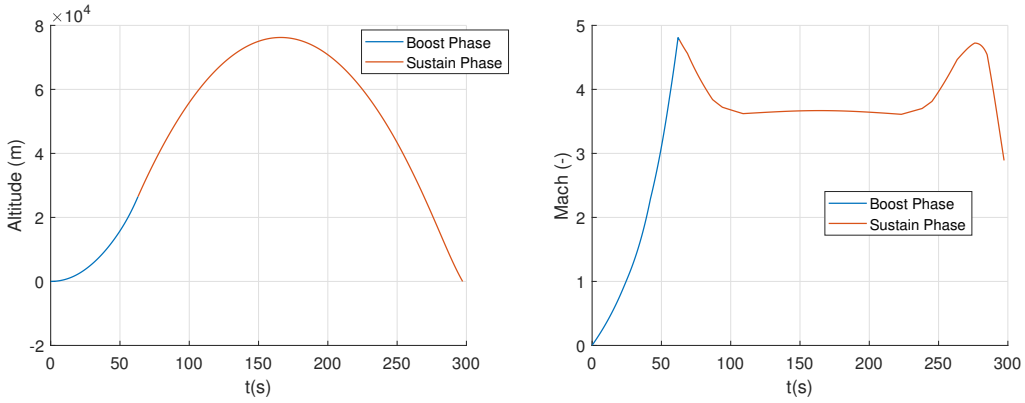

(a) Modelled Scud Altitude

(b) Modelled Scud Mach number

Figure 4.1: Ballistic Missile Model

4.2. Electrical Sensor Equipment

The BM target is to be tracked using one IR sensor on the NCADE and two IR systems of the launch aircraft. The provided EKF at TNO features a random noise input, which is chosen to be improved, by estimating the pixels of the sensor and its viewing angle. The quality of the track prediction of the filter depends on the filtered states, so the deterioration of the signal should be modelled accurately. First, the tracking scenario is modelled, after which the IR sensors are analysed.

4.2.1. Tracking Application Scenario

To model the flight of the NCADE, a fly-out scenario is sketched (Figure 4.2). An aircraft equipped with IR sensors scans the territory for BMs, with can be performed by the DAS system of the Joint Strike Fighter (JSF), a 5^{th} generation fighter (Lamar, 2017 [17]). Once an IR spike is observed, the aircraft will direct its radar and its Infrared Search and Track (IRST) sensor towards the threat. The radar is used for a distance measurement, and the IRST sensors are designed for a more accurate angle reading. The onboard computers will perform the tracking process, and decide if firing the NCADE will be effective. The NCADE is fired with a protective cap covering the vulnerable IR sensor. To refrain the NCADE from flying blind, the aircraft will guide the missile by commanded guidance, whilst continuing tracking the BM with radar and the IRST sensor. When the aerodynamic heating does not pose a danger for the IR sensor, the cap is disposed. The launch aircraft updates the location of the target to the NCADE during its flight, which is therefore able to point the IR sensor in the correct direction. Both the NCADE's and the aircraft's IR sensors measure observation angles which are combined using radio communication. The NCADE's computer will provide the guidance towards interception. The tracking algorithm however, applies the theory that the cap is absent, and the radar does not have a function in the EKF. Rework to apply the radar into the tracking algorithm is beyond the scope of this thesis.

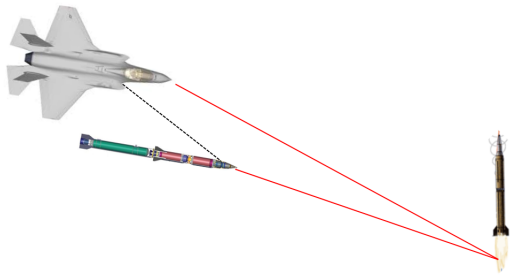

Source: Broekhuizen, 2018
Figure 4.2: Measurement of the Observation Angles Using IR Sensors

4.2.2. IR Sensors

An InfraRed (IR) sensor is able to provide an angle measurement of a bundle of IR signals, transmitted by any object or fluid. Molecules with a higher temperature transmit a higher amount of IR signals, which is discriminated by the IR sensor. Infrared signals will enter the dome which protects the IR sensor for aerodynamic heating. The cap is round, to prevent fragmentation from taking place. Aft of the dome, the IR signals proceed via mirrors past a lens, from where the focused beam illuminates a certain part of the sensor. The diameter of the beam is commonly smaller than a pixel. Depending on which pixel is illuminated, the IR sensor can determine the observation angle between the missile and the target. The amount of pixels in the sensor therefore defines the accuracy of the sensor. Larger pixels result in a worsened distinction in observation angles. Several examples from other kill vehicles in the industry show that the amount of pixels in the Focal Plane Array (FPA) vary between 64x64 and 265x256 pixels (Yingbo and Yong, 2010 [44]). One pixel is therefore responsible for a range of observation angles, which is to be minimised for the best accuracy (Figure 4.3). This accuracy is quantified by determining the range of angles which one pixel measures, being the Instantaneous Field Of View (IFOV) (Equation 4.1). N_{pixels} is the amount of pixels in 1 direction.

$$IFOV = \frac{\angle_{FOV}}{N_{pixels}} \tag{4.1}$$

The mirrors are focused in such a way that only a certain angle is observed, which is the Field Of View ($\angle_{FOV}$). Using additional gimbal suspension, the IR sensor is able to be directed towards the threat. Scanning patterns can be applied to increase the FOV to a wider range of angles, which is then called the Total Field Of View (TFOV) (Yilin Jiang and Ji, 2017 [43]). The target is to remain inside the TFOV, so when the gimbal is not aimed correctly to the threat, the threat can be lost. Therefore, the IR sensor is always directed in such a position that the illuminated pixel is in the centre of the sensor, where the orientation of the gimbal provides the observation angle.

Launch Aircraft

As launch platform, the aircraft is assumed to be equipped with IR sensors for initial detection. The JSF is a typical example of a 5^{th} generation fighter, equipped with a Distributed Aperture System (DAS), able to provide readings all around the aircraft. When a threat is detected and an observation angle is measured, the JSF's radar system could provide a distance measurement. Radar instruments operate in scanning patterns, so the DAS reading is used to aim the radar in the correct direction, keeping the signal signature of the aircraft as low as possible. The DAS exists of six sensors and is designed to scan all around the aircraft, providing high update frequencies. With an optimum distribution, the TFOV per sensor should cover at least 90^o, which is received by one non-scanning FPA. This means that the TFOV and FOV are the same for the DAS. The amount of pixels in the sensor is assumed to be a minimum of 1024x1024, giving an IFOV of 1.534 mrad per pixel. In perspective, on a detection distance of a BM of 250 km, this gives a maximum error of 384 m.
The reading of the DAS is used to aim the IRST, which is assumed to feature a moving IR sensor, to be able to scan a smaller angle range with an amount of pixels. The FPA is assumed to have 1024x1024 pixels at minimum, scanning a 6^o angle. The IFOV comes down to 0.1023 mrad, a much smaller amount than the DAS. At a 250 km range distance, the measurement error would be a maximum of 26m.

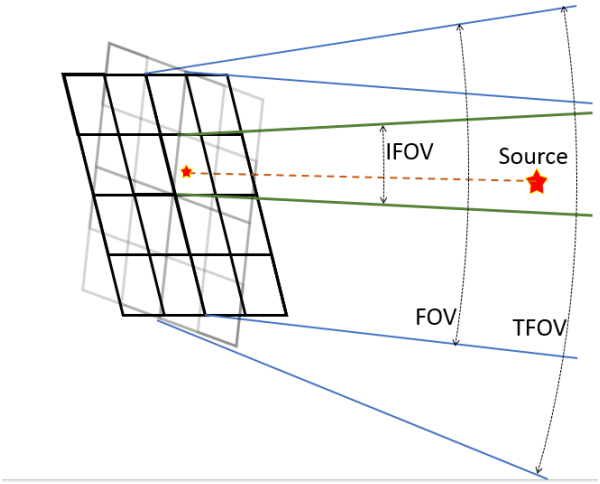

Source: Broekhuizen, 2018
Figure 4.3: Viewing Angles of an example IR sensor, with 4x4 pixels

NCADE IR Sensor
A higher amount of pixels is favoured for a better discrimination between observation angles, but complexity and therefore costs increase. The AIM-132 ASRAAM, an IR sensor equipped missile, was developed in the late 90's. Its IR sensor, manufactured by Raytheon, features 128x128 pixels, so a minimum of that value is to be expected from the NCADE. Other examples from literature show a maximum of 512x512 pixels of IR sensors of KVs (Yingbo and Yong, 2010 [44]). So a FPA with 256x256 pixels is assumed. An assumption must also be made for the IFOV. The launch aircraft will update the target's location to the missile, so the gimbal can be set to a certain angle. It therefore needs to cope with the error in the target's location, measured by the launcher using both the IR sensor and the radar. If the gimbal is not aimed correctly, the target will fall out of scope and the missile cannot provide a reading of the target. When an FOV of 3.0^o is assumed, the IFOV comes down to 0.205 mrad (Equation 4.1). Scanning must be avoided to minimise complexity of the gimbal. An overview of all IR assumptions can be found in Appendix A.

4.2.3. Embedding the IR Disturbance to the Filter Algorithm

The IFOV is used to determine the noise of the sensor. Both the sensor of the launch platform and the sensor of the NCADE are disturbed with Equation 4.2. This equation represents the range of angles which are received by a single pixel, among which the correct one is present.

$$\epsilon = IFOV \cdot \sqrt{2}(Rd - 0.5) \tag{4.2}$$

With Rd being a random number between 0 and 1.

Disturbances
Other sources of disturbances to IR sensor measurements could be the measurement errors and the inertia delays of the gimbal. These could be discarded to the pixel angle errors, which are assumed to be of a larger significance. Also, modern missiles are equipped with sensors which are able to accommodate for the delays (Schleijpen, 2017 [33]). Vibrations during flight are also neglected.

Endgame
During the endgame of the interception, the infrared sensor is to shift focus from the hot exhaust plume to the BMs body. This is programmed to refrain the intercepting from pursuing the plume, and aim for penetration of the BM instead. The control deflection required for the final endgame applied is assumed to be small compared to the sustain phase of the NCADE, and is therefore omitted in the guidance algorithm.

4.3. Ballistic Missile Boost Phase Tracking Filter

For the tracking of the BM in its boost phase, an Extended Kalman Filter is used (Riegman, 2016 [31]). It is able to filter the noise from the sensors and calculating dependent states. The states are used to predict the trajectory of the BM, so the quality measurement of the EKF is shown and its results are discussed.

4.3.1. Non-Linear Extended Kalman Filters

In short, a KF is able to filter sensor noise in real time. The filter receives a measurement, and using the linearity of the observation, it predicts the next future measurement. This prediction is then combined with the next measurement, for which a Kalman gain is used to weight the prediction in relation to the measurement. The difference between the prediction and the measurement is used to calculate the next Kalman gain. At high noise levels, the filter relies more on the prediction, while at low noise levels, the sensor data is used at a larger extend. The filter used in this thesis is an Extended Kalman Filter (EKF), which solves non-linear relations between the perceived states, to perform the prediction for the next reading.

4.3.2. Extended Kalman Filter Operation

The used EKF receives readings of the IR sensor, by a horizontal and vertical angle for both the sensor of the launcher and the missile. Using this information, a position can be measured. BMs are known for their non-changing azimuth angle, so a custom North-East-Down (NED) frame is used (Figure 3.3), reducing the amount of states which updates. The states applied in the Kalman filter are determined with a state transition equation (Equation 4.3).

$$\begin{bmatrix} \dot{X} \\ \dot{Y} \\ \dot{Z} \\ \dot{V}_t \\ \dot{\gamma} \\ \dot{\chi} \\ \dot{m} \\ \ddot{m} \\ \dot{\xi} \end{bmatrix} = \begin{bmatrix} V_t \cos\gamma \\ 0 \\ -V_t \sin\gamma \\ \frac{F}{m}\cos\xi - g\sin\gamma \\ (\frac{F}{m}\sin\xi - g\cos\gamma + \frac{V^2}{r}\cos\gamma)/V \\ 0 \\ -\dot{m} \\ 0 \\ 0 \end{bmatrix} \tag{4.3}$$

In this equation, γ is the flight path angle, χ is the azimuth and ξ expresses the angle between acceleration and velocity. These states are expressed in the modified ENU frame. The linearisation is used to perform the Kalman state prediction. One can observe the change in azimuth, the change in mass flow and the Y coordinate being zero. This is clarified with the governing assumptions of a BM target, being at first a fixed mass flow. As guidance, the BM is assumed to apply a fixed azimuth and is assumed to avoid turning in Y direction. Note that the target model applies these assumptions as well. In the Kalman filter, the ECEF coordinates are calculated from the modified NED frame, and the observation angles of both the launch platform and the missile are determined. These angles are therefore a prediction. The deviation between the actual sensor measurement is defined as the noise which is to be filtered, which therefore could be caused by actual sensor noise, or deviating Kalman states.

4.3.3. Testing the Extended Kalman Filter

The accuracy of the filtered states is important for the trajectory prediction to work accurately. The results of the EKF are therefore investigated, by taking the deviation between the actual states and the EKF's estimation. KF performance can be assessed with the error between the actual state, and the result from the filtering process (Simpson and Revell, 2009 [34]). The error should converge to 0 as tracking time goes to infinity. To test this, both the launcher and the interceptor (the NCADE) are placed at a random location and the filter is run. For the first case, the launcher is placed 400 km from the target's location, which is larger than initial estimations of the range of the NCADE (Halswijk and Benoist, 2014 [10]). The interceptor is placed 10 km away from the launcher, so that triangulation can occur.

4.3.4. EKF Quality

The error is shown in Figure 4.4a, and again for a distance of 50 km in Figure 4.4b. Note that the error in X,Y,Z is chosen, which are the coordinates of the BM in the ECEF frame. As can be observed, the results of the tracking are not converging, which is not a good sign when it comes to Kalman Filter assessment. The filter however receives continuously new readings, retaining the error from diverging. Showing derived states

from the position, for example the mass and the mass flow, the EKF definitely improves (Figure 4.5). The initiation values for all Kalman states are chosen as common values for ballistic missiles. When initial KF variables are being used which are far off, a converging pattern is recognisable. The initial increase of the mass flow however is wrong and worsens the first trajectory predictions. During convergence, the mass flow decreases below zero, being physically wrong. When providing the KF with correct initial values, it shows that the quality of the filter again not perfect. This indicates the necessity for an adapting flight guidance algorithm of the NCADE, which should handle the uncertainties resulting from the EKF.

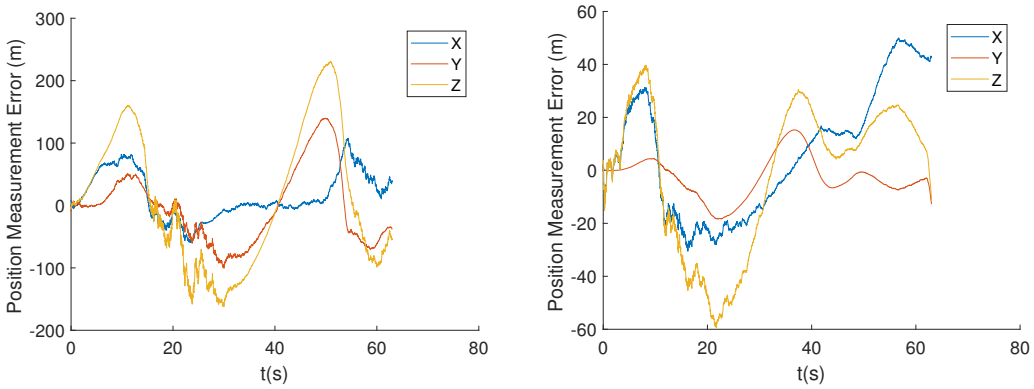

(a) Launch Platform distance of 400km (b) Launch Platform distance of 50km

Figure 4.4: Performance of the EKF Measured in State Deviation

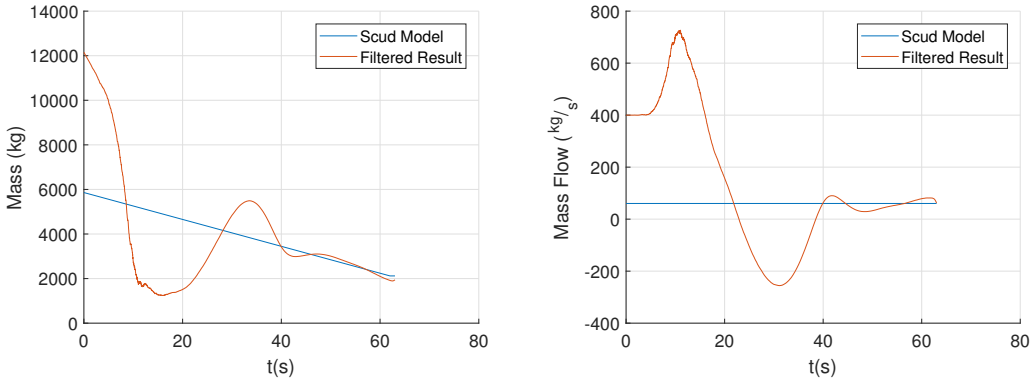

(a) Mass (b) Mass flow

Figure 4.5: Kalman States Filtering Result

When the interceptor is located too close to the launch platform, triangulation would not be successful. This is due to the small difference between the angles of the missile and the platform, giving large variations in distance measurements when triangulating. This is solved by the complimentary radar system of the JSF, which together with the IR sensor provides a location reading of the target. Chosen is to not model the radar system, and it is assumed the position error of the radar is not too large to pose issues. Multiple JSFs together on patrol missions are also able to share IR readings, which is the most likely engagement scenario, decreasing the error.

4.4. Ballistic Missile Trajectory Prediction

The tracking algorithm produces besides the filtered Kalman states of the target a prediction of the trajectory, using which the guidance algorithm of the NCADE can determine a Predicted Interception Point (PIP). This study will use the outputs of the prediction to perform a quality assessment, to investigate certain settings of the EKF giving best performance of the trajectory prediction. For this purpose, the Certainty Score C_S has been defined.

4.4.1. Track Prediction Model

The track prediction requires the integration of the states. Position, velocity and acceleration are directly applied from the filtered states. The mass and mass flow are also taken from the EKF. The acceleration is split in a forward acceleration component, which results from propulsion and drag, and a gravity component. The orientation and state give directly an input to the track prediction itself, which integrates all states through time. Included in the integration is the change in mass, which is used to estimate the change in acceleration.

4.4.2. Certainty Score

Because of the large uncertainties of the target and the prediction of its trajectory, the prediction is rated on certainty. This must be performed without the knowledge of the actual track of the target. To score the prediction, the trajectory prediction algorithm determines Jacobian H_C, which quantifies the influence of the errors of the Kalman states on the trajectory prediction, in X, Y and Z direction (Equation 4.4). Subscription 0 indicates the values of the states at the current simulation time step, after which the prediction is performed. The Kalman states are transformed to the ECEF reference frame for the track prediction. The partials are determined numerically, by adding a small increment to each state individually, whereafter the track prediction is performed. The result, the ECEF coordinates at a certain time step, is subtracted from the main result, from which each partial derivative is determined.

$$H_C = \begin{bmatrix} \frac{\partial X}{\partial X_0} & \frac{\partial X}{\partial Y_0} & \frac{\partial X}{\partial Z_0} & \frac{\partial X}{\partial U_0} & \frac{\partial X}{\partial V_0} & \frac{\partial X}{\partial W_0} & \frac{\partial X}{\partial m_0} & \frac{\partial X}{\partial \dot{m}_0} \\ \frac{\partial Y}{\partial X_0} & \frac{\partial Y}{\partial Y_0} & \frac{\partial Y}{\partial Z_0} & \frac{\partial Y}{\partial U_0} & \frac{\partial Y}{\partial V_0} & \frac{\partial Y}{\partial W_0} & \frac{\partial Y}{\partial m_0} & \frac{\partial Y}{\partial \dot{m}_0} \\ \frac{\partial Z}{\partial X_0} & \frac{\partial Z}{\partial Y_0} & \frac{\partial Z}{\partial Z_0} & \frac{\partial Z}{\partial U_0} & \frac{\partial Z}{\partial V_0} & \frac{\partial Z}{\partial W_0} & \frac{\partial Z}{\partial m_0} & \frac{\partial Z}{\partial \dot{m}_0} \end{bmatrix} \tag{4.4}$$

Together with the covariance matrix P from the Kalman prediction itself, the covariance matrix R_C is determined (Equation 4.5).

$$R_C = H_C \cdot P \cdot H_C' \tag{4.5}$$

This covariance matrix can therefore be used to quantify the quality of the trajectory prediction. If all the values of the matrix are low, the Kalman states have converged and the prediction is more accurate. An indication of the magnitude of the matrix R_C is summarised using the determinant, now called the certainty score (C_S) (Equation 4.6):

$$C_S = \det(R_C); \tag{4.6}$$

To review what C_S represents, the offsets of the trajectory prediction have been plotted (Figure 4.6). In this graph, the track prediction is started at a simulation time (x-axis), towards the moment the boost phase is completed, at $t_s = 63s$. The offsets resulting from changing the Kalman states, are plotted as dX, dY and dZ. C_S shows a similar trend, and as the determinant takes all three directions in account, it is used to quantify the quality of the trajectory prediction. In Figure 4.6, the 100 km threshold is shown, which is an order of magnitude of the range of common air-to-air missiles (Parsch, 2007 [29]). An usable threshold of about 40 km corresponds to a C_S of $1.3 \cdot 10^{16} m$, shown with the circle.

4.4.3. Model Performance

A study has been performed to determine the performance of the EKF and the trajectory prediction. The determinant is calculated with an increasing simulation time, to review the effect of an increased amount of measurements. Next, at certain time steps, the prediction is performed with a range of prediction periods lengths, so at several time nodes in the future. To visualise the effect of the IR sensors disturbance of the measurements, the analysis is performed with disturbances modelled into the angle measurements of the sensors compared to the disturbance being absent. In this simulation, both the missile and the launch platform travel at a constant speed.

Local Linearisation Influence

The EKF operates using the Jacobian of the states, which is determined using numerical differentiation. A certain time step has to be taken for this process, which affects the performance of the filter. Trajectory predictions are performed and assessments are made at certain time steps in the simulation, to investigate the effect of the time step on the tracking result. The end of each trajectory prediction of the BM is $t = 63s$, which is the burn-out time of the BM. When changing the time step of the calculation of H_C, results are observed as shown in Figure 4.7, in form of C_S. The x-axis shows the time step on which the trajectory prediction is initiated, with at the y-axis the resulting Jacobian determinant at $t = 63s$.

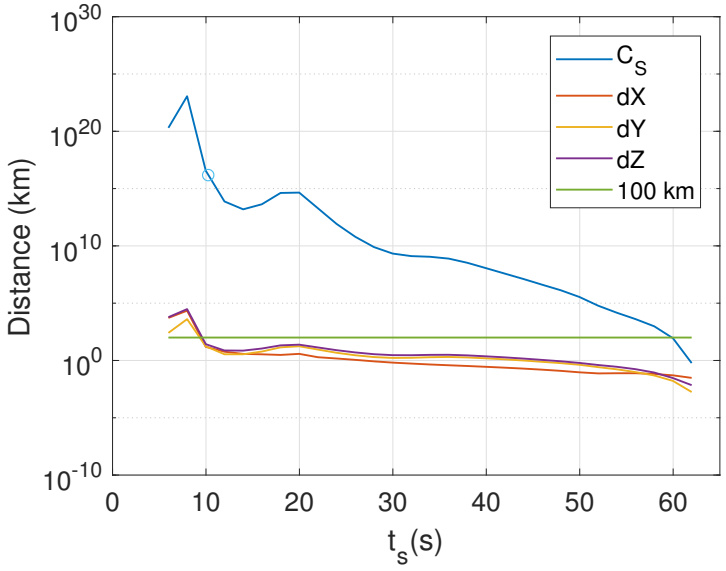

Figure 4.6: Certainty Score and Offsets

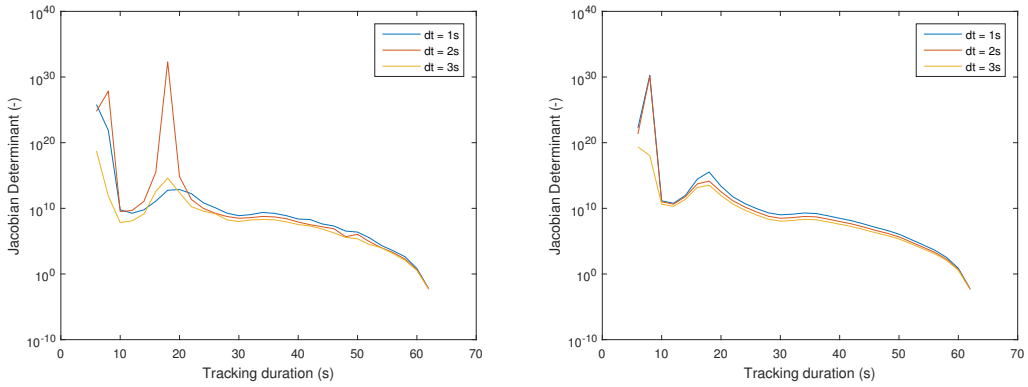

(a) Sensor noise modelled

(b) Sensor noise omitted

Figure 4.7: Effect of Different Time Step Sizes for States Linearisation in Jacobian Calculation

The time step of $3s$ shows best results for the prediction and is therefore applied for the linearisation of the states and determining the Jacobian. It seems more logical that a smaller time step improves results. However, since the EKF generates errors, the impact of those errors is decreased if those deviations are relatively smaller, which occurs at larger time steps. The sudden increase in Figure 4.7a at $t = 18s$ could possibly be explained by a large error in measurement, however it is immediately followed by a decrease. An improved linearisation procedure could possibly solve this problem, but is beyond the scope of this thesis.

Sensor Noise

Effort has been put in to model the IR sensors accurately, to model the effect of the sensor noise on the trajectory prediction. The results of which are shown in Figure 4.8. Initially, the sensor noise has a large effect on the score of the prediction, but as the duration of the tracking increases, the noise does not affect the error anymore. The noise could even be said to be a smoothing factor, which reduces the steep peaks in the graph. A possible explanation is that at first, the measurements are slightly disturbed. Later through the tracking process, the disturbances could cause the filter to rely on the Kalman prediction rather than the measurement, omitting wrong measurements. The error of the prediction is accredited mostly to the filtering process of the Kalman states, as further in time, the noise of the sensor does not influence the results much (Figure 4.5).

EKF Performance With Increasing Tracking Periods

The effect of the tracking duration on the trajectory prediction can also be observed (Figure 4.7a). As more data is processed by the filter, the Kalman states converge towards their correct values. C_S becomes lower as the tracking duration increases, which indicates a better result.

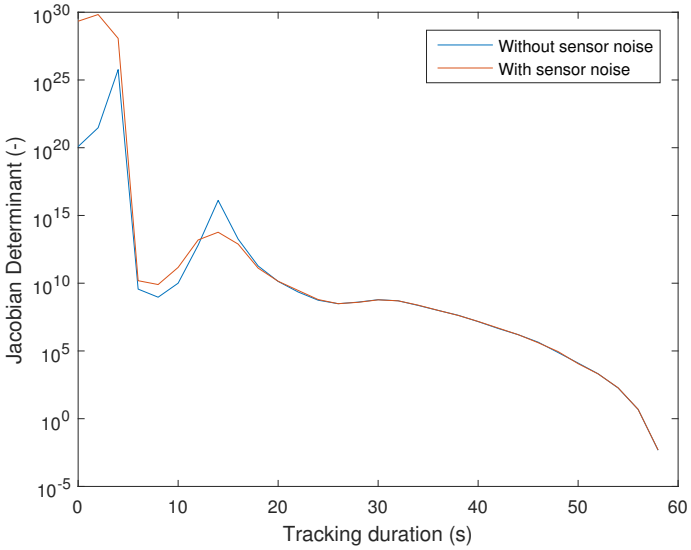

Figure 4.8: Comparison the Sensor Noise on the Jacobian Determinant

EKF Performance With Increasing Prediction Duration

The effect of increasing the prediction period on the performance is investigated. During the tracking of the BM, four time nodes are chosen, at which several trajectory predictions are simulated and rated. For all predictions, a Jacobian linearisation time step of 3 seconds is chosen, which proved to be most suitable. First, the simulation of the tracking procedure is paused at $t_{start} = 4s$ and a trajectory prediction is performed to $t = t_{end} = 63s$. This prediction is rated at certain time steps, as shown in Graph 4.9a. Starting the trajectory prediction at an early time step, it becomes clear that C_S grows relatively fast when the prediction proceeds into the future. The simulation is again paused at $t_{start} = 20s$ for a second analysis, shown in Graph 4.9b. The error grows at a lower and more predictable rate. This effect continues as the tracking duration increases (Figure 4.10). The effects of the noise of the sensor becomes less prominent.

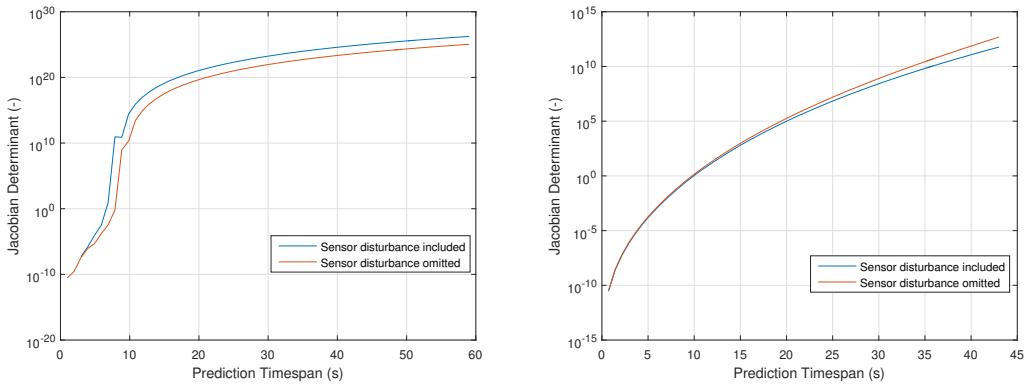

(a) t_{start} = 4s (b) t_{start} =20s

Figure 4.9: Trajectory Prediction Assessment (1)

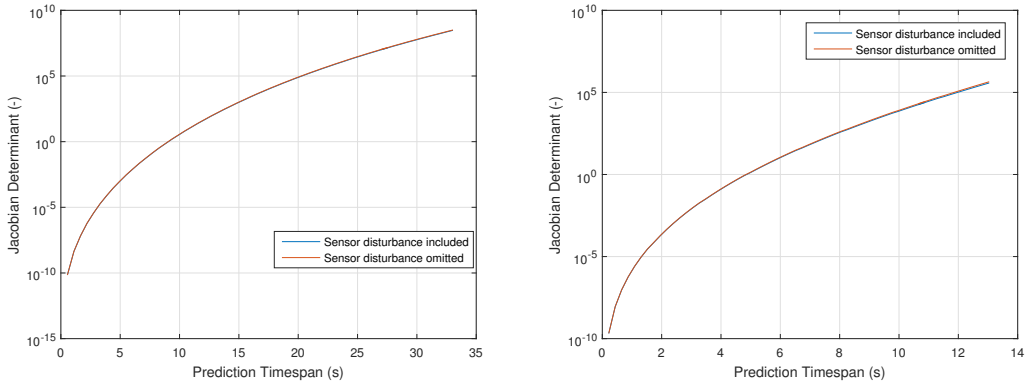

(a) t_{start} = 30s (b) t_{start} =50s

Figure 4.10: Trajectory Prediction Assessment (2)

4.5. Guidance Algorithm Interaction

The prediction is to be forwarded to the flight trajectory optimiser. This algorithm will calculate the trajectory of the interceptor, based on the Predicted Interception Point (PIP), located somewhere on the predicted trajectory of the BM. At the PIP, both the interceptor and the BM must arrive simultaniously, resulting in a hit. Since the PIP varies during the optimisation routine due to the evaluation of multiple trajectories, the score must be available at all times of the BM's trajectory prediction. When investigating Graphs 4.9 and 4.10, one can observe an increasing determinant at a smoothly increasing rate. To prevent time consuming evaluations at each iteration of the guidance algorithm, interpolation is chosen to forward the trajectory prediction uncertainty score to the guidance algorithm. Three equally spread prediction time nodes are applied, where the trajectory prediction is evaluated. The result, the sizes of the three uncertainty ellipses P_E, are interpolated using a 3rd degree polynomial, at which no Runge phenomenon will be expected for low amount of points. The Runge phenomenon is the unwanted oscillation of the polynomial at the begin and end, when too much nodes are applied. The coefficients of the polynomial, along with the time nodes where interpolation took place, are forwarded to the optimisation routine. The 3rd degree polynomial requires one target prediction, which score is determined using eight target predictions for eight Kalman states, performed at three time nodes. This totals to 25 target prediction calculations for one target prediction iteration.

4.6. Conclusions

The EKF has been implemented in the trajectory guidance algorithm, with the most optimal linearisation time step. The EKF performs poorly, due to the target decreasing in mass, and the initial mass, thrust and acceleration are unknown. However, the convergence rates of the determinant of the Jacobian shows the decreasing error when the tracking period is lengthened, or when a prediction shorter into the future is used. The sensor noise is now modelled more accurately, but shows little effects compared to the EKF errors. Without knowledge of the actual target trajectory, the EKF is able to assess its prediction, and using polynomials, it is forwarded to the guidance algorithm.

5

Trajectory Optimisation Algorithm

With an acceptable tracking result, the guidance of the NCADE towards an interception point can be established. The guidance must accommodate for the uncertainty of the prediction, a staging event with a changing control system and a complex consideration of applying the available monopropellant for propulsion or direction control, so a common proportional navigation strategy would not suffice. In theory, an infinite number of trajectories is possible, so a trajectory optimisation algorithm is presented which aims to find the most optimal solution, by minimising a performance index J while applying constraints to have a physical possible solution. Using NLP, candidate solutions are evaluated and adjusted, so that an optimum is found. This Chapter will first describe the control problem, and will elaborate the chosen optimisation strategy. Next, the choices of the implementation of the optimiser are explained.

5.1. Optimisation Control Problem Definition

First, the control problem is described. The control problem at hand is that control functions must be defined which guides the missile towards the interception of the BM. The performance index is a value which defines the most optimal trajectory, when minimised (Equation 5.1).

$$\min_{t_0, t_f, \mathbf{x}(t), \mathbf{u}(t)} = J\left(t_0, t_f, \mathbf{x}(t_0), \mathbf{x}(t_f\right) + \int_{t_0}^{t_f} w\left(\tau, \mathbf{x}(\tau), \mathbf{u}(\tau)\right) d\tau \tag{5.1}$$

subject to the state equations (Equation 5.2):

$$\dot{\mathbf{x}}(t) = \mathbf{f}(t, \mathbf{x}(t), \mathbf{u}(t)), \; 0 \leq t \leq t_f \tag{5.2}$$

and the dynamic constraints (Equation 5.3 and 5.4):

$$\mathbf{c}_{equal}(t, \mathbf{x}(t), \mathbf{u}(t)) = 0 \tag{5.3}$$

$$\mathbf{c}_{inequal}(t, \mathbf{x}(t), \mathbf{u}(t)) \leq 0 \tag{5.4}$$

The launch conditions and interception states are also bounded by constraints (Equation 5.5):

$$\mathbf{x}_0 = \mathbf{S}_0 \tag{5.5}$$

$$\mathbf{x}_{tf} = PIP$$

In these equations, t_0 is the start of the time line of the interceptor's flight, t_f is the final time on which the interception takes place. $\mathbf{x}$ describes the states and $\mathbf{u}$ describes the control vector, and J is the performance index.

5.1.1. Performance Index

The performance index J is to be minimised by the optimisation strategy. The ultimate goal of the flight of the NCADE would be to intercept the target and destroy it, given a certain amount of trajectory prediction uncertainty. As seen in Chapter 4, the results of the EKF are the target's position at a certain time span and the uncertainty ellipse P_E. For J, The interceptor divert ellipse E is defined, which quantifies the ability of the NCADE to divert, given its values of the states at a certain time step. This value is elaborated below. Both E and P_E quantify the probability of a successful interception, which together define J (Equation 5.6). Note that the Predicted Interception Point (PIP) is included in the constraints, since an infinite amount of trajectories is possible. The missile is now forced to achieve interception, so it is deemed unnecessary to focus on solutions which do not reach a useful destination. Mechanical failures of the missile or fabrication inaccuracies are not applied in the kill probability prediction.

$$J = P_E \cdot J_E - E \cdot J_D \tag{5.6}$$

Where J_D and J_E are weights, controlling the priority of the performance index elements. P_E and E are the target prediction certainty ellipse size, and the interceptor divert ellipse size respectively, elaborated below.

Target Prediction Certainty Ellipse

The target prediction certainty ellipse size (P_E) should be minimised for the best interception probability. This can be achieved by the optimiser by decreasing time to flight t_f, for which the tracking results are more reliable. A second option would be to extend the flight trajectory, and allow the tracking to continue for a longer period so the EKF is able to converge. This option is not considered for a few reasons. The first is that the divert ellipse size is increased by the optimisation procedure (as seen below). This most likely results in the t_f to increase, which results in a longer tracking duration. This way, the tracking duration is already increased. The second reason is that the EKF shows indeed better results when the tracking duration is extended, but the rate is hard to predict, especially further in time.

Interceptor Divert Ellipse

The target will be tracked with a certain uncertainty volume, which the trajectory optimiser must consider. It does so by means of the divert cone, which is an estimation of the volume which can be covered by the missile, given the amount of propellant, the current velocity and altitude (Figure 5.1). The divert cone is defined in this study as follows: in black, the calculated trajectory of the missile is shown. At a certain time during the flight, an amount of three flights is calculated which describes all locations the missile is able to reach. For the NCADE specifically, this cone is dominated by the amount of reserve propellant available, which is used for propulsion and turning. The optimum solution would be an as large as possible cone, so that the missile can accommodate the largest uncertainties of the BM's trajectory prediction.

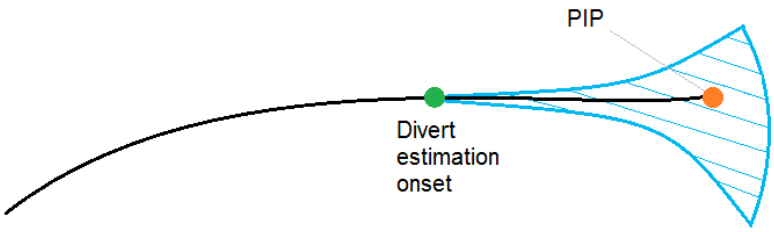

Figure 5.1: Divert Cone

The size of the cone is determined by an extra optimisation routine, which aims to maximise the distance from the original PIP, with the same time to flight (t_f) applied. It does so three times, in east, north and up direction in the local ENU frame. The average distance of the results is a measurement for the divert cone, noted as E, which can be compared to the uncertainty ellipse dimensions. Therefore, during the optimisation iterations, the cone is to be calculated at some point on the trajectory. To investigate the most useful divert estimation onset, a range of time-to-flight ratios has been used to investigate the divert ellipse size , for two launch conditions. The concept is visualised in Figure 5.2, where the prediction of the BM's trajectory is shown in yellow, with the interceptor flying at the black line. The green dots represents three of the

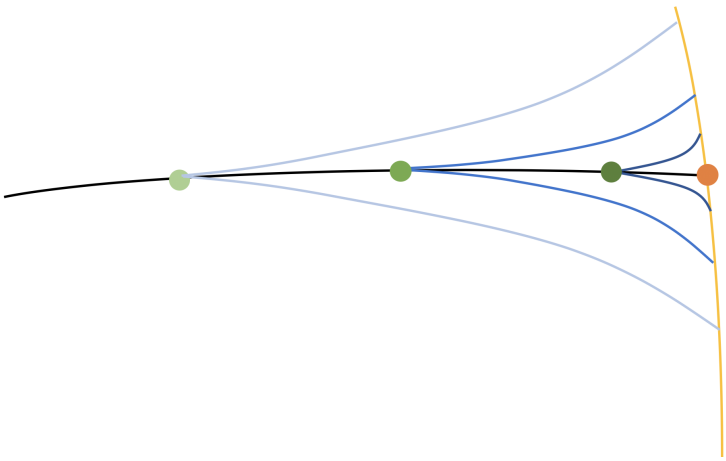

Figure 5.2: Divert Cone Study Strategy

points chosen to investigate the size of the divert cone. The flight trajectories used for this study are a result of the final guidance algorithm described in this chapter, without considering the divert cone in J. The first graph shows a missile launch from $20km$ behind the BM, at $15km$ altitude (Figure 5.3a). In this figure, the relative time is plotted, on which the divert cone is calculated. The boost phase is omitted in this study, which explains why the t_f ratio does not start at 0%. At t_f, all propellant is consumed, because the optimiser will apply all propellant to decrease the time to flight, which is in this case $19.68s$. Therefore, there is no more room for corrections, as control deflections can only be applied using propellant. The missile has a relative large amount of potential energy, but a small amount of time to make control deflections. At the start of the flight, the deflection possibility is large, as more propellant is available for deflections. Notable difference is the possibility to change the upward distance, as potential energy is required, which consumes more propellant. The second case applies a NCADE launch from $30km$ sideways, at $12km$ altitude (Figure 5.3a). t_f is reached after $26.18s$, which is a longer duration than the first scenario. The increased sizes of the divert cones are due to the ability of the NCADE to provide a heading change, after which the NCADE has a longer period to increase the distance relative to the PIP.

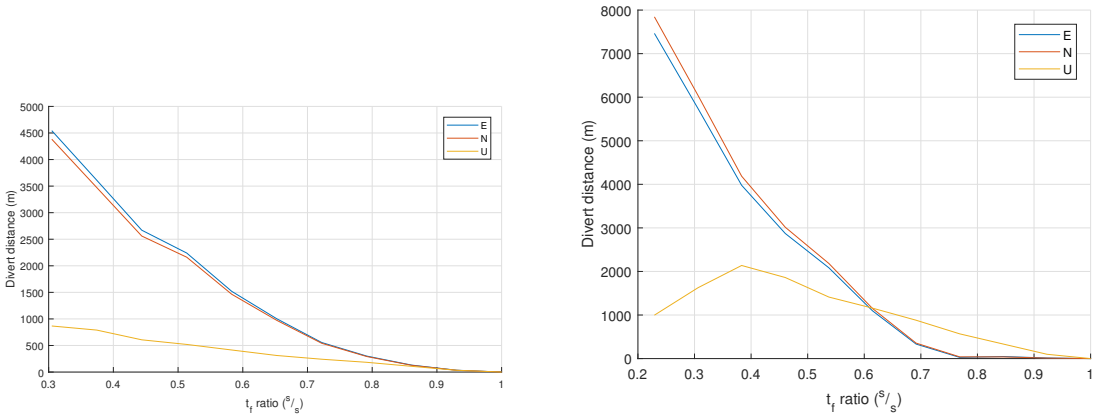

(a) Launched from Behind

(b) Launched from the Side

Figure 5.3: Interceptor Divert Cone Sizes at Increasing Onsets

The divert estimation onset is chosen at $0.65 \cdot t_f$. An onset closer to the PIP would result in a smaller cone, where changes in the flight path and control deflections are relatively small. An onset further away would not provide an effective divert estimation, since the divert cone is meant to cover tracking inaccuracies, which becomes clearer as the interceptor approaches its target.

Relative Velocity Difference
The relative velocity difference between the Kill Vehicle (KV) and the target contributes whether or not the target is actually penetrated and killed. No explosive charge is applied in the KV, so the destruction of the BM is accomplished by a kinetic energy impact. If the relative velocity between the two is small, the target could possibly survive the unsuccessful penetration. The interception is not useless, since systems could damage and which causes the BM to miss its target, which is however not the ideal situation. The relative velocity difference is however not included in the performance index, since the optimiser aims to increase the reserve propellant at 65% of the flight. This reserve could be used for divert manoeuvres and if those are not required, it can be applied to increase the velocity difference.

5.1.2. Constraints

Constraints are imposed on the optimisation problem, either to set physical requirements or to guide the optimisation routine away from non-optimal solutions. This prevents the optimiser from solutions which are technically not feasible and errors due to abnormal control inputs and states. Both equality and inequality constraints are applied. One set of three equality constraints is set for the PIP at $t = t_f$. Every set of inequality constraints are valid for each time node of the trajectory.

Equality Constraint
A set of equality constraints is applied, being that the last ECEF location of the NCADE at time $t = t_f$ must be equal to the location of the BM at that same time step (Equation 5.7). The final coordinates of the trajectory is an interception point on the prediction of the trajectory of the BM. It would also be possible to incorporate this as part of the performance index, however, within the range of the NCADE, an infinite amount of trajectories is possible reaching an aiming point, so this idea is disregarded. The equality constraint is defined in the ECEF frame, and should be zero in the final optimum solution.

$$X_M(t_f) - X_T(t_f) = c_{equal} \tag{5.7}$$

With X_M and X_T being the ECEF coordinates of the interceptor and the BM target respectively.

Physical Inequality Constraints
The altitude of the missile should always be higher than sea level (Equation 5.8. This is a physical constraint as the missile would crash in the ground, and a constraint to prevent error when calculating the density. The ground elevation is not included, since the missile would most likely remain above the altitude of the BM in the optimum solution. The constraint is set for all time nodes of the trajectory.

$$-\left(\sqrt{X_M^2}\right) + r \leq c_{ineq} \tag{5.8}$$

With r being the radius of the earth, $6371 \cdot 10^3 m$.

Control Inequality Constraints
The maximum inputs of the controls are implemented using inequality constraints, for both the boost stage and the sustain phase (Table 5.1). The chosen NLP algorithm (elaborated in Section 5.3 requires inequality constraints to be equal to or smaller than zero. All maximum inputs have been established in Chapter 3 and are summarised in Appendix A. They are implemented for both a positive and negative inputs, defined at all time nodes. For the boost phase, the α and the β are both limited using inequality constraints. Note that solid propellant consumption is not included in the constraints, as the burn is not controllable. Since the controls are an input, one could apply bounds instead of constraints to increase the calculation speed. However, the applied parametrisation makes this impossible (Section 5.3), so constraints are to be applied.

Table 5.1: Boost Control Constraints

Constraint	Equation
α (max)	$\alpha(t_i)$ - 0.524 rad $\leq c_{ineq}$
α (min)	- 0.524 rad - $\alpha(t_i) \leq c_{ineq}$
β (max)	$\beta(t_i)$ - 0.524 rad $\leq c_{ineq}$
β (min)	- 0.524 rad - $\beta(t_i) \leq c_{ineq}$

The second stage employs a more complex control layout, where controls and velocity increase are regulated using monopropellant, which originates from the same tank. Constraints are applied to the maximum mass flows and the minimum amount of total propellant (Table 5.2). First, the minimum and maximum DACS control inputs are limited, expressed in an amount of mass flow. The DACS control input is possible in Y direction and Z direction of the body frame. One control function is applied per direction, so positive and negative values can be applied. For propulsion, the control is also expressed as a mass flow. The first constraint of the mass (M_1) keeps the mass flow for thrust within the maximum. The second mass constraint (M_2) states that the mass flow should never increase, i.e. the thrust is positive at all time nodes. The last mass constraint (M_3) prevents the total use of propellant from exceeding the available amount, which is carried in the tanks. The mass flow of both the DACS and the thrusters is integrated to obtain the mass. Again, due to the parametrisation strategy, bounds are not possible to implement.

Table 5.2: Kill Vehicle Control Constraints

Constraint	Equation
$DACS_Y$(max)	$DACS_Y(t_i)$ - 0.53 $^{kg}/_s \leq c_{ineq}$
$DACS_Y$(min)	- 0.53 $^{kg}/_s$ - $DACS_Y(t_i) \leq c_{ineq}$
$DACS_Z$(max)	$DACS_Z(t_i)$ - 0.53 $^{kg}/_s \leq c_{ineq}$
$DACS_Z$(min)	- 0.53 $^{kg}/_s$ - $DACS_Z(t_i) \leq c_{ineq}$
M_1	$-\dot{m}_{KV}(t_i)$ - 11.25 $^{kg}/_s; \leq c_{ineq}$
M_2	$-\dot{m}_{KV}(t_i) \leq c_{ineq}$
M_3	$\int_{(t_i)}^{t_{(i+1)}} \dot{m}_{KV} dt + \int_{(t_i)}^{t_{(i+1)}} (\lvert DACS_Y(t_i) \rvert) dt + \int_{(t_i)}^{t_{(i+1)}} (\lvert DACS_Z(t_i \rvert) dt$ - $45kg \leq c_{ineq}$

Optimisation guiding inequality Constraints

To guide the optimiser in the correct direction, a few inequality constraints are implemented (Table 5.3). These constraints should not be active at the optimum solution, but act as a limitation so that calculation errors are prevented. The set constraints are dealing with the velocity, path, the heading and the position. A velocity maximum of 2310 $^{m}/_s$ is set, which is in the vicinity of Mach 7. After this value, the values for the aerodynamic coefficients become questionable, as the Prodas software is validated up to Mach 7. Minimum velocities below 100 m/s should not be present in the optimum solution, refraining the optimiser from negative velocities. Path angle γ should remain between $\pm 0.5\pi$, straight up or straight down. Heading Ψ should also limit to the maximum of a full circle ($\pm 2\pi$), since the missile is already being fired in the correct direction due to the minimum tracking duration. This prevents the interceptor from flying in circles, which will most likely not be the optimum solution.

Table 5.3: Non-equal Constraints for Directing the Optimiser

Constraint	Equation
V(max)	$V(t_i)$ - 2310 $^{m}/_s \leq c_{ineq}$
V(min)	100 $^{m}/_s$ - $V(t_i) \leq c_{ineq}$
γ(max)	$\gamma(t_i)$ - $\frac{\pi}{2} \leq c_{ineq}$
γ(min)	$-\frac{\pi}{2}$ -$\gamma(t_i) \leq c_{ineq}$
Ψ(max)	$\Psi(t_i)$ - 2 $\pi \leq c_{ineq}$
Ψ(min)	-2 π -$\Psi(t_i) \leq c_{ineq}$

5.2. Optimisation Strategy Choice

The control problem is optimised using a trajectory optimisation strategy. One could argue that a non-optimisation flight guidance algorithm is able to guide the missile to a certain point, which is considered as well. The discussed optimisation strategies of Chapter 2 are assessed and a choice is made.

5.2.1. Non-optimum Trajectory Optimisation Algorithm

The EKF provides a prediction of the location and an acceleration term of the target, which in theory could be included in a non-optimised PN algorithm (Nesline and Zarchan, 1981 [25]). A simple algorithm could calculate a suitable interception point, given the distance to be covered, which has the advantage that the calculation effort is greatly reduced. However, the tracking comes with a large uncertainty, and the strategy of the monopropellant consumption for either control or propulsion makes the flight planning too complex. For these, and more reasons, PN is deemed unsuitable.

5.2.2. Indirect Methods

Indirect trajectory optimisation strategies require a mathematical derivation of the problem (von Stryk and Bulirsch, 1992 [41]). Non-linear phenomena make the derivation difficult, and when boundary conditions are updated, the derivation has to be redone. Due to the high non-linearity of the problem and the updating target trajectory prediction, indirect trajectory optimisation is discarded.

5.2.3. Direct Collocation

Initially, the collocation scheme showed best properties for the optimisation problem. Collocation is known for its fast convergence and a lower tendency to converge to a local optimum, as non-feasible solutions can be explored (Betts, 1998 [4]). Because both the states and the controls for the flight are defined at each iteration, the calculation time decreases as calculations are performed parallel. In contrary, for example a shooting method requires integration of the controls to find the states of the next time step, which means that all calculations are performed sequentially at each time node. For this optimisation problem however, convergence of the constraints linking controls and states was not achieved. Possible cause for this divergence is thought to be the discontinuity in the problem due to the staging event, as the mass decreases instantly and the control system layout changes. Also, during the boost phase of the interceptor, the effectivity of the control deflections varies due to large decrease of the mass. Therefore, collocation is discarded for this optimisation problem.

5.2.4. Direct Shooting

The direct shooting method is convenient to implement compared to other direct methods (Betts, 1998 [4]). Due to the complexity of the missile system and the performance index, the shooting method is chosen for this study. At each iteration, the five control functions of the missile are set up by the design vector parameters. These parameters are coefficients of basis functions, further elaborated below. The initial guess for the controls is chosen to give minimum control inputs, so that the probability of the optimiser for getting stuck in a local optimum is reduced. The EOM are then evaluated sequentially, giving first the acceleration, then the velocity and finally the position at each time node. The evaluated EOM provide a trajectory, using which the constraints can be evaluated, together with the constraints imposed on the controls. Finally, the performance index is calculated, after which the NLP will apply new control function coefficients.

5.3. Computational Trajectory Optimisation Implementation

The optimiser operates by changing parameters until a minimum of the performance index is achieved, considering the constraints. To reduce the calculation effort, the flight optimisation strategy employs basis functions to express functions for the controls. To finally solve the optimisation problem, a NLP tool is chosen.

5.3.1. Control Function Parametrisation

The control vector is the vector describing the controls deflections of the missile, which is adjusted to find the minimum performance index. This vector can consist of values of all control deflections at all time stepping nodes, which could results in hundreds of variables which must be optimised. To reduce the size of the control vector, parametrisation in form of basis functions is applied, where basis function parameters describe a function through time, which in turn describe all control deflections. For basis functions, an op-

timum choice for all conditions is absent (von Stryk and Bulirsch, 1992 [41]). Therefore, the choice is made to choose a polynomial for the boost phase, and splines for the sustain phase. The boost phase has a relatively short flight time of 4 seconds, for which third order polynomials are applied for the angle of attack and the sideslip control. A higher order polynomial would be a small calculation effort, however control inputs during the boost phase are expected to vary little, since only a certain velocity vector in the correct direction is to be achieved. Skidding turns generate a large drag, which in combination with the large velocity has a devastating effect on the final achieved burn-out velocity. The initial control input is also a free variable for the optimiser to adjust, which in reality can be set by the launch platform when the missile is not being fired yet. The sustain phase is subject to a larger amount of control variations, so the controls are represented by three 3^{rd} order splines, one set for each control deflection possibility. By using splines instead of single polynomials for the total time span, the Runge phenomenon is minimised. Only first order continuity conditions are imposed between the splines, as the control inputs are assumed to be able to adjust instantly. All coefficients which define the control functions are called design parameters, which together make up the design vector, which the NLP configures to minimise J (Table 5.4). Note that the first design variable is t_f, which the optimiser is able to increase or decrease. This way, the duration of the flight can be adjusted.

Table 5.4: Design Vector Parameters

Control function	Design Vector Parameter
t_f	a(1)
α	a(2:4)
β	a(5:7)
DACS_Y	a(8:14)
DACS_Y	a(15:21)
$\dot{m}_{KV}$	a(22:28)

Due to the design parameters of the controls being weights for basis functions, the imposed control constraints are evaluated after the design vector is evaluated in the EOM. This increases the calculation time compared to bounding the controls. However, the alternative is to apply actual control deflection magnitudes at all time nodes, which results in a higher amount of design parameters and therefore an even higher calculation time.

5.3.2. NonLinear Programming

A NLP solver is used to minimise the performance index. MATLAB is equipped with the function 'fmincon' (Mathworks, 2015 [22]). The use of this tool prevents extensive work in the programming of a NLP. Fmincon searches for a minimum of the objective function, by determining the local gradient of a design point. It does so, by changing the design variables and evaluating the effect on the objective. This gradient is determined for both the objective function and the imposed constraints. The applied settings for fmincon are shown in Table 5.5. The optimum is found, when either the change of J reduces below TolFun, or the design vector change decreases below TolX. TolCon sets a relaxation factor on the constraints.

Table 5.5: fmincon Options

Algorithm	SQP
TolFun	$1{\cdot}10^{-3}$
TolCon	$5\cdot10^{-5}$
TolX	$2{\cdot}10^{-3}$

5.3.3. Time Discretisation

In Chapter 3, the amount of time nodes is found to be 163. The discretisation of time is applied separately for the boost phase and the sustain phase. Since the duration of the boost phase is fixed at the $4s$, the discretisation steps do not change. The sustain phase has a variable time step during the iteration process, depending on t_f.

6

Guidance Algorithm Modelling Results

The optimisation algorithm described in Chapter 5 is the developed tool to calculate the trajectory to intercept the tracked target. To evaluate the functionality of both the optimisation routine and the NCADE, a series of simulations has been performed. In this chapter, the test cases are described and their corresponding results are presented and discussed. To clarify the different time lines, the simulation time is defined as t_s and starts when the BM is launched. The prediction time t starts from the beginning of the trajectory prediction, which is also when the NCADE is launched from the launch platform.

6.1. Boost Phase Interceptor Flight Guidance Test Cases

A set of test cases has been defined to investigate the operation of the guidance algorithm. To be able to answer the main research question, certain optimisation strategies are compared, which are defined by the different performance indices. For these performance indices, several launch locations will be adjusted, so that a wide range of launch scenarios is run. The tracking procedure is dependent on the simulation time, of which the effects are investigated as well. The following test cases are defined:

1. Minimum tracking uncertainty optimisation strategy
2. Divert cone maximisation
3. Interception probability maximisation
4. Maximum range
5. Tracking duration effects
6. Non-directed launch conditions

6.1.1. Performance Index Adjustments

The performance index in Chapter 5 defines the probability of interception. The probability is highest if J is minimised. To compare the compromise between minimising the target trajectory prediction uncertainty P_E and maximising the divert cone E, both P_E and E are optimised separately. A comparison is made to the performance index where both elements are included. A selection of launch conditions have been chosen to perform these studies.

6.1.2. Launch locations

Three headings are chosen relative to the heading of the BM, which in this simulation has a heading of 45^o. From a set of ranges, the missile is being fired from downrange, from behind, and from the side. A launch position from behind would require the interceptor to overtake the target BM, opposed to a downrange launch where the interception opportunity window would be much larger. The results of the optimisation can be compared with the sideways missile launch, which is less dependent on the horizontal distance travelled by the BM. A range from $10km$ to $50km$ will show the effects of the amount of distance which must be travelled. The launch location of the BM is randomly chosen at 48.861^o N 2.351^o E. The altitude is set as zero. Launch locations of the NCADE are placed relatively from the launch location of the BM.

6.1.3. Launch Altitudes

The altitude has a large influence on the performance of the interceptor. A lower density results in a lower drag, which increases the range which can be achieved. The NCADE is designed for high altitude interceptions, which is concluded from the DACS layout with aerospike engines consuming monopropellant (Chapter 3). The JSF fighter aircraft, due to its extended IR sensors being the example launch platform, has an estimated ceiling of $15km$ (ACCPAO, 2014 [1]). Note that the true ceiling is classified and therefore the exact value is unreliable. Three altitudes are tested, being $9km$, $12km$ and $15km$.

6.1.4. Launch Attitude and Velocity

All launches start with the correct heading relative to the launch location of the BM. The tracking filter will not be converged from the start of the simulation of the BM, but the location or at least the view angle will be measured with high accuracy. Therefore, the launch platform is assumed to be able to turn into the direction of the BM, as the tracking filter continues to converge. The IRST sensor has to be directed towards the BM for a more accurate reading than the DAS could achieve. A few cases are run to review the effects of incorrect launch directions. The cruising velocity of the launch aircraft is set as velocity magnitude, being 277.3 $^{m}/_{s}$, which is between Mach 0.9 and Mach 0.95 at the chosen altitudes. The initial path angle is set to 0° at t_0.

6.1.5. Tracking conditions

The tracking is run for the Scud Ballistic Missile, described in Chapter 4. The tracking procedure is performed once, where the initial Kalman states are randomly chosen variables, equal for all cases. At some moment in time, the prediction of the trajectory is sufficient enough to perform the trajectory optimisation calculations, when the deviation at the end of the prediction is a few kilometres. The resulting certainty score at that simulation time node can then be set as a minimum, so a threshold is defined. Next, if this condition is met, the interception can proceed. Two scenarios are tested, being the scenario when the threshold is just met, which provides a wide opportunity for interception. The second scenario is that the simulation of the BM is run until halfway, to investigate the effect of an increased quality of the trajectory prediction.

6.2. Tracking Results

The tracking procedure has been investigated in Chapter 4, where a score has been allocated for the quality of the trajectory prediction. The trajectory prediction is run a set of times, so a threshold can be determined which is usable for the guidance algorithm. A worse uncertainty ellipse will result in too large manoeuvres for the interceptor to perform, a too long tracking time will cause the BM to escape the Weapon Engagement Zone (WEZ). For this study, a threshold is found which is deemed usable for interception. A time node halfway the flight of the BM will also be used to review the effect of an increasing quality of the tracking. The EKF has been run for a duration between $t_s = 0$ and $t_s = 10s$ (Figure 6.1a), and $t_s = 11$ and $t_s = 16s$ (Figure 6.1b). The altitude is plotted against the longitude, as the latitude shows similar behaviour as the longitude. The results of the track prediction between 1 and 5 seconds are not shown, simply because the results are very far off. From $t_s = 9s$ onward, the prediction shows a similar shaped trajectory as the modelled BM. The trajectory of $t_s = 14s$ is chosen for the interception study. The uncertainty score P_E at this point increases exponentially to a maximum of almost 6 km in diameter (Figure 6.2).

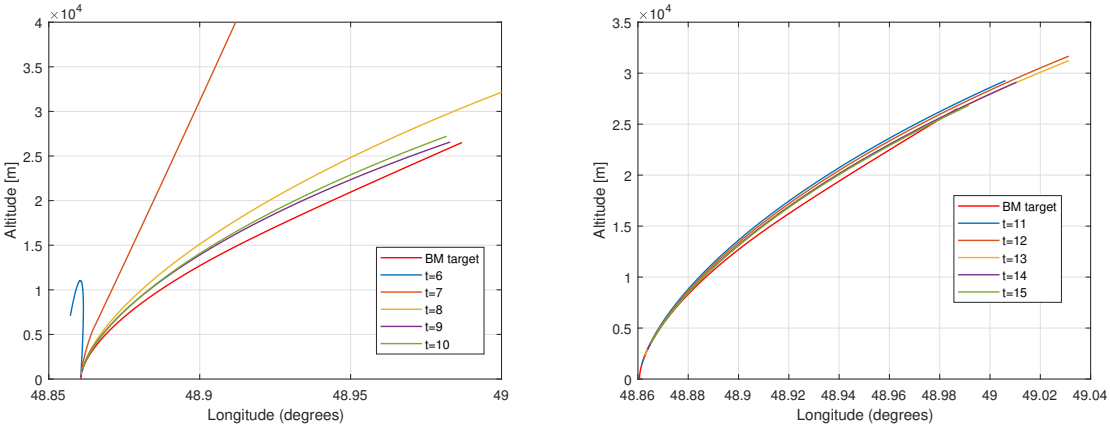

(a) Results up to 10 seconds of Tracking

(b) Results after 10 seconds of Tracking

Figure 6.1: 3D Trajectory Prediction Plots (LLA Frame)

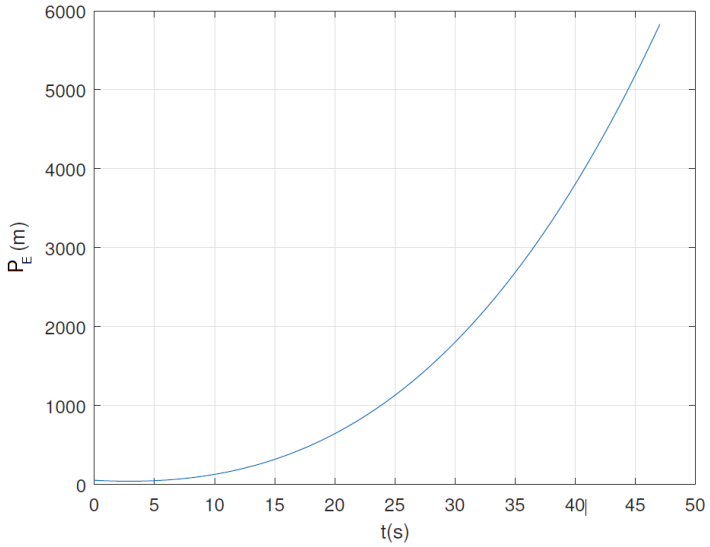

Figure 6.2: Uncertainty of the Predicted Trajectory of the BM, at t = 14s

6.3. Trajectory Guidance Results

The test cases have been set to investigate the behaviour of the trajectory guidance algorithm. First, the overall behaviour of flights have been investigated, where control inputs, states and a 3D profile of the interception are shown. Next, the performance index components are individually challenged, with first minimising the uncertainty of the target. Then, the divert cone size is maximised, and the results are compared. The optimum solution is a compromise of both, which is then investigated. A few cases have been explained for clarification of the results. The complete data of the results can be found in Appendix C.

6.3.1. Minimum Tracking Uncertainty Optimisation Strategy

A few of the test runs have been examined to review the strategy that the optimisation found to minimise P_E, and therefore t_f. Two cases are compared, the first case will be a launched with $40km$ range, $12km$ altitude, launched from behind the target, referred to as 'behind launch' (Figure 6.3). The conditions are non-optimal, as a longer distance flight must be performed starting at a non-optimum altitude. The second launch location will be downrange from a $10km$ range and $15km$ altitude, which means that the BM will head into the direction of the launch location.

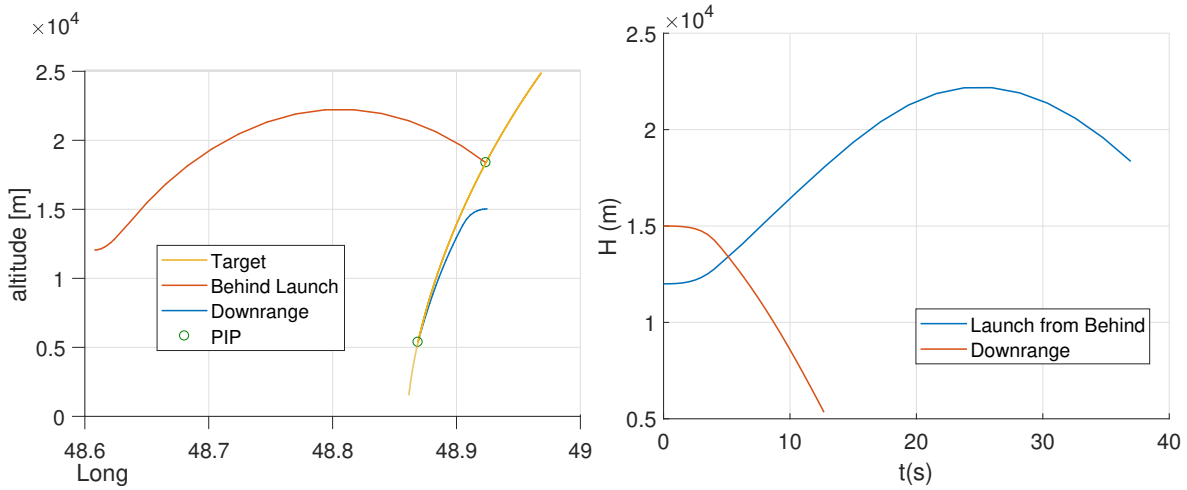

(a) 3D Trajectory

(b) Altitude

Figure 6.3: Visualisation of the Optimised Flights of the Interceptor

The 3D plot shows the difference between a small range flight and a longer range flight (Figure 6.3a). The downrange nearby launch dives down fast to keep the time to flight as small as possible. This is better shown in the altitude plot, where the dive flight is initiated during boost, and continued during the sustain phase. t_f is minimised to $12.60s$ (Figure 6.3b). The launch from behind has a much larger distance to complete. Increasing velocity by diving down would result in not being able to achieve interception, because the drag is larger due to the higher density of the surrounding air. The interceptor also takes a longer time to reach the BM's trajectory, during which the BM is able to achieve a higher altitude. Therefore, the optimiser increases altitude and applies thrust during climb. The resulting climb and descent towards the target shows a ballistic profile, and takes 37.0 seconds to complete.

Next, the consumption of propellant is investigated (Figure 6.4a). In this figure, the total mass of the active missile is plotted versus the time. The boost phase, taking $4s$, is similar for both flights, showing a fast decrease of mass. After the boost phase, the empty stage is dropped, showing a large mass decrease at an infinite small time. Next, the sustainer continues flight. The nearby launch shows a steady mass decrease, but does not consume all available propellant. This is due to the maximum control value of the thrust of $2.4^{kg}/_{s}$, as shown in Figure 6.6b, where all control inputs are plotted. The thrust of the sustain phase (3^{rd} plot) shows a steep ascend, from which it remains about the maximum value. This is also visible at the velocity plot, where velocity remains increasing (Figure 6.4b). The path angle confirms the fast dive towards the PIP (Figure 6.5a). As described before, the heading does not change much, as the launch platform is assumed to be able to turn into the correct heading before launch (Figure 6.5b). Launched from behind, the thrust maximises at $1.53{\cdot}10^{3}\ ^{m}/_{s}$ to increase the velocity. As the propellant is almost depleted at midway of the flight, both velocity and altitude are around their maximum values. The remainder of the flight is a descent towards the target.

Comparing the control inputs, the previous explained behaviour is confirmed (Figure 6.6a). The angle of attack is used to prepare the missile for the remainder of the flight. What cannot be easily explained is the large deflections of β. No notable heading changes are generated, but the deflections cause velocity decreasing forces. In Section 5, the choice for the shooting method was elaborated, where a drawback is that the optimiser tends to converge to local optima. Another drawback is the large effects of the control deflections during the first stage of the flight. The observed sideslip oscillation can therefore be set to compress the flight trajectory, without making large changes to the flight path angle. This will result in the final location constraints being satisfied, without having much influence on other flight parameters. As the range must be increased for the launch from behind, the deflections of β decrease. The deflections of the sustain phase are as expected, where the DACS deflections in z direction are applied to direct the flight path, but well within the limits, to perform a ballistically shaped flight. The y-direction is close to zero, as a large change in heading is not necessary. The forward thrust becomes for both cases at the maximum value. The advantage of applying thrust the beginning of the flight, is that velocity remains high and the decreasing mass is favourable.

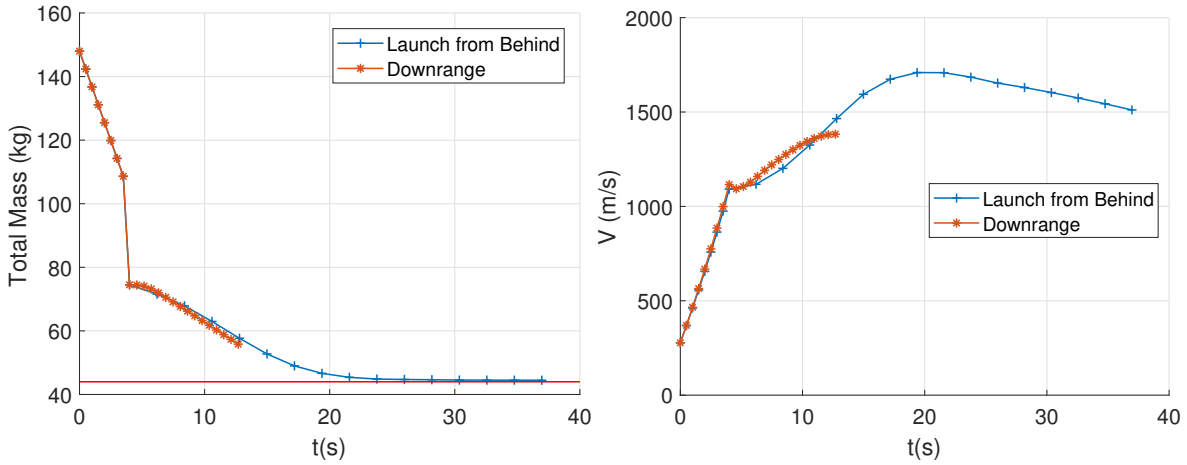

(a) Mass of the Interceptor (b) Velocity Vector (Magnitude V)

Figure 6.4: States of an Interception Flight, Both 1^{st} and 2^{nd} Stage (1)

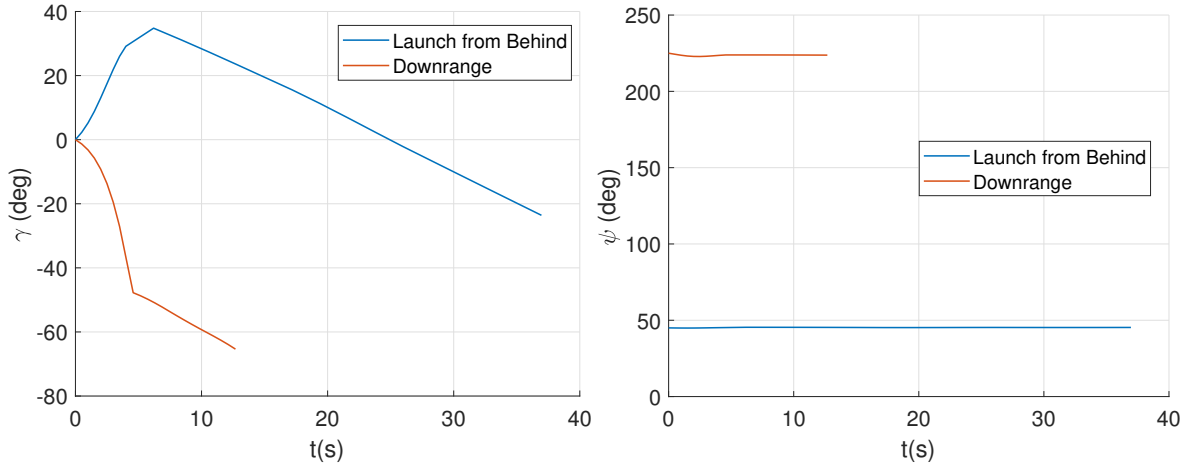

(a) Velocity Vector (Path Angle γ) (b) Velocity Vector (Heading Ψ)

Figure 6.5: States of an Interception Flight, Both 1^{st} and 2^{nd} Stage (2)

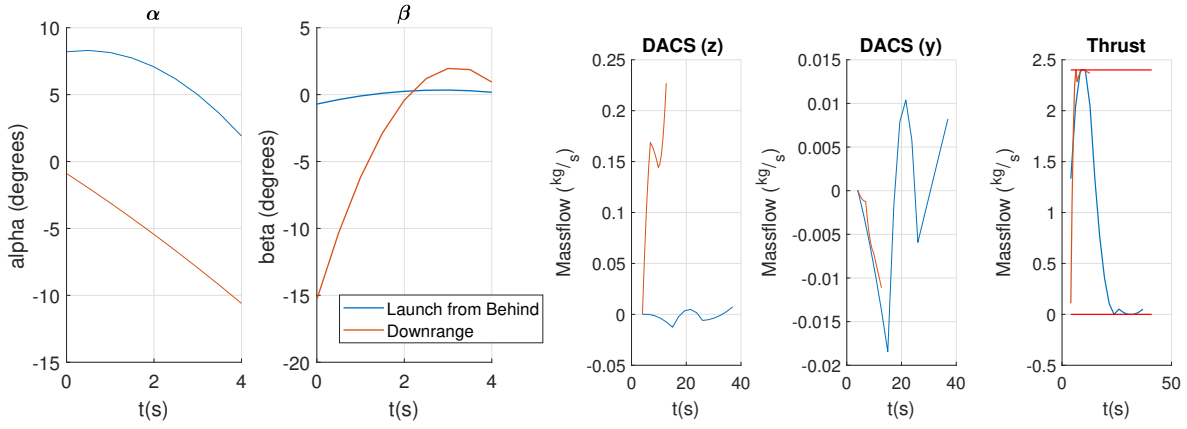

(a) 1^{st} stack (b) 2^{nd} stage

Figure 6.6: Control inputs of Interception Flights

6.3.2. Divert Cone Maximisation

The next study is to maximise divert cone E, without considering the uncertainty of the target prediction. The optimal solution for a maximised divert cone is a trade-off between velocity, altitude or reserve propellant, to obtain the widest range which the NCADE could still achieve. For the divert cone maximisation study, sideways launches are performed, so the distance flown by the BM influences the results minimal. Most interesting is how the optimiser regulates the energy balance of the missile, of which altitude and propellant are shown in Figure 6.7. The resulting flight trajectory is shown in Figure 6.8. Effort is put in minimising propellant consumption, which offers larger control inputs later in time. At the PIP ($t = t_f$), all propellant is used, but at the divert cone at $t = 0.65 \cdot t_f$ the amount of available propellant is maximised, which confirms that saving propellant is best method to increase the size of the divert cone. The altitude is also increased, because a lower amount of propellant is available for the first half of the flight, which decreases the velocity which can be achieved, so the missile must fly a propellant-saving ballistic trajectory. Since the missile flies at smaller velocities, control forces have more effect on a heading change, and the increased duration of the flight provides a larger divert cone, as a control force can be applied for a longer duration.

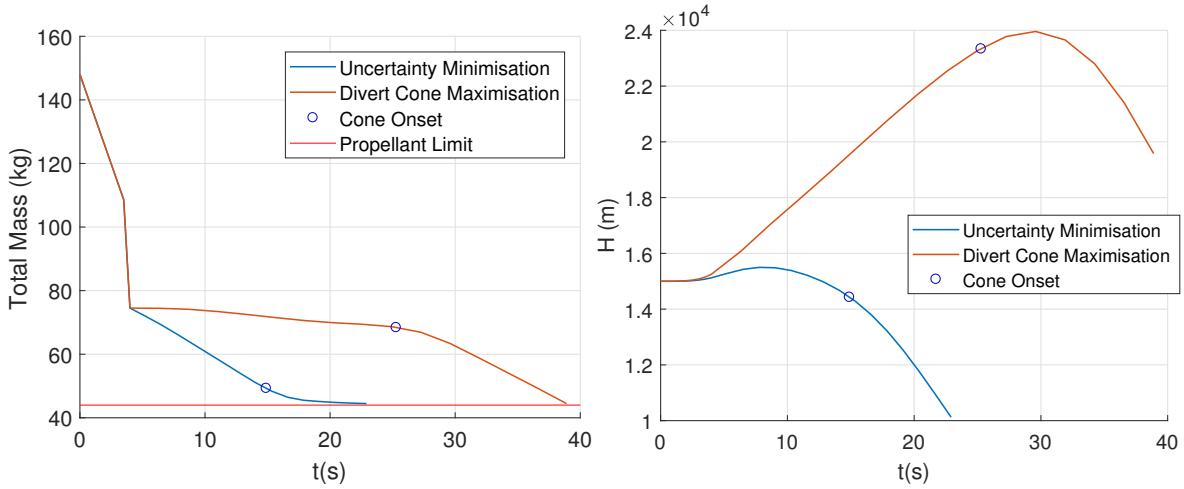

(a) Mass Comparison

(b) Altitude Comparison

Figure 6.7: Energy Plots of Maximisation of the Divert Cone

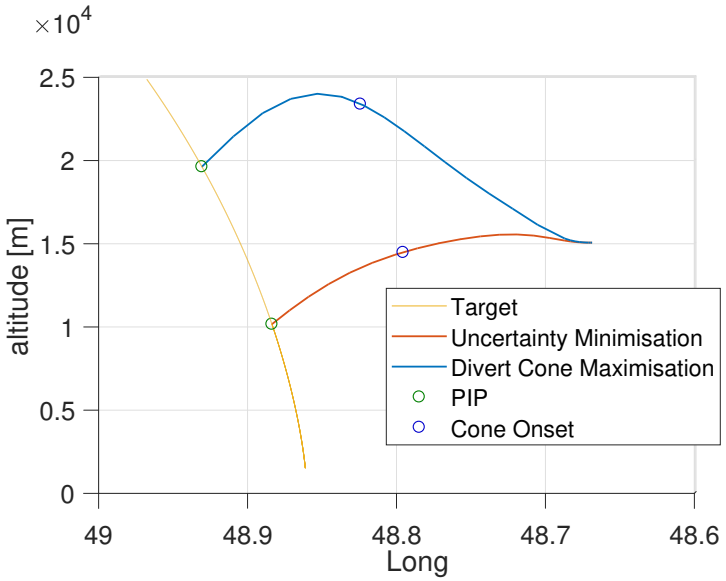

Figure 6.8: Divert Cone Maximisation Interception, 3D Trajectory

The divert cone maximisation produces very diverse results (Appendix C, Table C.4). As the range between the missile launch and the target increases, a larger portion of the propellant is required to actually reach the PIP, and cannot be applied for divert. However, a too close launch means that there a smaller time window to apply a diversion, making the divert cone smaller than that of a launch further away. The negative effect of maximising the divert cone is also visible. As lower velocities are achieved by not applying thrust and by gaining altitude, a longer time to flight is planned, which results in a higher uncertainty of the target.

6.3.3. Interception Probability Maximisation

The combination of minimising the tracking uncertainty and maximising the divert cone results in an optimum probability of interception. Downrange launches, sideways launches and launches from behind are compared. For each direction, four cases have been chosen to present the behaviour of the flight optimisation algorithm. For the weights J_D and J_E, a value of 1 has been selected (Equation 6.1). The complete set of plots of the results are shown in Appendix D.

$$J = P_E \cdot J_E - E \cdot J_D \tag{6.1}$$

Downrange Launches

A selection of downrange launches shows the complexity of the compromise between the sizes of the uncertainty ellipse and divert cone (Figure D.1a). The four cases are defined in Table 6.1, given the start conditions and the end results. The first case plotted starts at the lowest altitude. This will result in a ballistically shaped flight profile, also seen in Figure 6.3a where a longer flight has to be covered. An extra advantage for this flight strategy is the reduced velocity, which increases the divert cone size, as control forces are more effective considering heading and path angle changes. Compared to the cases of minimisation of the uncertainty ellipse (Figure 6.4a), where propellant is used as fast as possible by the thrusters, the use of monopropellant for thrust have been postponed, to about the point where $t = 0.65 \cdot t_f$ (Figure D.2a). After the time node where the divert cone is determined, propellant is applied at all four cases, decreasing t_f and therefore the uncertainty ellipse.

Table 6.1: Maximum Interception Probability, Downrange Launches Cases

Case	Distance (km)	Altitude (km)	t_f (s)	P_E (km)	E (km)
1	30	9	28.3	1.54	2.77
2	40	15	31.5	2.05	2.41
3	20	15	19.4	0.59	1.36
4	30	15	24.4	1.06	1.94

Sideways Launches

The start conditions and end results of the launches from the side are shown in Table 6.2, and the more extended results are included in the Appendix (Table C.6). Launched from the side, the effects of the horizontal distance covered by the BM are not assisting with the interception, so larger distances are to be covered compared to the downrange launches (Appendix C, Figure D.6a). This has the effect that t_f is relatively higher, and therefore the ballistic shape of the trajectory of the interceptor is more present. For these trajectories to be possible, a larger amount of propellant is required during the begin of the flight, which has the effect that a smaller amount is possible to increase the divert cone (Figure D.7a). Notable is the difference between the first and second case, which are positioned at an equal distance from the target. Case 1 has a lower altitude, so the larger density causes the missile to arrive at a later time. A larger amount of propellant is required to cope with the increased drag. Case 2 starts higher, so it requires a smaller effort to glide down towards the target. The larger velocity however causes a smaller divert cone, but the lower t_f compensates for this effect (Figure D.7b). Common with the downrange launches, is the velocity dip at $t = 0.65 \cdot t_f$ for the nearby launches, to increase the effectivity of the control inputs and therefore to increase the size of the divert cone. As the distance increases, this tactic will take more time, so the altitude is increased, giving the highest altitudes at $t = 0.65 \cdot t_f$.

Table 6.2: Maximum Interception Chance, Sideways Launches Cases

Case	Distance (km)	Altitude (km)	t_f (s)	P_E (km)	E(km)
1	20	9	23.0	0.91	1.67
2	20	12	21.9	0.80	1.51
3	30	12	27.5	1.44	2.13
4	40	15	34.0	2.49	2.64

Launches From Behind

Four cases have been chosen for the launches from behind, shown with their results in Table 6.3. In this scenario, the BM moves horizontally away from the interceptor, requiring a longer flight at the investigated launch distances. This can be observed in the 3D flights of three of the four cases (Figure D.11a). Case 4, fired from 40km away, has the largest distance to cover. The monopropellant decreases the fastest from all cases to increase the velocity to be able to achieve interception (Figures D.12a and D.12b). The maximum achieved altitude is about 23 km, which is the highest of the investigated cases (Figure D.11b). Case 1, fired closest of the four cases, shows an increase in altitude, increasing the divert cone. It has the lowest velocity of all cases, retaining a large portion of the monopropellant to increase the divert cone. P_E is increased, however case 1 has a lower interception chance compared to case 2, launched from further away. Decreasing the altitude decreases the possibility to divert as the remaining distance decreases. Due to the BM moving away, more space becomes available to extend the divert cone, from which can be concluded that shooting from a nearby distance does not automatically result in a better interception chance, given the specific solid booster phase of the NCADE which increases the velocity to very high values. This is also confirmed by the control inputs of the nearby case (Figure D.14). The sideslip angle reaches its limits, to decrease the velocity as much as possible. The inputs of the DACS are maximised in positive z direction, to make the ballistic arc as tight as possible. The third case shows an interesting optimum. The ballistic shape is not required as the launch altitude is already 15 km. Focus has been shifted towards the minimisation of the time to flight. To achieve the smallest t_f of the investigated cases, the NCADE applies a relative large amount of monopropellant. As an effect, the divert cone is relatively small. This shows the very different solutions for each launch condition.

Table 6.3: Maximum Interception Chance, Behind Launches Cases

Case	Distance (km)	Altitude (km)	t_f (s)	P_E (km)	E(km)
1	10	9	26.1	1.27	2.18
2	20	12	24.7	1.1	2.23
3	20	15	21.0	0.73	1.5
4	40	15	29.2	2.3	1.3

6.3.4. Maximum Range

The missile has been tested for a set of launch conditions, up to 50km downrange. It would be interesting to review the range limitation of the NCADE for the scud missile. The maximum range study will be conducted with downrange missile launches, as the horizontal distance covered by the BM helps with closing in. The launch altitude will be the ceiling of the JSF of $15km$. As seen from the velocity vector, the launches from further away are shaped ballistically, which is initiated by a control input resulting in a larger drag force during boost. Therefore, an initial path angle of 25^o is provided and to further assist interception, velocity is increased to a supersonic 354 $^m/_s$. The 3D plot of the long range interceptions is shown in Figure 6.9. The interception fails after a range of $90km$. This is not necessarily due to the NCADE not being able to achieve the range, however, the boost phase of the BM is finished at $t_f = 47s$, which is too soon to intercept from further away. The NCADE reaches an altitude of almost $30km$, due to its large fuel to weight ratio, giving an empty weight of only $44kg$ (Figure 6.10). The application of propellant is almost similar for all cases, as the longest range is reached by applying all available resources into thrust, decreasing overall weight and reaching the largest altitude. Note that the launch conditions are ideal for this case. When the NCADE is pushed further over its limits, constraints will be violated, resulting in a combination of not reaching the target with negative propellant amounts.

Figure 6.9: Maximisation Interception Range, 3D Trajectory

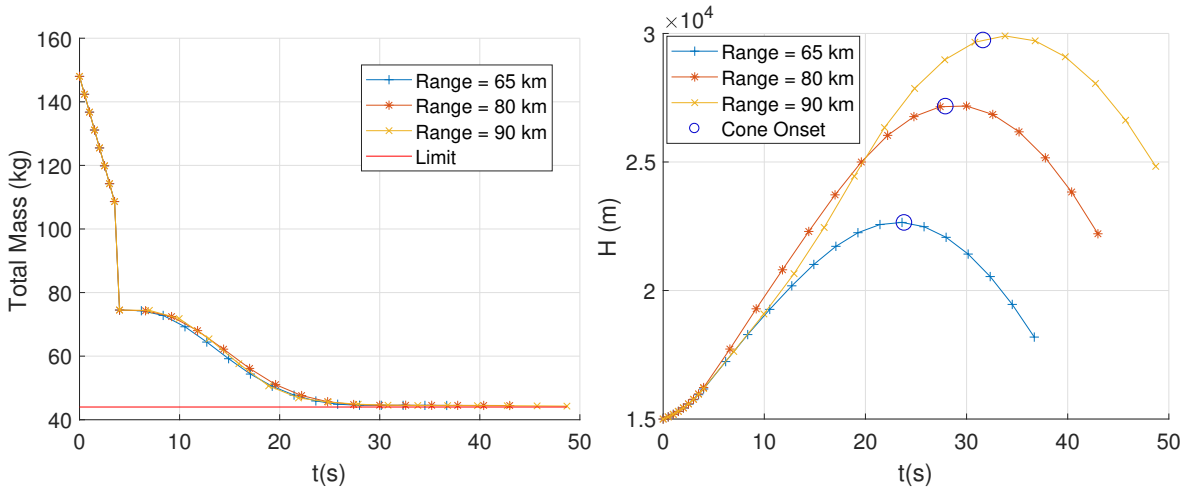

(a) Mass Comparison (b) Altitude Comparison

Figure 6.10: Energy Plots of the Maximum Range Trajectories

6.3.5. Tracking Duration Effects

The target track prediction reliability improves when more data is gathered and the Kalman states converge, so an improved track prediction can be performed. The actual tracking duration is not included in the guidance algorithm performance index, to avoid wishful thinking of the algorithm that the prediction reliability improves. This means that the guidance algorithm would not consider trajectories with a longer duration to wait for the filter to converge. It is however valuable to review the effects of launching at a later time step, so instead of $t_s = 14s$, $t_s = 30s$ is the time step of launch of the NCADE. The launch locations from behind are used, with the same launch attitudes.

The 3D plot comparison shows that the optimiser focuses less on the minimisation of t_f, as P_E has improved (Figure 6.11b). From both launch distances, the missile aims for a higher altitude, to increase E. This is also shown in the mass plot (Figure 6.11a), where the 10 km distance launch is able to deploy a larger amount of propellant than the reference launch. The launches further away from the BM are more similar, as the velocity must be sufficient to reach the target in time. The reason why this comparison does not consider any launches further from the BM, is that there is not sufficient time to actually accomplish interception.

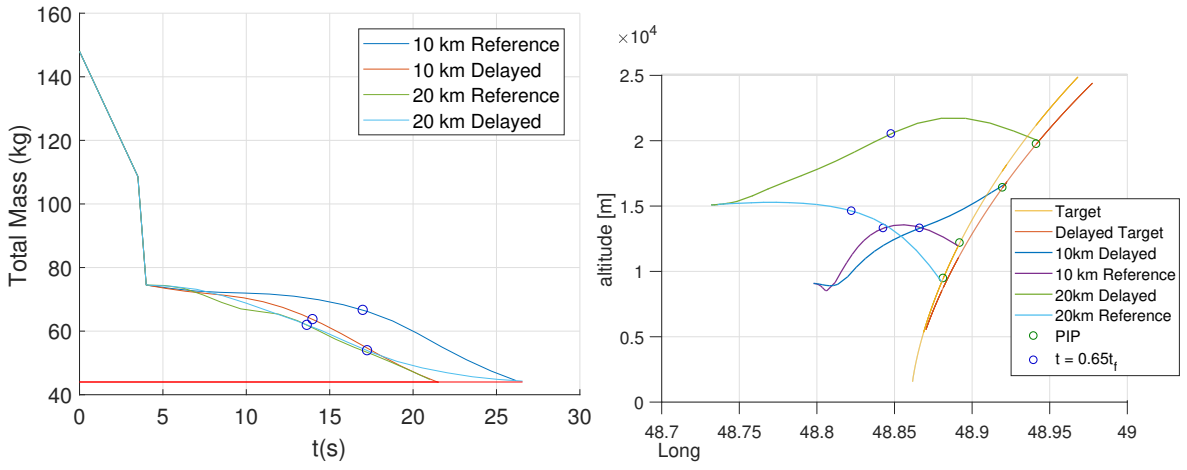

(a) Mass (b) 3D Plot

Figure 6.11: Comparison Between the Reference $t_s = 15s$ and the Delayed $t_s = 30s$ Tracking Time

6.3.6. Non-Directed Launch Conditions

The launch heading is assumed to be directed towards the target, as the launch platform is assumed to achieve the best attitude when the tracking procedure is performed. During the tracking procedure, the track prediction is unreliable as the derived Kalman states of the BM did not converge yet, but the location is directly found by an IR sensor and accurate enough for the fighter aircraft to turn into the correct launch heading. The launch heading is for this study changed, to explore the behaviour of the optimiser (Table C.9). The most interesting case is shown in Figure D.16a, where a heading shift of 90^o is applied at the launch conditions, where the missile has been launched from the side of the BM's trajectory. The missile is barely able to reach the target. Launches fired from further away or at lower altitudes start to violate the enforced constraints. Reviewing the inputs of the control system, the NCADE applies a sideslip angle to turn towards the target, sacrificing the velocity, which results in the t_f to increase. This will lead to a PIP at a higher altitude and therefore reducing the size of the divert cone. Comparing the two launches, both the target uncertainty and the divert cone size are worsened greatly when the missile is not pointing towards the target when launched.

6.4. Observations and Conclusions

The test cases have been run and analysed. Most interesting was how the optimiser handled the uncertain BM's trajectory prediction, which answers the main research question of this thesis work. The chosen optimisation strategy is evaluated as well.

6.4.1. Tracking

A certain threshold for the EKF to converge has been found, which gives a P_E of a few kilometres at the end of the BM's boost phase. A study shows that longer tracking periods will increase E and decrease P_E, at the cost of the WEZ to decrease, both due to the lower time available for interception, and the higher altitude which must be achieved. Since it is also concluded that nearby launches try to reduce velocity to increase the divert cone, it could be favourable for the NCADE to wait a longer period than the allocated $14s$. The divert cone is increased by either saving propellant for the longer ranged flights, or by creating extra drag, reducing velocity to increase flight time, and therefore improve the effects of the control inputs. Both strategies have as effect that t_f increases, which results in the tracking result to improve further during the flight.

6.4.2. Shooting Method

The disadvantages of applying the shooting method, found in literature, where also confirmed in the interception simulations. The first seen disadvantage is that convergence to a local optimum is more present. Velocities, headings and control inputs show some oscillatory behaviour, where optimum solutions would be expected to show much more gradual behaviours. The second observation was that the control inputs during the beginning of the flight have great influence in the final location where the missile ends. This translated to a sideslip control input to the left and right during the boost phase, where the achieved heading change is negligible. This is a quick fix to satisfy the constraints, as the angle of attack has also an effect on the achieved path angle, resulting in more drastic changes to the final position of the missile. Still, an optimum answer the optimisation problem has been found.

6.4.3. Uncertainty Handling

The uncertainty is handled by applying a performance index of the optimiser which maximises the interception probability. It does so by minimising the $\sigma = 1$ uncertainty ellipse P_E of the BM track prediction tool, and by maximising divert cone E which the NCADE still is able to achieve, which is determined at 65% of the flight duration. These two oppose each other, as P_E decreases, time to flight t_f decreases, which can be achieved by using all available propellant as fast as possible. E grows as the amount of available propellant is larger, so the final solution is a compromise of both. This results in the trajectories to be still aiming for a low t_f, retaining a larger amount of propellant at the $t = 0.65t_f$ mark. Reserving a larger amount will result in lower velocities which results in a higher t_f. Also, since the altitude of the target increases at increasing rates, a smaller t_f results in a lower amount of energy to be required. Divert cone E is increased by saving propellant. At nearby launches, the divert cone is increased by applying sideslips, as the decreased velocity allows for a longer flight, where the control inputs have more effect. Launching from further away, this effect decreases.

6.5. Validation

True validation is unfortunately not possible, since a prototype of the NCADE does not exists to the best knowledge of the author. If data becomes available for the NCADE if it is actually build and tested, the resulting performance will not be made available to the public, further complicating the ability for validation.

7

Conclusions

The main research question is formulated as:

How can the guidance of an air launched missile with the purpose of intercepting a ballistic missile in its boost phase be developed, by applying a flight trajectory optimisation algorithm to cope with the uncertainties of the prediction of the ballistic missile's trajectory?

The answer is provided by first investigating the current technologies of ballistic missile defence. Next, a dedicated air launched interception missile has been modelled, after which the tracking procedure has been implemented. A trajectory optimisation strategy is found and a study is performed to investigate the tactics the optimiser finds to cope with the trajectory prediction uncertainties.

7.1. Conclusions

The literature study found the current state of ballistic missile defence, which is most commonly performed by launching an intercepting missile towards the threat. Development of this kind of missiles tends toward more precise guidance, so that a smaller warhead is required, or a warhead is even absent. This increases the deployability of the defence systems. The development in trajectory optimisation has been investigated, where a distinction between indirect and direct methods has been made. Indirect methods provide a precise answer after a case-specific mathematical derivation, where a direct method is chosen in this study to better cope with different launch scenarios and flight conditions.

A study has been performed earlier to model the NCADE, a dedicated BM BPI in development [10]. The NCADE is a two stage air launched missile, which outer shape is based on the AMRAAM AIM 120D. It is equipped with a fast-burning booster for a high initial velocity, after which the kill vehicle proceeds with the interception. The DACS provides control possibility by means of monopropellant thrusters. The EOM have been set up, for which the remaining assumption have been performed. The assumptions considered the performance system and the control system. An empirical software package has been used to find the aerodynamic coefficients, and the equations are verified using a different but validated Simulation program.

A tracking algorithm was made during an earlier study, which applied an EKF [31]. The error resulting from the sensors has been updated to be more realistic than the original random error, by making assumptions of the used IR technology. The sensor disturbance itself shows a limited influence on the BM boost phase track prediction results. The trajectory prediction score has been investigated by defining the determinant of the Jacobian. The uncertainty of the track prediction has been forwarded to the missile system by means of an uncertainty ellipse. The trajectory prediction score improves with longer tracking durations, or shorter trajectory prediction periods.

Next, the flight optimisation strategy has been defined. The complexity of both the target and the control system motivated the choice to apply trajectory optimisation. The performance index to be maximised is the interception probability, measured by a distance. The interception probability is calculated by subtracting the divert cone size, providing the divert possibility of the interceptor at $t = 0.65\,t_f$, from the uncertainty ellipse of the target's trajectory prediction. Due to the uncertainty of the target and the non-linear behaviour of the two stage missile, the indirect method was deemed unsuitable for the problem, as adapting boundary conditions

require updates of the mathematical derivation. The direct collocation method was initially chosen, however implementation posed problems, which presented itself in the divergence of the equality constraints linking the states and controls of the candidate solutions. Therefore, the shooting method has been applied. The NLP algorithm used is Matlab's 'fmincon.' Constraints are applied to find a PIP on the trajectory prediction, so that interception is enforced. The t_f is set free so that an optimum can be found at all times and locations of the BM's predicted trajectory. Constraints are further applied to limit the control inputs and to prevent the guidance algorithm from generating errors, due to for example negative velocities. Basis functions are applied for the five controls of the NCADE, giving α and β control polynomial functions for the boost phase, and splines for the DACS and thrust for the sustain phase, for the purpose of reducing calculation load.

The guidance algorithm has been tested for multiple cases, where variation is applied for launch position, tracking conditions and performance index. The trajectory prediction becomes less reliable when t_f is increased. The strategy to intercept without considering the divert cone is to use all monopropellant as soon as possible, increasing the velocity to a maximum and therefore to minimise t_f. At the maximum interception probability strategy, some of the initial thrust is traded off to increase the divert cone size. Besides saving propellant, the velocity is decreased by either increasing the drag during the boost phase for nearby launches, and/or by increasing the altitude. Increasing the altitude also reduces propellant consumption due to lower drag, increasing the saved propellant. When launched from nearby, the divert cone is larger than the $\sigma = 1$ uncertainty ellipse, which difference decreases when launched from further away, depending on the direction.

7.2. Recommendations

The main conclusion of this thesis is the behaviour of the interceptor, given an uncertain prediction of the target's trajectory. During the thesis work, potentially new research subjects have been identified, described below.

7.2.1. Radar Integration

As explained in Chapter 4, radar is assumed to be applied for measuring the distance from the launch platform to the BM, because the NCADE features a protective cap over the IR sensor. Also, when the distance between the NCADE and the launch platform is initially small, the noise of the sensor combination is too large for the filter to work, as both sensors provide about the same reading. The applied EKF however does not feature a model of a radar, which would increase the authenticity of the model.

7.2.2. Kalman Filtering and Track Prediction

The applied Kalman Filter shows room for improvement. The reasoning for the choice of the Kalman Filter itself has not been clarified, so perhaps other tracking algorithms could suit the filtering of the process better. The Batch-Least-Squares algorithm shows promising results [32]. Another improvement idea is to provide the filter with a better understanding of BMs. The initial guesses first used are a lot different from the real values, which could be concluded from the initial measurements. The track prediction tool could be more specified for use on BMs, preventing for example the first prediction results from going through the centre of the earth.

7.2.3. Time Lines

This thesis work focused on the guidance algorithm, by applying trajectory optimisation for a single static simulation time. This means, given one ballistic missile trajectory prediction with its uncertainty cone, and given the launch location of the fighter aircraft, a trajectory is calculated for the interceptor, which considers the tracking quality and its own divert possibility. A fixed tracking quality threshold is defined, after which the missile launch is initiated to intercept as fast as possible. Extending the launch time however will improve the tracking quality of the EKF, and therefore more chance to a certain trajectory prediction. Decreasing the threshold could be usable if the distance is large. Two questions appear: the first being how long the missile should wait before launching. As seen in the results, waiting for a longer period will result in a smaller chance of actual hitting the BM, of which the velocity, altitude and acceleration increases. The second question will be what the launch vehicle can do during this time period. It could use its available engine power to accelerate closer, increase altitude or even decrease power if the target is already close. This can make the optimisation a whole lot more complex.

7.2.4. Collocation

A large portion of the thesis work was the failed attempts to implement the collocation method. Collocation is argued to be the most suitable optimisation strategy, as computations are faster than the shooting method and the tendency for reaching a local optimum is minimised.

Bibliography

[1] Air Combat Command Public Affairs Office ACCPAO. F-35a lightning ii, apr 2014. https://www.af.mil/About-Us/Fact-Sheets/Display/Article/478441/f-35a-lightning-ii-conventional-takeoff-and-landing-variant/.

[2] Arrow-Tech. Arrow tech software products catalog, jun 2013. http://www.prodas.com/.

[3] Florios Bardanis. Kill vehicle effectiveness for boost phase interception of ballistic missiles. Master's thesis, Monterey, California. Naval Postgraduate School, jun 2004.

[4] John T. Betts. Survey of numerical methods for trajectory optimization. *Journal of Guidance, Control and Dynamics*, 21(2):193–207, apr 1998.

[5] Missile Defense Project CSIS, nov 2016.

[6] Marnix F.E. Dillenius Daniel J. Lesieutre, John F. Love. Recent applications and improvements to the engineering-level aerodynamic prediction software misl3. *AIAA Aerospace Sciences Meeting & Exhibit*, 40, jan 2002.

[7] Tom P. Thorvaldsen David A. Benson, Geoffrey T. Huntington and Anil V. Rao. Camtos - a software suite combining direct and indirect trajectory optimization methods. 29, nov 2006.

[8] Maruizumi Haruki Ayabe Muneo Fukuchi B. Apollo, Nagase Sakae. Han/hn-based monopropellant thrusters. *Engineering Review*, 43(1):22–28, 2010.

[9] M. Guelman and O.M. Golan. Minimum energy guidance for boost phase ballistic missile interception. *American Control Conference Seatlle*, jun 1995.

[10] B.Sc. Ir. B.J.N van de Laar Ir. M. Brodecki Dr. Ir. H.M.A. Schleijpen Halswijk, J.S.F. Kerkkamp and Drs. K.W. Benoist. Fifth generation fighters in a bmd role. 1(0.1), 2014. Confidential.

[11] C.R. Hargraves and S.W. Paris. Direct trajectory optimization using nonlinear programming and collocation. *Journal of Guidance*, 10(4):338–342, 1987.

[12] He Huang and Zhifu Zhu. Guidance law design for space-based anti-missile boost phace intercept. *Advanced Materials Research*, 301-303:1749–1753, jul 2001.

[13] H. F. R. Schöyer J. W. Cornelisse and K. F. Wakker. *Rocket Propulsion and Spaceflight Dynamics*. Pitman, 1979.

[14] Robert S. Jankovsky. Han-based monopropellant assessment for spacecraft. *AIAA*, 96(2863), 1996.

[15] John P. Janus. Homing guidance (a tutorial report). Technical report, Aerospace Corporation, dec 1964.

[16] Julie L. Webster John C. Lonnquest, David F. Winkler. *To Defend and Deter: The Legacy of the United States Cold War Missile Program*. Department of Defense Legacy Resource Management Program, nov 1996.

[17] Northrop Grumman: Janis Lamar. An/aaq-37 distributed aperture system (das) for the f-35, 2017. URL `http://www.northropgrumman.com/Capabilities/ANAAQ37F35/Pages/default.aspx`.

[18] Daniel J. Lesieutre. Prediction of sparrow missile aerodynamic characteristics with a non-linear engineering-level missile prediction method. *AIAA Applied Aerodynamics Conference*, 35(3399), 2017. http://www.nearinc.com/pubs/AIAA-2017-3399.pdf.

[19] Zheng Liang Lu. *Ballistic Missile Interception from UCAV*. Naval Postgraduate School, dec 2011.

[20] John A. Lukacs. *Hit-To-Kill Guidance Algorithm for the Interception of Ballistic Missiles in the Boost Phase*. Naval Postgraduate School, jun 2006.

[21] P. Mantle. *The Missile Defense Equation*. American Institute of Aeronautics and Astronautics, mar 2004.

[22] Mathworks. Mathworks fmincon documentation (r2015b), 2015. Accessed 06-11-2017.

[23] D. Maynes and G. A. Gebert. High-angle-of-attack aerodynamics of a missile geometry at low speed. *Journal of Spacecraft and Rockets*, 36(5):772–774, oct 1999.

[24] Thomas L. Moore. Solid propulsion enabling technologies and milestones for navy air-launched tactical missiles. *American Institute of Aeronautics and Astronautics*, sep 2011.

[25] F. William Nesline and Paul Zarchan. A new look at classical vs modern homing missile guidance. *Journal of Guidance, Control and Dynamics*, 4(1):78–85, 1981.

[26] Micheal J. Neufeld. *The Rocket and the Reich*. The Free Press, 1995.

[27] Mark B. Milam Nicolas Petit and Richard M. Murray. Inversion based constrained trajectory optimization. *IFAC Proceedings Volumes*, 34(6):1211–1216, 2001.

[28] Andreas Parsch. Directory of u.s. military rockets and missiles, western electric sam-a-7/m1/mim-3 nike ajax, 2001. URL `http://www.designation-systems.net/dusrm/m-3.html`.

[29] Andreas Parsch. Directory of u.s. military rockets and missiles, aim-120, 2007. URL `http://www.designation-systems.net/dusrm/m-3.html`.

[30] Theodore A. Postol. Size of boost-phase region of ballistic missile flight. Technical report, Carnegie, jun 2001.

[31] E.J.P. Riegman. Boost phase ballistic missile target characterization using the ncade system, nov 2016.

[32] Haywood Satz and Thomas H. Kerr. Comparison of batch and kalman filtering for radar tracking. *AIAA/BMDO Technology Conference*, 1, jul 2001.

[33] H. M. A. Schleijpen. Interview with tno electronic defence technology scientist dr. ric h. m. a. schleijpen (personal communication). Interview, dec 2017.

[34] R. Simpson and J. Revell. Towards a taxonomy of performance metrics, bounds and tests for tracking and slam algorithms. *4th SEAS DTC Technical Conference - Edinburgh*, 2009.

[35] George M. Siouris. *Missile Guidance and Control Systems*. Springer, 2004.

[36] Everett Tackett. Raytheon, aerojet test new propulsion system for air-launched missile defense system, may 2006. URL `http://investor.raytheon.com/phoenix.zhtml?c=84193&p=irol-newsArticle&ID=999828`.

[37] Christian Funk Thomas Tyrell and Nagy Marton. Aim-120c-5 performance assessment for digital combat simulation enhancement. Revision 2, 2014.

[38] TNO. Math tools. Matlab Scripts, jan .

[39] TNO. Simulink generic missile model, aug 2012.

[40] H.G. (Dries) Visser. *Aircraft Performance Optimisation (AE4447)*. Lecture Notes. TU Delft, jan 2014.

[41] O. von Stryk and R. Bulirsch. Direct and indirect methods for trajectory optimisation. *Annals of Operations Research*, 37:357–373, 1992.

[42] Mark Wade. R-11, jul 2016. URL `http://www.astronautix.com/r/r-11.html`.

[43] Haiyan Wang Zhigang Yang Yilin Jiang, Qi Tong and Qingbo Ji. Image recovery of an infrared sub-imaging system based on compressed sensing. *Symmetry*, 9(11):260, nov 2017.

[44] He Yingbo and Qiu Yong. Thaad-like high altitude theater missile defense: Strategic defense capability and certain countermeasures analysis. *Science & Global Security*, 11(2-3):151–202, jun 2010.

A

NCADE Model Assumption Data

In this appendix, all assumptions of the NCADE are summarised. Note that the found design impressions could deviate from the final design of the NCADE. The first stack is the combination of the boost stack and the kill vehicle, where the second stage is the kill vehicle only.

A.1. Dimensions

The missile system exists of two stages, with wings mid of the stack or aft at the second stage, and controllable fins aft of the first stage. The ogive of a missile defines the shape of the nose.

Table A.1: NCADE Dimensions Assumptions

Parameter	Value
Total length	$3.65 \cdot 10^3 mm$
Booster stage length	$1.676 \cdot 10^3 mm$
Sustainer stage (2^{nd}) length	$1.9740 \cdot 10^3 mm$
Diameter (excluding fins)	$1.8 \cdot 10^2 mm$
Wing span	$4.5 \cdot 10^2 mm$
Wing root chord	$3.02 \cdot 10^2 mm$
Wing tip chord	$84\ mm$
Wing thickness	$5\ mm$
Fin span	$4.5 \cdot 10^2 mm$
Fin root chord	$3.20 \cdot 10^2 mm$
Fin tip chord	$1.68 \cdot 10^2 mm$
Fin thickness	$5\ mm$
Ogive Length	$4.5 \cdot 10^2 mm$

A.2. Mass

THe Empty mass of the first stage includes the total mass of the second stage

Table A.2: NCADE Mass Assumptions

Parameter	1^{st} stage	2^{nd} stage
Total mass	$148\ kg$	$74\ kg$
Propellant mass	$45\ kg$	$30\ kg$
Empty mass	$103\ kg$	

A.3. Propulsion

Table A.3: NCADE Propulsion Assumptions

Parameter	1^{st} stage	2^{nd} stage
Isp	250 s	230s
Max. mass flow	11.25 $^{kg}/_{s}$	2.4 $^{kg}/_{s}$
Max. thrust	$2.76{\cdot}10^{4} N$	$5.41{\cdot}10^{3} N$

A.4. Controls

Table A.4: NCADE Control assumptions

Parameter	Value
Maximum AoA (1^{st} stage)	30^{o}
Maximum sideslip (1^{st} stage)	30^{o}
Maximum DACS thrust	$1.20{\cdot}10^{3} N$
Maximum DACS divert mass flow	0.53 $^{kg}/_{s}$

A.5. Sensor

Table A.5: Infrared sensor Assumptions

IR Sensor	Pixels	FOV	IFOV
JSF (DAS)	1024x1024	90^{o}	1.534 mrad
JSF (EOTS)	1024x1024	6.0^{o}	0.1023 mrad
NCADE	256x256	3.0^{o}	0.205 mrad

B

NCADE Aerodynamic Coefficients

This Appendix contains an extended set of aerodynamic coefficient plots of the NCADE model, generated using PRODAS software.

B.1. Boost Stage Results

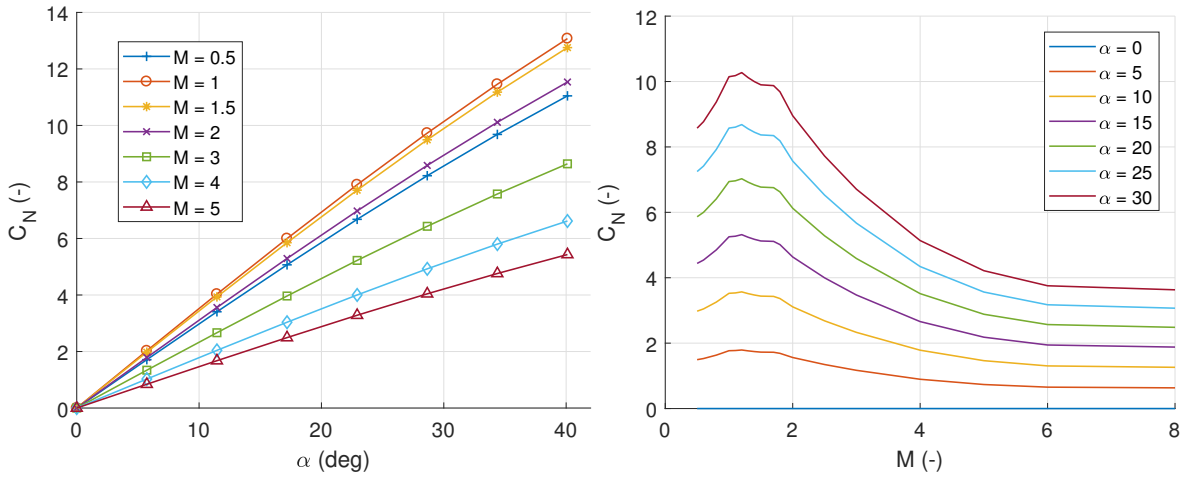

(a) Plot with the Angle of Attack on the x-axis, at Various Mach Numbers

(b) Plot with the Mach Number on the x-axis, at various Angles of Attack

Figure B.1: Normal Coefficient plots, 1^{st} stage

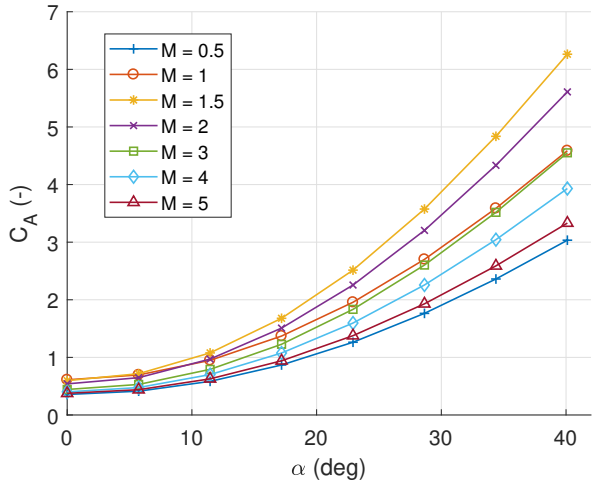

(a) Plot with the Angle of Attack on the x-axis, at Various Mach Numbers

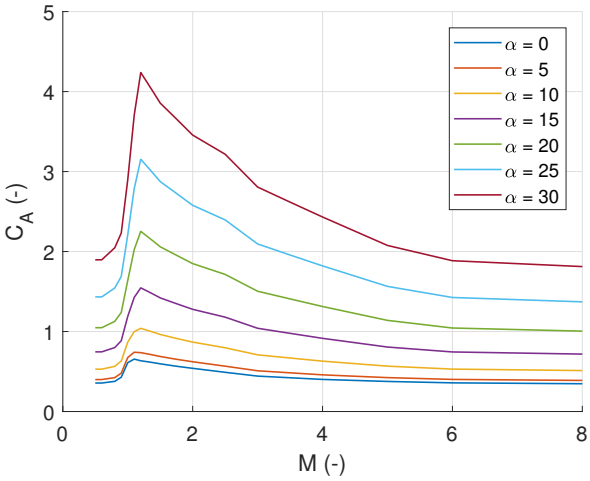

(b) Plot with the Mach Number on the x-axis, at various Angles of Attack

Figure B.2: Axial Coefficient plots, 1^{st} stage

B.2. Sustain Stage Results

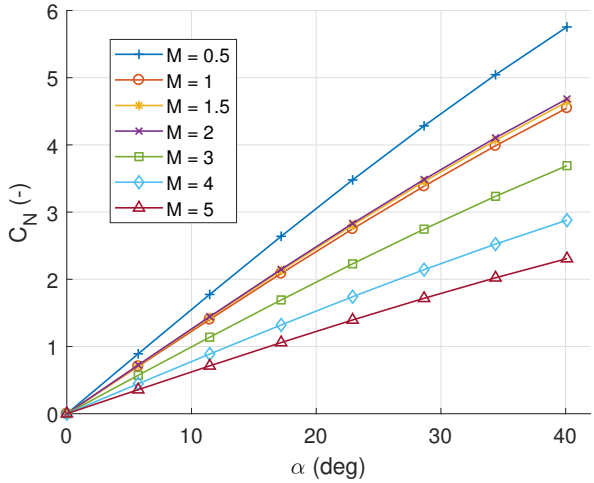

(a) Plot with the Angle of Attack on the x-axis, at Various Mach Numbers

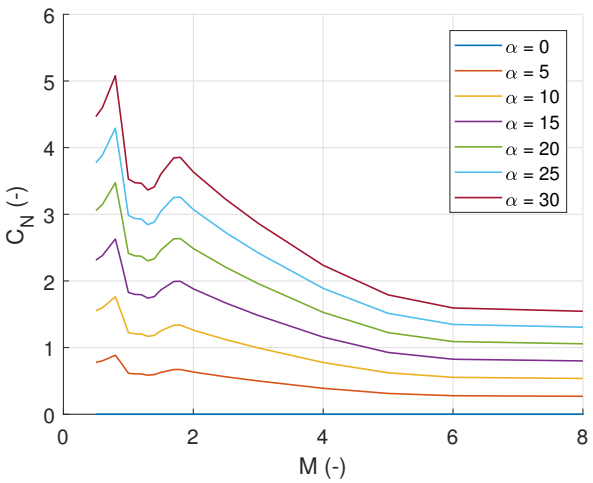

(b) Plot with the Mach Number on the x-axis, at various Angles of Attack

Figure B.3: Normal Coefficient plots, 2^{nd} stage

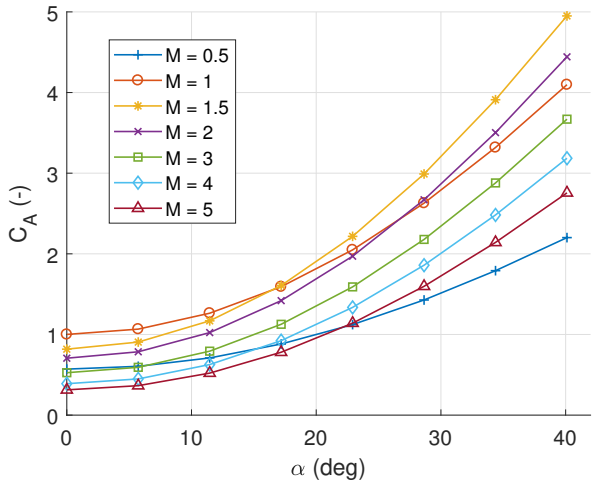

(a) Plot with the Angle of Attack on the x-axis, at Various Mach Numbers

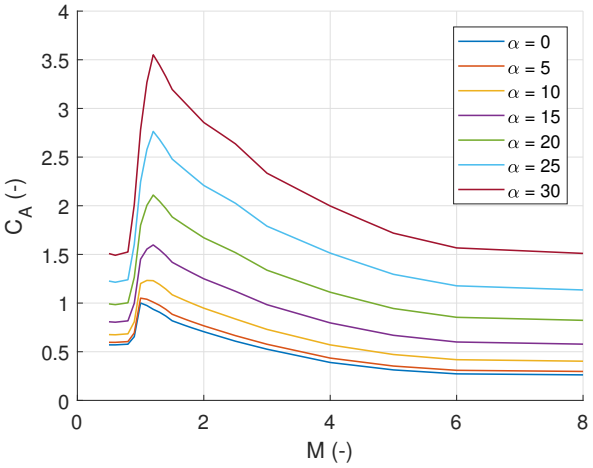

(b) Plot with the Mach Number on the x-axis, at various Angles of Attack

Figure B.4: Axial Coefficient plots, 2^{nd} stage

C

Trajectory Guidance Result Tables

C.1. Minimum Target Trajectory Prediction Uncertainty

The first set of results is for the minimisation of the certainty ellipse P_E, without considering the divert cone E.

Table C.1: Minimum Target Trajectory Prediction Uncertainty Results, Fired Downrange

Launch Conditions		Results		
Distance (km)	Altitude (km)	t_f	P_E (km)	E (km)
10	9	10.7	0.15	0.37
10	12	11.7	0.18	0.4
10	15	12.7	0.21	0.49
20	9	17.0	0.43	0.97
20	12	16.8	0.41	1.01
20	15	16.8	0.42	1.05
30	9	23.3	0.94	1.25
30	12	22.1	0.82	1.35
30	15	21.4	0.76	1.36
40	12	27.4	1.43	1.28
40	15	25.6	1.20	0.87
50	15	31.3	2.02	1.26

Table C.2: Minimum Target Trajectory Prediction Uncertainty Results, Fired Sideways

Launch Conditions		Results		
Distance (km)	Altitude (km)	t_f	P_E (km)	E (km)
10	9	11.2	0.16	0.4
20	9	18.4	0.52	1.16
20	12	17.8	0.48	1.07
30	9	25.7	1.21	0.88
30	12	24.6	1.09	1.33
30	15	22.9	0.9	1.01
40	12	31.2	2.00	1.16
40	15	29.5	1.73	1.28
50	15	36.4	2.98	1.53

Table C.3: Minimum Target Trajectory Prediction Uncertainty Results, Fired From Behind

Launch Conditions		Results		
Distance (km)	Altitude (km)	t_f	P_E (km)	E (km)
10	9	12.1	0.19	0.5
10	12	12.7	0.21	0.58
10	15	13.7	0.25	0.65
20	9	20.7	0.7	1.25
20	12	19.4	0.59	1.31
20	15	18.4	0.52	1
30	9	31.8	2.1	0.95
30	12	26.6	1.32	0.68
30	15	25.1	1.14	0.94
40	15	33.3	2.35	1.3
40	12	37.0	3.09	1.48
50	15	46.6	5.68	0.63

C.2. Maximum divert Cone

Table C.4: Maximum Divert Cone Size Results, Fired Sideways

Launch Conditions		Results	
Distance (km)	Altitude (km)	P_E (km)	E (km)
10	9	0.28	0.65
20	9	5.27	3.72
20	12	0.85	1.58
30	9	5.83	3.89
30	12	1.31	1.65
30	15	3.53	3.15
40	12	3.24	1.40
40	15	2.19	2.92
50	15	4.05	2.26

C.3. Maximum Interception Probability

Table C.5: Maximum Interception Probability Results, Fired Downrange

Launch Conditions		Results		
Distance (km)	Altitude (km)	t_f	P_E (km)	E (km)
10	9	11.3	0.16	0.34
10	12	12.2	0.19	0.43
10	15	13.0	0.23	0.67
20	9	18.0	0.49	0.64
20	12	17.4	0.45	0.9
20	15	19.4	0.59	1.36
30	9	28.3	1.55	2.67
30	12	26.0	1.25	2.69
30	15	24.4	1.06	1.71
40	12	33.4	2.37	3.52
40	15	31.5	2.05	2.45
50	15	37.8	3.28	3.48

Table C.6: Maximum Interception Probability Results, Fired Sideways

Launch Conditions		Results		
Distance (km)	Altitude (km)	t_f	P_E (km)	E (km)
10	9	13.5	0.25	0.66
20	9	23.0	0.91	1.67
20	12	21.9	0.8	1.51
30	9	31.6	2.05	3.41
30	12	27.5	1.44	2.13
30	15	29.7	1.75	3.56
40	12	29.3	1.69	3.22
40	15	34.0	2.49	2.64
50	15	36.9	3.07	2.3

Table C.7: Maximum Interception Probability Results, Fired from Behind

Launch Conditions		Results		
Distance (km)	Altitude (km)	t_f	P_E (km)	E (km)
10	9	26.1	1.27	2.18
10	12	19.6	0.61	1.36
10	15	14.4	0.29	0.71
20	9	30.6	1.9	3.16
20	12	24.7	1.1	2.23
20	15	21.0	0.73	1.5
30	9	32.7	2.25	2.01
30	12	33.2	2.33	3.02
30	15	29.2	1.67	2.67
40	15	38.8	3.52	1.49

C.4. Maximum Range Study

Table C.8: Long Range Trajectories, Fired Downrange

Launch Conditions		Results
Distance (km)	Altitude (km)	P_E (km)
65	15	3.0
80	15	4.6
90	15	6.4

C.5. Launch Conditions Study

Table C.9: Launch Conditions Study Results, Fired Sideways

Launch Conditions		Results			
Distance (km)	Altitude (km)	Heading (deg)	t_f	P_E (km)	E (km)
30	15	29.7	1.75	3.56	
30	15	46.7	5.71	0.81	

D

Trajectory Guidance Result Plots

D.1. Maximum Interception Probability

The maximum interception chance plots show the flight of the interceptor, when a compromise is made between the quality of the BM's trajectory prediction, and the size of the divert cone. Three launch directions are investigated, being downrange from the direction where the BM is headed, sideways, and launches from behind where the interceptor has to catch up.

D.1.1. Downrange Launches

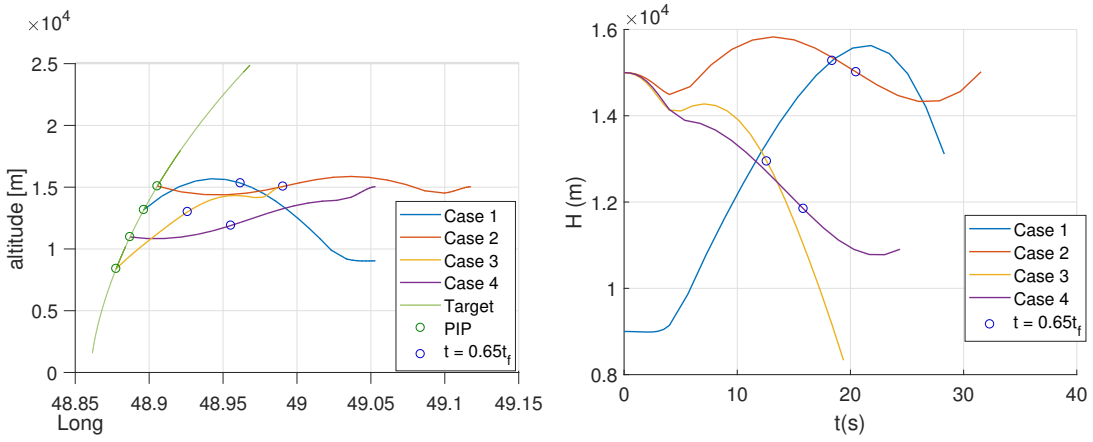

(a) 3D Flight Profile

(b) Altitude of the Interceptor

Figure D.1: 3D Plot and altitude of Intercepting Flights, Launched Downrange with Maximum Interception Chance

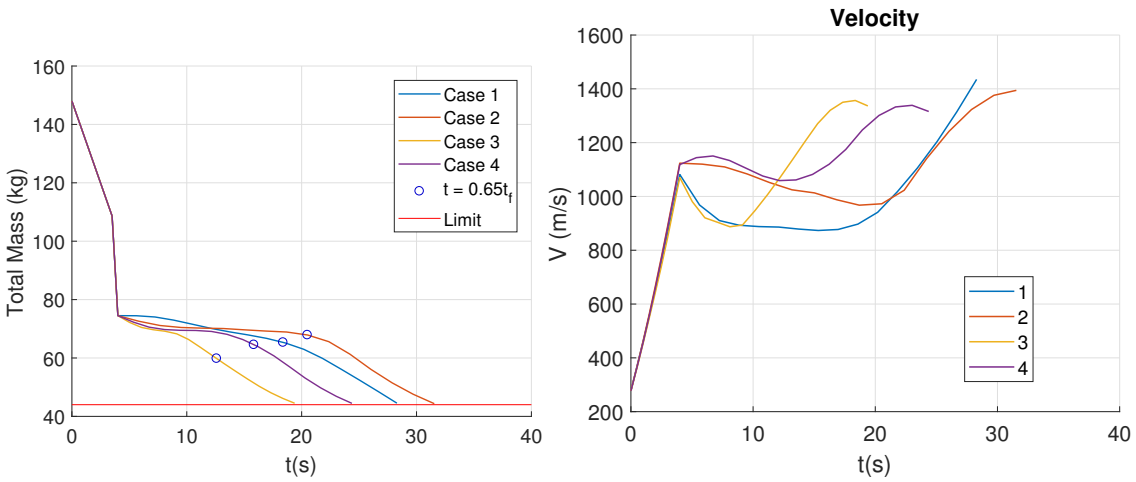

(a) Mass of the Interceptor

(b) Velocity Vector (Magnitude V)

Figure D.2: States of an Interception Flight, Launched Downrange with Maximum Interception Chance (1)

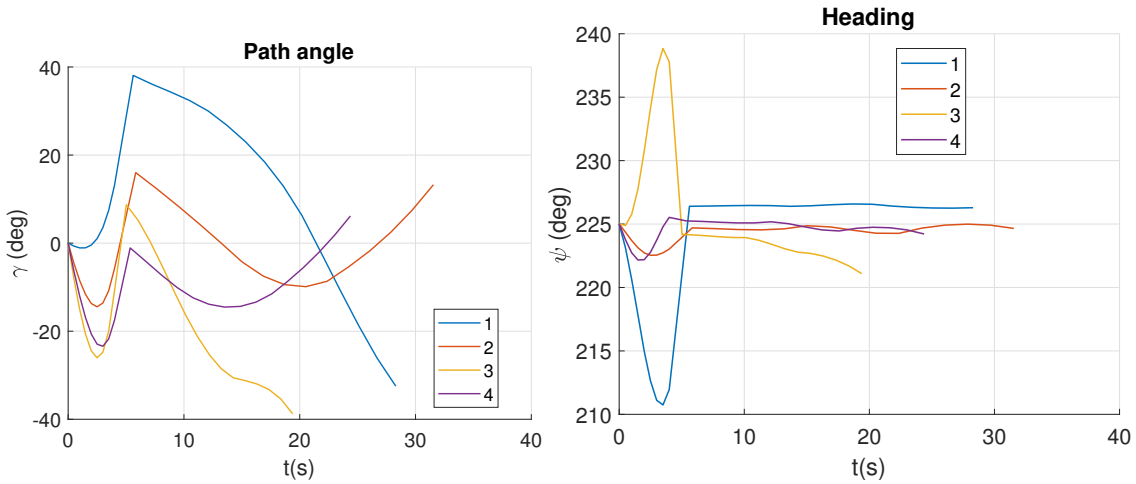

(a) Velocity (Path Angle (γ)

(b) Velocity (Heading (Ψ)

Figure D.3: States of an Interception Flight, Launched Downrange with Maximum Interception Chance (2)

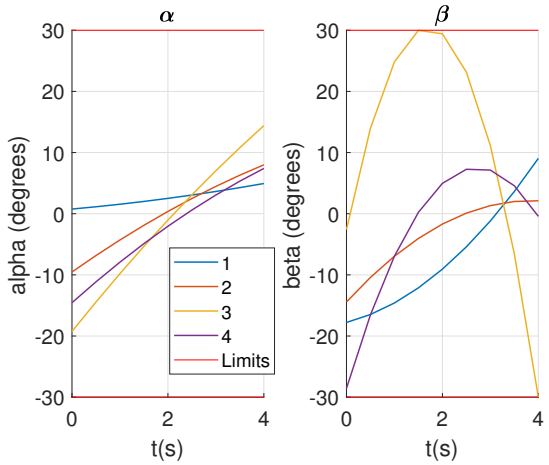

Figure D.4: Boost Phase Controls, Launched Downrange with Maximum Interception Chance

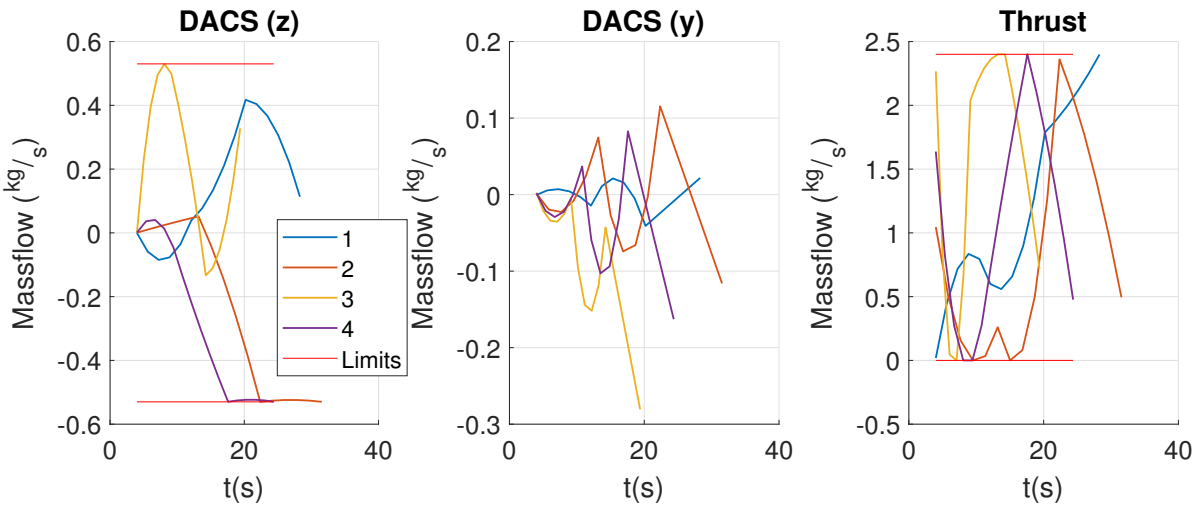

Figure D.5: Sustain Phase Controls, Launched Downrange with Maximum Interception Chance

D.1.2. Sideways Launches

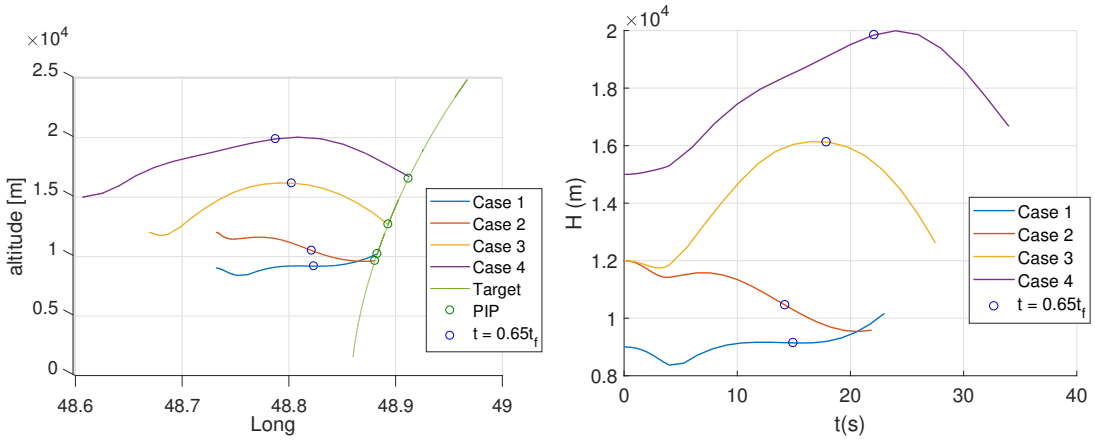

(a) 3D Flight Profile

(b) Altitude of the Interceptor

Figure D.6: 3D Plot and altitude of Intercepting Flights, Launched from the Side with Maximum Interception Chance

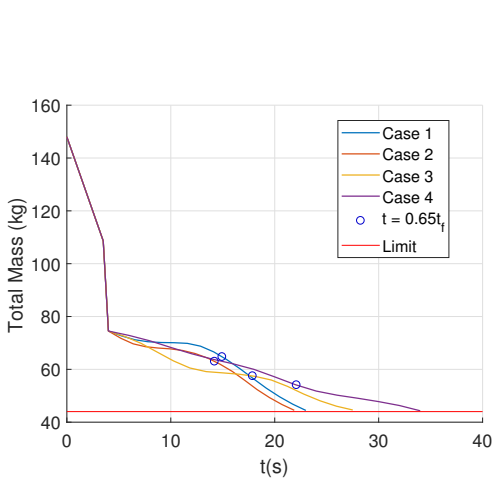

(a) Mass of the Interceptor

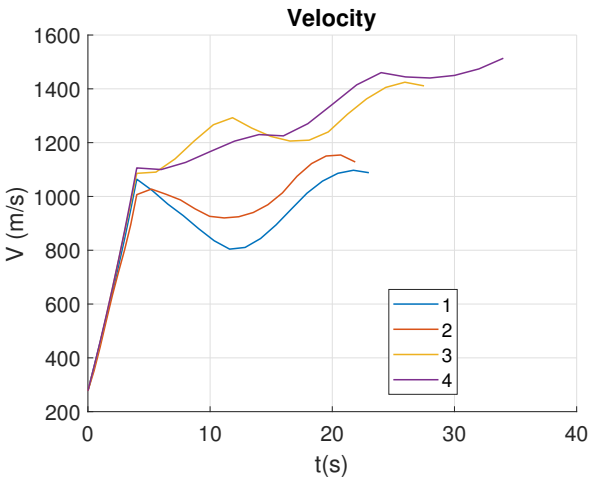

(b) Velocity Vector (Magnitude V)

Figure D.7: States of an Interception Flight, Launched from the Side with Maximum Interception Chance (1)

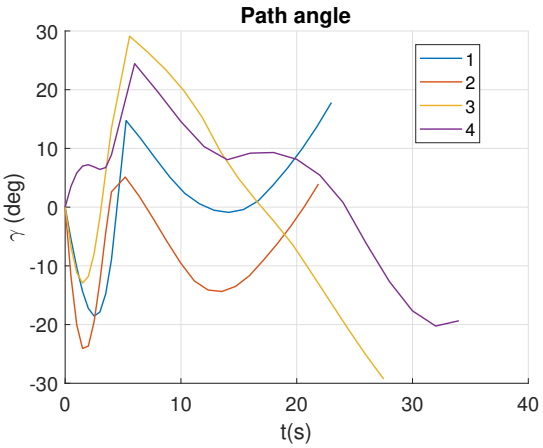

(a) Velocity (Path Angle γ

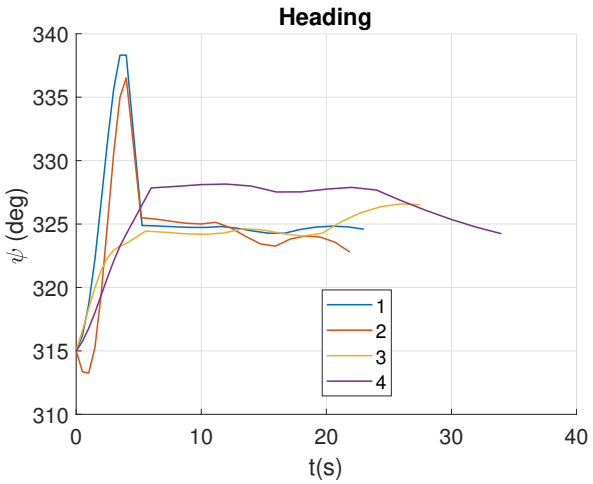

(b) Velocity (Heading Ψ

Figure D.8: States of an Interception Flight, Launched from the Side with Maximum Interception Chance (2)

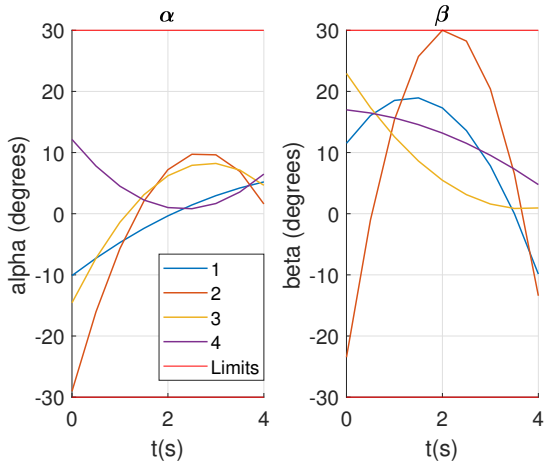

Figure D.9: Boost Phase Controls, Launched from the Side with Maximum Interception Chance

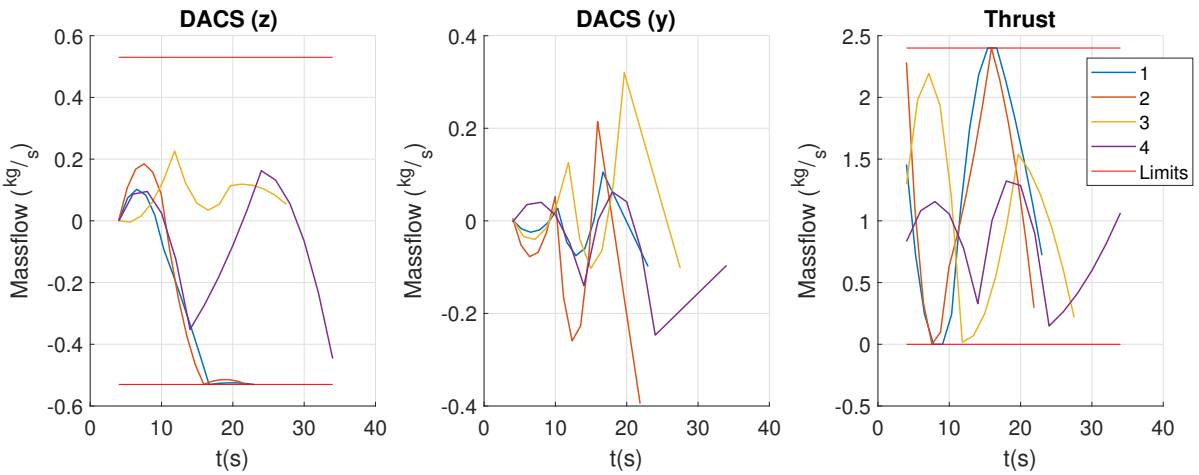

Figure D.10: Sustain Phase Controls, Launched from the Side with Maximum Interception Chance

D.1.3. Launches From Behind

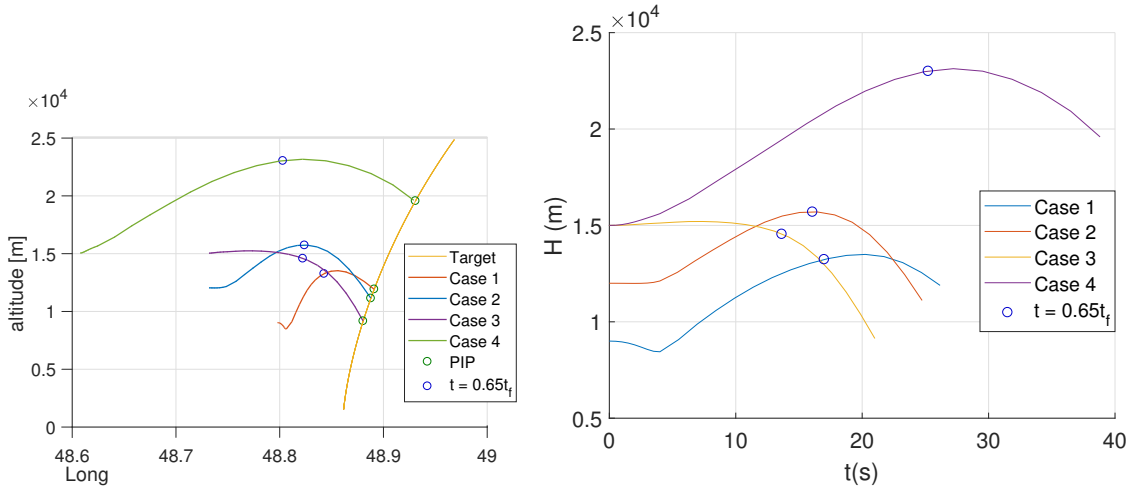

(a) 3D Flight Profile

(b) Altitude of the Interceptor

Figure D.11: 3D Plot and altitude of Intercepting Flights, Launched from Behind with Maximum Interception Chance

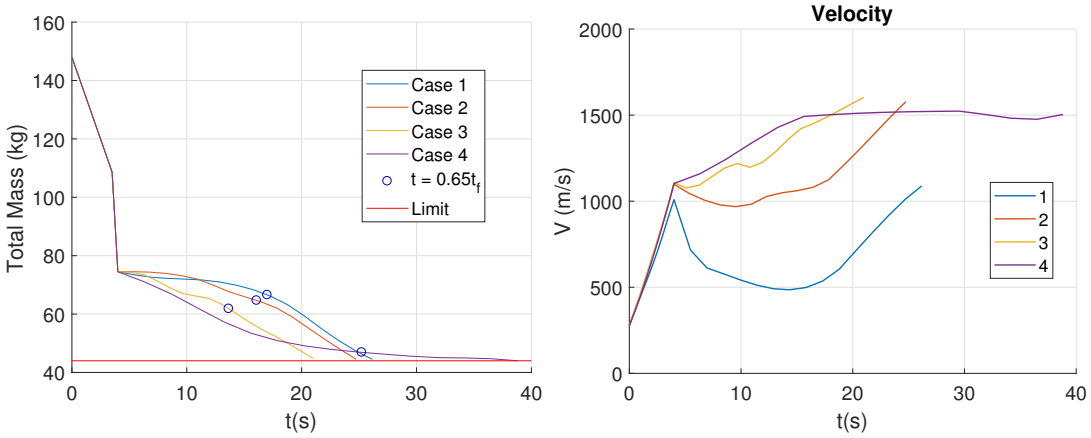

(a) Mass of the Interceptor (b) Velocity Vector (Magnitude V)

Figure D.12: States of an Interception Flight, Launched from Behind with Maximum Interception Chance (1)

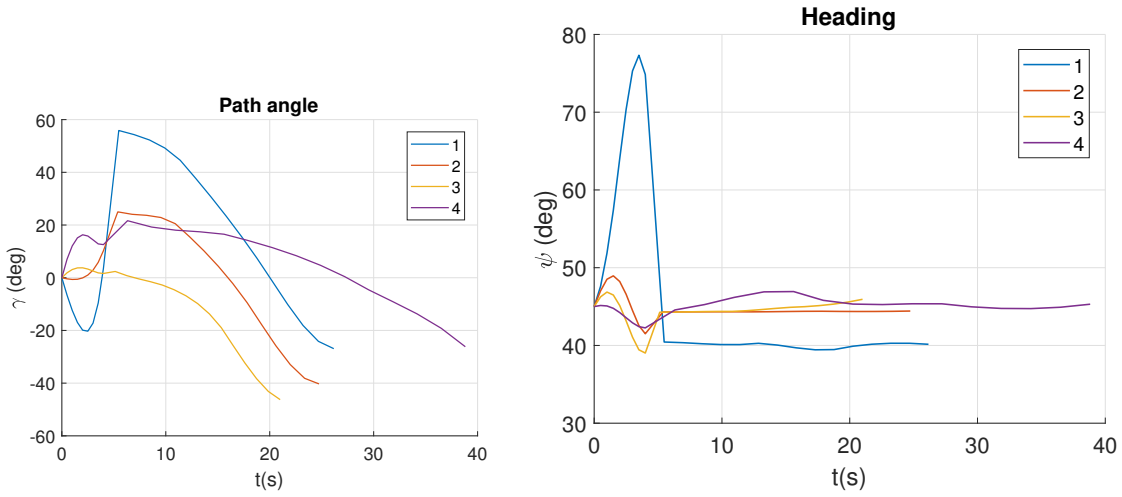

(a) Velocity (Path Angle (γ) (b) Velocity (Heading (Ψ)

Figure D.13: States of an Interception Flight, Launched from Behind with Maximum Interception Chance (2)

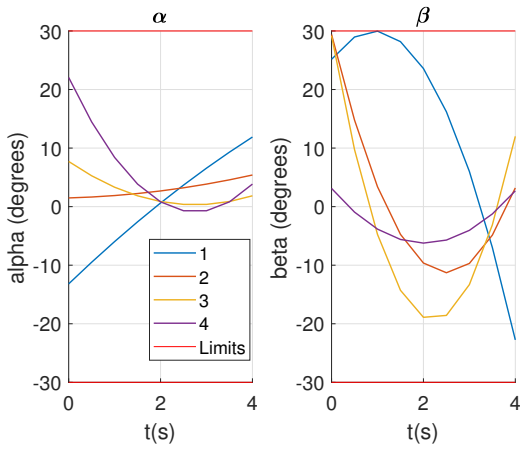

Figure D.14: Boost Phase

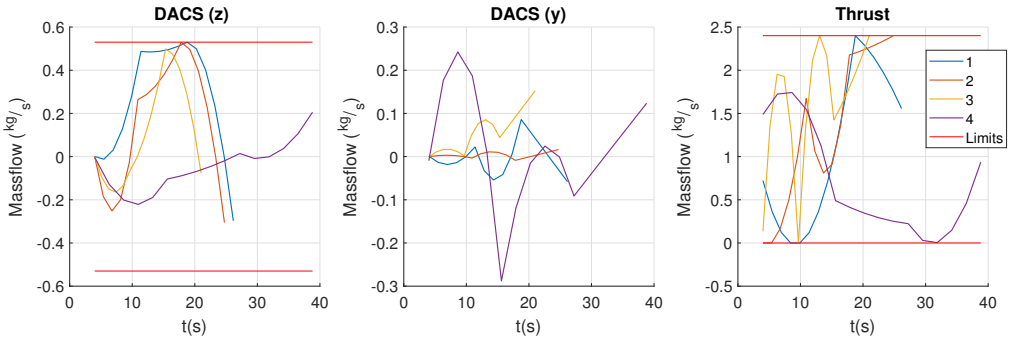

Figure D.15: Sustain Phase Controls, Launched from Behind with Maximum Interception Chance

D.1.4. Launch Conditions Study

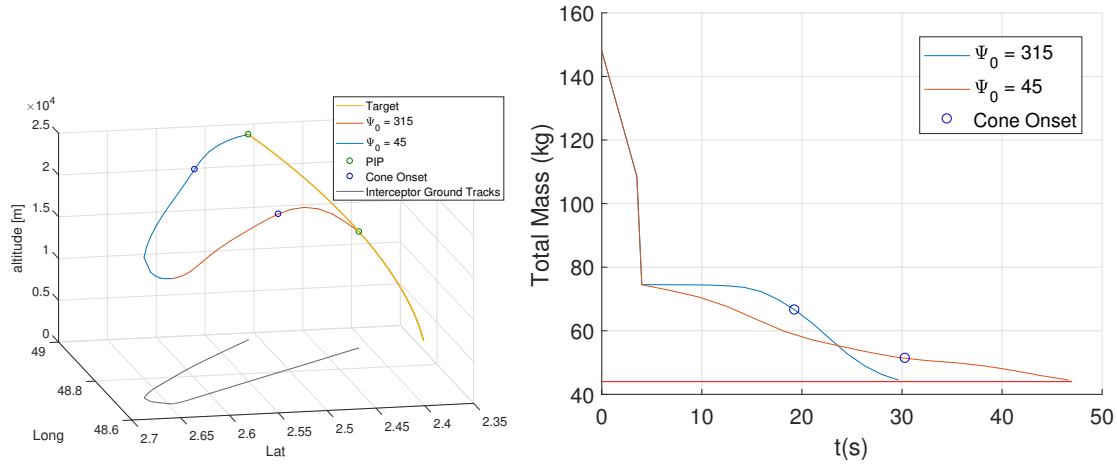

(a) 3D Flight Profile

(b) Mass of the Interceptor

Figure D.16: 3D Plot and Mass of Intercepting Flights, Launched with Various Start Headings

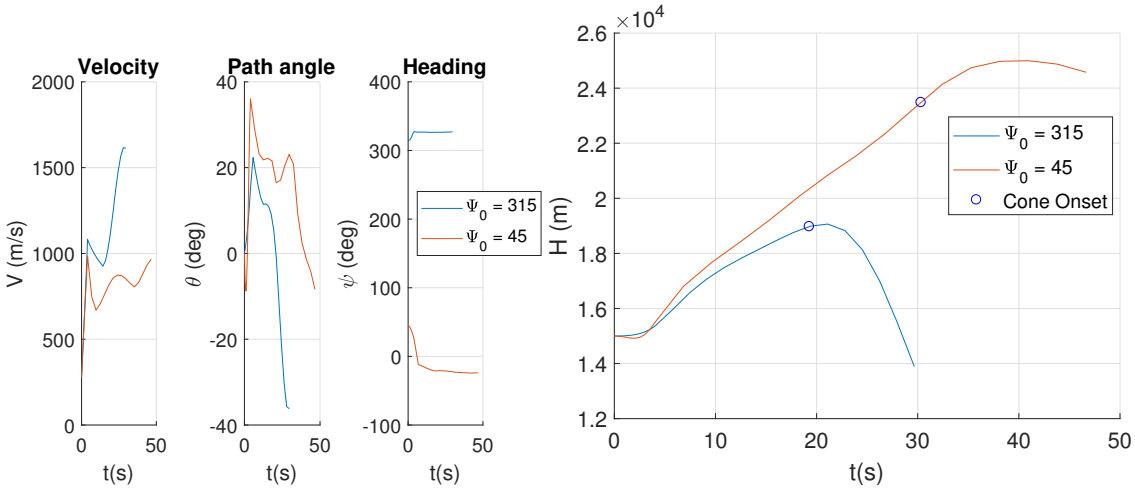

(a) Velocity of the Interceptor

(b) Altitude of the Interceptor

Figure D.17: Velocity and Altitude of an Interception Flight, Launched with Various Start Headings

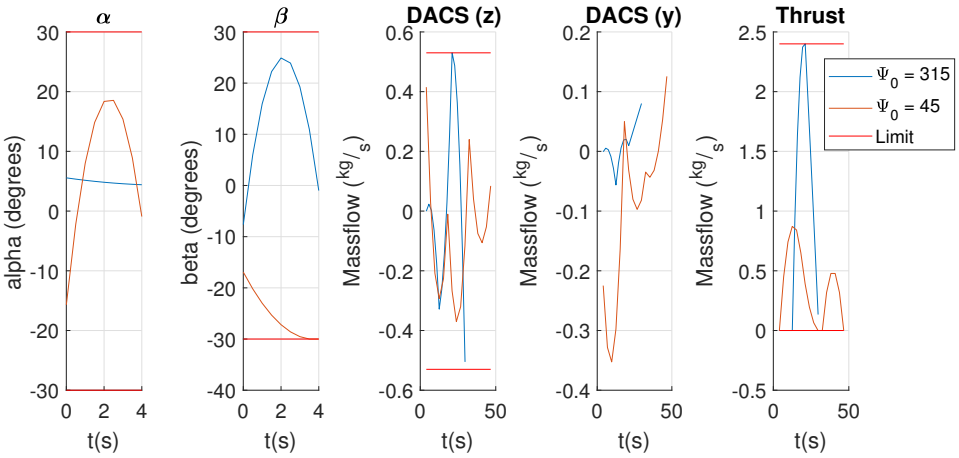

Figure D.18: Control Deflections of the Missile Launches, Launched with Various Start Headings